Sediment fluxes dominate glacial-interglacial changes in ocean carbon inventory: results from factorial simulations over the past 780,000 years

Markus Adloff[1,2], Aurich Jeltsch-Thömmes[1,2], Frerk Pöppelmeier[1,2], Thomas F. Stocker[1,2], and Fortunat Joos[1,2]

[1]Climate and Environmental Physics, Physics Institute, University of Bern, Switzerland
[2]Oeschger Centre for Climate Change Research, University of Bern, Switzerland

Correspondence: Markus Adloff (markus.adloff@unibe.ch)

Abstract. Atmospheric CO_2 concentrations ~~changed~~ varied over ice age cycles due to net exchange fluxes of carbon between land, ocean, ~~ocean sediments, atmosphere~~marine sediments, lithosphere, and the ~~lithosphere. Marine sediment and ice cores preserved~~ atmosphere. Marine sediments and polar ice cores archived indirect biogeochemical evidence of these carbon transfers, which resulted from ~~sensitivities~~ poorly understood responses of the various carbon reservoirs to climate forcing~~, many of which remain poorly understood. Numerical~~ . Modelling studies proved the potential of several physical and biogeochemical processes to impact atmospheric CO_2 under steady-state glacial conditions. Yet, it ~~is~~ remains unclear how much they affected carbon cycling during transient changes of repeated glacial cycles, and what role burial and release of sedimentary organic and inorganic carbon and nutrients played. Addressing this ~~uncertainty~~knowledge gap, we produced a simulation ensemble of various idealized physical and biogeochemical carbon cycle forcings over the repeated glacial inceptions and terminations of the last 780 kyr with the Bern3D Earth system model of intermediate complexity~~including~~ , which includes dynamic marine sediments. This ensemble allows for assessing transient carbon cycle changes due to these different forcings and gaining a process-based understanding of the ~~associated carbon fluxes and isotopic shifts~~ carbon fluxes resulting from the forcings, and the associated isotopic shifts that could serve as proxy data, in a continuously perturbed Earth system. We present results of the simulated Earth system dynamics in the non-equilibrium glacial cycles and a comparison with multiple proxy time series. In our simulations~~the ocean inventory changed by 200-1400 GtC and the atmospheric inventory by 1-150 GtC over the last deglaciation. DIC~~ , the forcings cause sedimentary perturbations that have large effects on marine and atmospheric carbon storage. Dissolved Inorganic Carbon (DIC) changes differ by a factor of up to 28 between simulations with and without interactive sediments, while CO_2 changes in the atmosphere are ~~at most~~ up to four times larger when interactive sediments are simulated. ~~Simulations with interactive sediments show no clear correlations between DIC or nutrient concentrations~~ The relationship between DIC (200-1400 GtC) and atmospheric CO_2 change (1-150 GtC) over the last deglaciation is strongly setup-dependent, highlighting the ~~likely need for~~ need for considering multiple carbon reservoirs and multi-proxy analyses to ~~understand~~ more robustly quantify global carbon cycle changes during glacial cycles~~in practice. Starting~~ . Finally, initiating transient simulations with an interglacial geologic carbon cycle balance causes isotopic drifts that require several 100 kyr to

overcome~~, and needs~~ . These model drifts need to be considered when designing spin-up strategies.

1 Introduction

During the Quaternary, the Earth's carbon cycle repeatedly shifted between low atmospheric CO_2 ~~concentrations~~ during glacial periods and elevated ~~concentrations~~ mixing ratios during interglacials in orbitally-paced cycles (Petit et al., 1999; Siegenthaler et al., 2005; Lüthi et al., 2008). The reconstructed evolution of atmospheric CO_2 ~~concentrations~~ from Antarctic ice cores aligns closely with temperature and ~~, with a delay,~~ is lagged by ice sheet extent, suggesting a close coupling of climate and the carbon cycle (e.g. Shackleton, 2000; Bereiter et al., 2015). Yet, simulating atmospheric CO_2 changes that are consistent with ~~reenstructed~~ reconstructed CO_2 and other proxy data is challenging because the observed carbon cycle changes were the result of complex Earth system responses to climate forcing (Schmittner, 2008).

Changing ocean chemistry is often attributed an important role in these cycles because of the considerable size of the marine carbon reservoir (Broecker, 1982a) and because reconstructions ~~imply smaller carbon stocks in vegetationand soils~~ show that overall there was likely less carbon stored on land (in vegetation, permafrost, peatlands and soils) at the Last Glacial Maximum (LGM) than during the current warm period ~~(Lindgren et al., 2018; Jeltsch-Thömmes et al., 2019)~~(Yu et al., 2010; Lindgren et al., 2018; Je . A multitude of physical and biogeochemical processes have been assessed for their contribution to changes in the marine carbon storage on these timescales ~~(e.g. Sigman et al., 2010; Fischer et al., 2010)~~(e.g. Kohfeld and Ridgwell, 2009; Sigman et al., 2010; Fisch , and their relative importance for the CO_2 difference between the ~~last glacial maximum~~ LGM and the late Holocene have been tested in numerical simulations with dynamic ocean models (e.g. Brovkin et al., 2012; Menviel et al., 2012). Changes in ocean circulation and increased CO_2 solubility due to lower temperatures contributed to the lower glacial atmospheric CO_2 concentration (Broecker, 1982a; Smith et al., 1999; Brovkin et al., 2007; Sigman et al., 2010; Fischer et al., 2010), while increased salinity and surface ocean dissolved inorganic carbon (DIC) concentrations due to lowered sea levels ~~added~~ tend to counteract this effect by stimulating CO_2 ~~back~~ outgassing to the glacial atmosphere (Weiss, 1974; Broecker, 1982a; Brovkin et al., 2007). Furthermore, reduced ~~carbon~~ CO_2 outgassing from the Southern Ocean due to a greater extent of sea ice isolating the surface ocean from the atmosphere, and enhanced stratification due to brine rejection during sea ice formation are other physical processes suggested to have affected the glacial carbon cycle (Stephens and Keeling, 2000; Bouttes et al., 2010).

~~Biogeochemical~~ Marine biogeochemical processes that lead to ~~increased ocean carbon storage include reduced~~ lower atmospheric CO_2 include a shift of organic carbon remineralization ~~rates in the colder ocean~~to greater depths, as well as increased export production due to increased nutrient supply from emerged shelves (phosphate) ~~,~~and enhanced dust deposition (iron, silica) and ~~supply from the deep Southern Ocean~~ changes in Southern Ocean dynamics and nutrient utilization, which would have counteracted the effect of ~~low temperatures~~ colder temperatures and large sea ice extent on surface ocean ~~productivity and increased export production~~ export production and nutrient utilization (Broecker, 1982b; Martin, 1990; Pollock, 1997; Deutsch et al., 2004). In a (hypothetical) closed atmosphere-ocean system, the combination of these processes ~~result~~ results in increased

marine carbon storage during glacials, but not necessarily in ~~open systems (i.e. considering dynamic land and lithospheric carbon reservoirs) (e.g. Buchanan et al., 2016; Kemppinen et al., 2019).~~

~~Little is known about the changes of carbon stored as organic and inorganic carbon in a fourth reservoir: marine sedimentsand the lithosphere. It has since long been assumed~~ the open Earth system because the carbon removed from the surface ocean and atmosphere by these processes could have been sequestered in the water column as DIC or particulate carbon but also in marine sediments. Carbon can also be transferred to the land. Constraints on glacial atmospheric CO_2 can be reconciled with increased and decreased marine DIC inventory in an open system (Jeltsch-Thömmes et al., 2019; Kemppinen et al., 2019) , though reproducing reconstructed carbon isotopic changes in atmosphere and ocean seems to require elevated DIC at the LGM (Jeltsch-Thömmes et al., 2019).

It is very probable that changing sedimentary carbonate and particulate organic carbon (POC) burial played a relevant role in glacial-interglacial carbon cycle changes by altering seawater carbonate chemistry, ~~particularly on continental shelves which would~~ carbonate ion concentrations, carbon isotope ratios, and oxygenation. Particularly, continental shelves have emerged from the ocean during glacial sea level low stands and provided new reef habitats and carbonate deposition environments during deglaciations and interglacials (e.g. Broecker, 1982b; Opdyke and Walker, 1992; Ridgwell et al., 2003; Brovkin et al., 2007; Menviel and Joos, 2012). Additionally, carbonate burial changes in the open ocean have been considered as amplifiers of marine carbon uptake (e.g. Archer and Maier-Reimer, 1994; Kohfeld and Ridgwell, 2009; Schneider et al., 2013; Roth et al., 2014; Kerr et al., 2017; Kobayashi et al., 2021). ~~Consistently, reconstructions~~ Organic carbon burial is also prone to vary in response to changes in the rain rate of POC sinking to the sea floor and altered oxygenation. Previous model simulations, that included POC burial, showed that interactive sediments greatly affect atmospheric CO_2 and carbon isotope variations through the burial-nutrient feedback, whereby enhanced burial of organic-bound carbon and nutrients reduces export production (Tschumi et al., 2011; Roth et al., 2014; Jeltsch-Thömmes et al., 2019; Jeltsch-Thömmes and Joos, 2023). Reconstructions of marine burial changes over the last glacial cycle suggest a reduction in ~~globally-averaged~~ globally-integrated inorganic carbon burial (Cartapanis et al., 2018; Wood et al., 2023) during the last glacial period, but increased organic (Cartapanis et al., 2016) sedimentary carbon burial. The extents of both changes are uncertain due to the spatial heterogeneity of sedimentary burial and the inherently local nature of marine ~~sediment cores~~archives, but possibly of comparable magnitude to terrestrial carbon stock changes (Cartapanis et al., 2016, 2018).

~~Previous model simulations, that included organic carbon burial, showed that interactive sediments greatly affect atmospheric CO_2 and carbon isotope amplitudes through the burial-nutrient feedback (Tschumi et al., 2011; Roth et al., 2014; Jeltsch-Thömmes et al., 2 . Dynamic sedimentary adjustment and imbalances in weathering-burial fluxes also increase the equilibration time of atmospheric CO_2 by a factor of up to 20 to several tens of thousands of years and the resulting $\delta^{13}C$ perturbations take hundreds of thousands of years to recover (Roth et al., 2014; Jeltsch-Thömmes et al., 2019; Jeltsch-Thömmes and Joos, 2023).~~ These findings demonstrate that organic and inorganic sedimentary changes and imbalances ~~between the weathering and burial fluxes to the consolidated sediments and lithosphere~~ with weathering fluxes need to be considered when quantifying carbon reservoir changes of the ocean, atmosphere, and land and interpreting the reconstructed changes in CO_2, carbonate ion concentrations, isotopes, and nutrients over glacial cycles.

Model-based estimates of carbon and carbon isotope inventory differences between glacial and interglacial periods are complicated by temporal carbon cycle imbalances during the continuously evolving climate of glacial cycles. This is particularly challenging when simulating dynamic elemental cycling in and burial from reactive marine sediments and the input of elements by weathering and volcanic outgassing ~~and the loss of elements by burial in reactive sediments and the lithosphere,~~ because of long-lasting re-equilibration and memory effects in carbon and nutrient fluxes and particularly isotopic changes (Tschumi et al., 2011; Jeltsch-Thömmes and Joos, 2020). ~~Importantly, sedimentary fluxes and related weathering-burial imbalances never reached true equilibrium during glacial cycles, which implies~~ Dynamic sedimentary adjustment, i.e. the equilibration of sedimentary dissolution and remineralization to changes in bottom water which slowly diffuse into sedimentary porewater, and imbalances between the supply (weathering) and loss (sedimentary burial) of carbon and nutrients also increase the equilibration time of atmospheric CO_2 by a factor of up to 20 to several tens of thousands of years and the resulting $\delta^{13}C$ perturbations take hundreds of thousands of years to recover (Roth et al., 2014; Jeltsch-Thömmes et al., 2019; Jeltsch-Thömmes and Joos, 2 . Importantly, the equilibration time scales are longer than typical interglacials in the late Pleistocene, which opens up the possibility for memory effects that span several glacial cycles.

A caveat of several modeling studies attempting to quantify carbon reservoir sizes at the LGM is that they assume a steady state carbon cycle in a closed (atmosphere-ocean only) system and do not account for the history of environmental changes that pre-dated the LGM but could have introduced long-lasting memory effects. Transient simulations of ~~a whole~~ an entire glacial cycle with a fully dynamic marine and sedimentary carbon cycle showed that time lags in the carbon cycle response to orbital forcing add constraints for the identification of the processes that caused glacial CO_2 changes (Menviel et al., 2012). In particular, imbalances between marine carbon burial and continental weathering and the long marine residence time of phosphate delay the CO_2 increase during the temperature rise of deglaciations. ~~Transient~~ Accounting for these long-term effects in their experimental design, transient simulations of more than one glacial cycle showed that reconstructed atmospheric CO_2 and benthic marine $\delta^{13}C$ changes over the last 400 kyr could be reasonably well simulated with a ~~combinations~~ combination of physical (radiative and ocean volume changes) and biogeochemical processes ~~(carbonate chemistry and land carbon changes, temperature-dependent remineralization depth, additional nutrient supply during glacials)~~ ~~if~~ ((carbonate chemistry and land carbon changes, temperature-dependent remineralization depth, additional nutrient supply during glacial . Yet, shallow water carbonate burial ~~changed too (Ganopolski and Brovkin, 2017). These burial changes were partially prescribed~~ was prescribed and POC burial not included in the simulations, which begs the question how ~~well~~ the effect of the considered processes ~~can explain~~ on glacial-interglacial atmospheric CO_2 ~~change if sedimentary burial and surface ocean carbonate chemistry are entirely dynamically simulated. Simulations~~ and carbon isotopic ratios changes if the sediments are dynamically calculated. Recently, simulations of glacial-interglacial cycles beyond the Mid-Brunhes transition (∼430 ka) were run with a box model (Köhler and Munhoven, 2020) and ~~purely physical models~~ a purely physical model (Stein et al., 2020) which are unable to capture transient and spatially heterogeneous interactive sediments. CLIMBER-2, a fully coupled intermediate-complexity Earth system model, was run stepwise over the last 3 Myr, but the results were not analysed for the carbon cycle dynamics (Willeit et al., 2019).

Here we examine systematically how the transient built-up and dissolution of marine sediments on glacial-interglacial timescales affects the carbon cycle changes produced by the various processes suggested to be relevant on these timescales, a gap left by previous studies. Instead of searching for the most likely scenario that reconciles the vast proxy evidence, we attempt to gain a more complete process understanding and overview of the proxy-relevant signals that these processes cause in the presence of weathering-burial imbalances. With this goal, we extend factorial simulations of multiple simplified physical and ~~biochemical~~ biogeochemical forcings in a marine sediment and isotope-enabled intermediate complexity Earth system model over the last 780 kyr ~~to understand how various processes affect carbon fluxes in response to continuously varying climate, and specifically how sediments affect the marine and atmospheric carbon cycle across repeated glacial cycles. To~~ and compare the resulting carbon and carbon isotopic signals to reconstructions. The long timescale is chosen to avoid biases resulting from steady state assumptions ~~, we simulated the last eight glacial cyclesfully transiently, so that~~ and account for the possibility of memory effects under continuously varying climate and carbon cycle that could span multiple glacial cycles. Consequently, all carbon stores ~~at the beginning of the last glacial cycle~~ are achieved dynamically rather than being prescribed. ~~Specifically, we~~ We present two sets of simulations with and without interactive sediments to distinguish the role of interactive sediments in the carbon cycle changes caused by ~~these different forcings over repeated glacial cycles~~ the tested forcings over reoccurring glacial cycles of the last 780 kyr.

2 Methods

2.1 Bern3D v2.0s

We simulated the Earth system's transition through the last 780 kyr of glacial cycles with the intermediate complexity Earth system model Bern3D v2.0s, which has ~~a resolution of~~ an irregular 41×40 grid (lowest resolution: lat×lon = 5°×10° in the North Pacific, highest resolution: lat×lon = 3°×7° in the Equatorial Atlantic) in the horizontal and 32 logarithmically spaced ocean depth layers. The model combines modules for 3D physical ocean dynamics, marine biogeochemistry, marine interactive sediments, and atmospheric energy-moisture balance. ~~The geostrophic-frictional balance ocean circulation is calculated explicitly (Edwards et al., 1998; Müller et al., 2006), and parameterizations are included to represent the effects of dia- and isopycnal diffusion and eddy-induced transport (Griffies, 1998). The NCEP/NCAR monthly wind stress climatology (Kalnay et al., 1996) is used to prescribe wind stress at the ocean surface. Atmosphere-ocean gas exchange and carbonate chemistry are simulated according to the OCMIP-2 protocols (Najjar et al., 1999; Orr et al., 1999, 2017; Wanninkhof, 2014; Orr and Epital , and gas transfer velocities are scaled with wind speed (Krakauer et al., 2006). The global mean sea-air gas exchange was then reduced by 19% to achieve agreement with radiocarbon distribution estimates (Müller et al., 2008).~~

The physical ocean component transports tracers through the ocean by advection, convection, and diffusion. Euphotic zone production depends on temperature, light, sea ice cover, and nutrient (phosphate, iron, silica) availability ~~, with a full description of the model biogeochemistry in Parekh et al. (2008); Tschumi et al. (2011) and of~~ (Parekh et al., 2008; Tschumi et al., 2011) and explicitly calculates carbon isotope dynamics ~~in Jeltsch-Thömmes et al. (2019)~~(Jeltsch-Thömmes et al., 2019). In our setup, a fraction of the particulate organic matter formed in the surface ocean is instantly remineralized following an oxygen con-

centration dependent version of the globally-uniform Martin curve (Battaglia and Joos, 2018) and particulate inorganic carbon and opal dissolution occurs according to globally-uniform e-folding profiles. The remaining solid particles reaching the sediment-ocean interface enter reactive sediments, where they are preserved, remineralized, or redissolved depending on dynamically calculated porewater chemistry, and mixed by bioturbation (Tschumi et al., 2011). ~~The sediment model includes~~ $CaCO_3$ dissolution rates in the sediments are determined from the pore water saturation state, and POC remineralisation is parameterised by a linear dependence on porewater O_2 (Heinze et al., 1999; Tschumi et al., 2011). The model contains 10 layers ~~and computes fluxes of carbon, nutrients, alkalinity, and isotopes between the ocean, reactive sediments, and the lithosphere. Loss fluxes to the lithosphere are compensated for at equilibrium~~ of reactive sediments. As matter gets pushed downward out of the bottom layer ('sedimentary burial'), it is lost to the modelled inventories. These loss fluxes are at equilibrium compensated for by a corresponding solute input flux from ~~weathering. The ocean model includes diagnostic tracers for preformed DIC and phosphate, which track the fractions of DIC and phosphate that are not incorporated into marine organic carbon during surface ocean production~~land into the coastal surface ocean. The (pre-industrial) land-sea mask and bathymetry are fixed throughout the spin-up and simulations.

2.2 Model spin-up with interglacial boundary conditions

We spun up the model with pre-industrial boundary conditions in three stages, sequentially coupling all modules, for computational efficiency. First, we forced the ocean circulation and then the atmosphere-ocean carbon cycle as a closed system with pre-industrial climatic conditions and prescribed CO_2 for 20 kyr. In the next step, the sediment module is coupled and terrestrial solute supply (phosphate, alkalinity, DIC, $DI^{13}C$ and Si) to the ocean is ~~prescribed to balance loss to the lithosphere over~~ set to dynamically balance the loss through sedimentary burial for 50 kyr. ~~Then, this weathering input flux is diagnosed~~ At the end of this stage, the solute input flux required to balance sedimentary burial is diagnosed (Table S1) and kept constant ~~thereafter~~for the rest of the spin up procedure and throughout our transient experiments. Until this stage, atmospheric CO_2 and $\delta^{13}C$ were prescribed. The spun up model for the pre-industrial was then run for 2000 years as an open system (freely evolving CO_2 and $\delta^{13}C$) with radiative forcing that varied linearly from PI to the slightly different MIS19 conditions, the starting point of our experiments. The total length of the spin-up to this point was 72 kyr. To avoid large drifts in carbon isotopes and alkalinity ~~(Jeltsch-Thömmes and Joos, 2023)~~ (Jeltsch-Thömmes and Joos, 2023, explained at the end of our results section) in the simulations with the forcings that perturbed the carbon cycle the most (PO4, REMI, LAND, CO2T, BGC, ALL, described in the next section), we ran the fully-interactive model with ~~the~~ each respective forcing for ~~three glacial cycles~~ two glacial cycles (215 kyr) before starting our experiments. We discuss the relevance of initial conditions and imbalances of the geologic carbon cycle at the end of the manuscript. Model limitations due to constant terrestrial solute supply are discussed in SI.5.

2.3 Experimental design

~~We~~ Data constraints on carbon cycle forcings are too sparse to know exact magnitudes and timings of the forcings that might have varied spatially and temporarily over the last eight glacial cycles. An inverse estimation of the forcings from the resulting proxy signals requires a different simulation ensemble and is beyond the scope of our study. Rather than trying to guess

the most proxy consistent forcing amplitudes and patterns, we designed seven simplified forcings~~(table 1)~~ , each with one exemplary magnitude, to simulate the ~~effects of Earth system changes~~ generic effects of processes that have been identified as glacial-interglacial carbon cycle drivers~~(similar to the study of long-term circulation changesin Adloff et al. (2023)): expanded Antarctic Bottom Water (AABW), here simulated by increased wind stess over the Southern Ocean, reduced sea-air gas exchange in the Southern ocean, reduced solar radiation due to increased dust and aerosol fluxes, enhanced supply of nutrients, reduced particulate organic carbon remineralization, lower rain ratio of particulate inorganic carbon (PIC, $CaCO_3$) to particulate organic carbon (POC), and reduced terrestrial carbon storage during glacial times~~. Except for the orbital changes, which were calculated following Berger (1978); Berger and Loutre (1991) and the reconstructed CO_2, N_2O and CH_4 curves (Loulergue et al., 2008; Joos and Spahni, 2008; Bereiter et al., 2015; Etminan et al., 2016), which we used to calculate the radiative forcing of greenhouse gas changes, the amplitudes of the forcings were set to cause noticeable CO_2 or circulation shifts, informed by previous studies (e.g. Tschumi et al., 2011; Menviel and Joos, 2012; Menviel et al., 2012; Jeltsch-Thömmes et al., 2019 . We produced timeseries of these forcings by defining a maximum forcing amplitude for the LGM, a minimum for the Holocene and then modulating this amplitude by reconstructed relative changes in the temporal evolution of either Antarctic ice core δD (Jouzel et al., 2007) or benthic δ^{18}O (Lisiecki and Raymo, 2005) for each year (Fig. 1). The choice of the isotope record for calculating the instantaneous forcing depends on whether we expect the forcing to evolve synchronously with temperature like δD or have a time lag similar to δ^{18}O ~~.~~

~~Forcing scenarios. Simulations are run in two configurations: the standard setup with interactive sediments and a closed-system setup without sediments (except PO4).~~ (see section SI.5 for a discussion of the limitations). In all simulations, we prescribed the radiative effect of CO_2 in the atmosphere, so that all simulations have the same radiative forcing from greenhouse gasses despite differences in simulated CO_2.

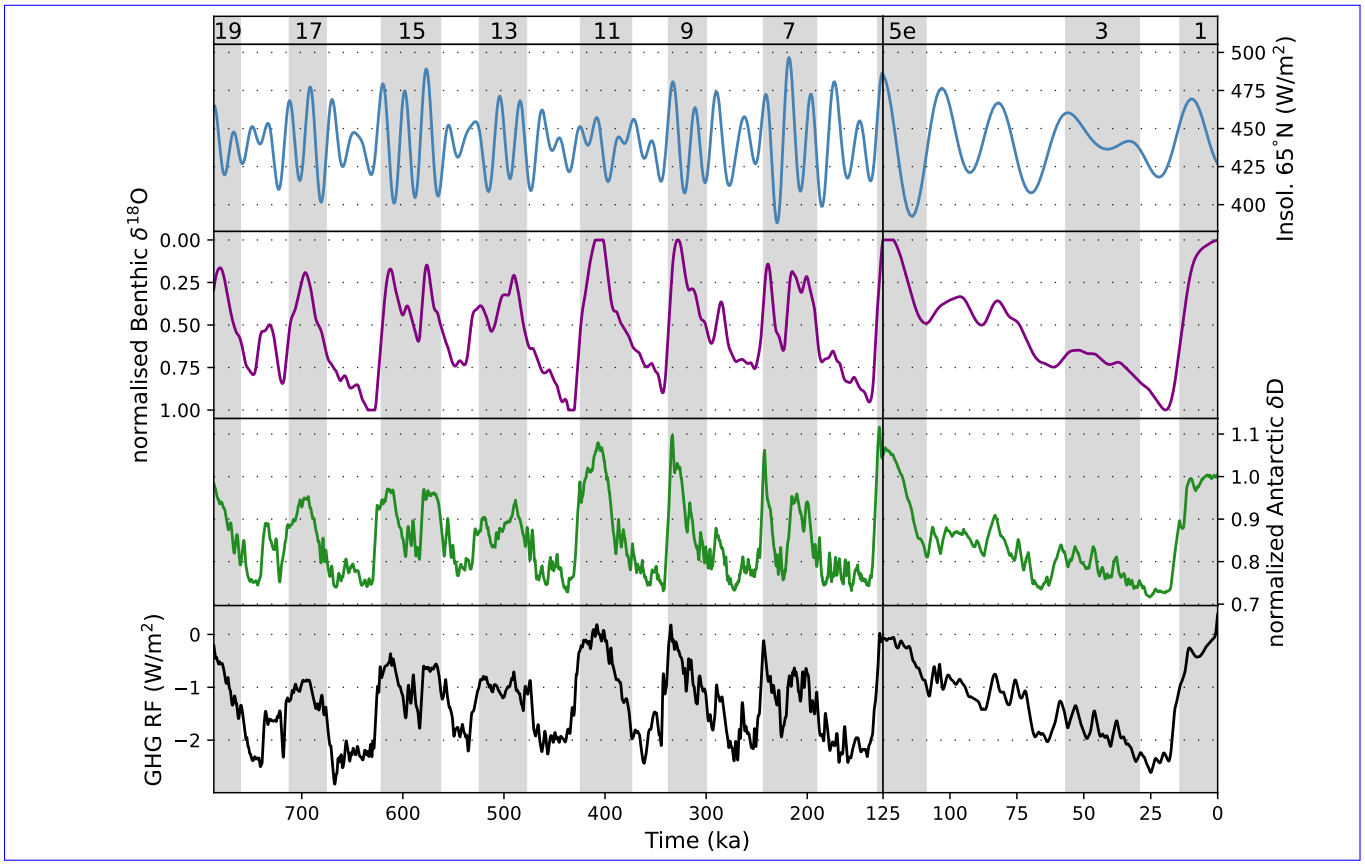

Figure 1. Forcing timeseries. Insolation changes (top panel) are calculated according to Berger (1978); Berger and Loutre (1991). The δ^{18}O forcing (second panel) is the LR04 stack (Lisiecki and Raymo, 2005), smoothed by averaging over a 10000-year moving window and normalized to the LGM-PI difference. The δD forcing (third panel) is taken from Jouzel et al. (2007) and normalized to the LGM-PI difference. The radiative forcing (RF) of CO_2, N_2O and CH_4 (greenhous gasses 'GHG', bottom panel) is calculated from Bereiter et al. (2015); Loulergue et al. (2008); Joos and Spahni (2008) following Etminan et al. (2016). Gray shading indicate uneven Marine Isotope Stages (MIS).

Specifically, we performed one 'base' run with orbital and radiative forcing only, one model run for different forcings, each added to the base forcing, and combinations of the individual forcings to study non-linear effects that appear when processes interact. All of these experiments are run once with and once without interactive sediments, to examine the effect of sediment perturbations on the results. The forcings and their rationale are described below. The experiments are summarized in Table 1.

The application of the standard forcing in simulation BASE ~~results~~ causes temperature changes associated with orbital, albedo, and greenhouse gas changes which affect solubility, sea ice and circulation, e.g. slightly weakening AMOC (by up to 4.5 Sv, Fig. S8) and resulting in younger deep water masses in the Atlantic and Pacific during the LGM than at the PI, which is inconsistent with proxy data and thus indicates that additional Earth system changes must have occurred (Pöppelmeier et al., 2020). To achieve an older glacial deep ocean (diagnosed with an ideal age tracer), we reduced the wind stress south of 48 °S by a maximum of 40% ~~temporally changing proportionally~~ (simulation SOWI) temporally changing

proportionately to the δD change because we assume that wind strength over the Southern Ocean evolved without temporal lags to Antarctic temperature. As a result, the South Pacific downwelling is strengthened by up to 1.5 Sv locally in glacials, AMOC strength is further reduced by up to 1 Sv and the simulated deep ocean age is ~100 years older in the LGM than in the PI, close to published model estimates (Schmittner, 2003). ~~Changing~~ In this set-up, changing wind stress only affects the circulation, not the piston velocity of gas exchange, which is forced by a wind-speed climatology. For an independent assessment of the effect of wind speed changes on sea-air gas exchange, we ~~added~~ performed a simulation in which we decreased the piston velocity in the Southern Ocean by a maximum of 40% (KGAS), also following the evolution of δD. ~~Finally~~Next, we tested ~~a~~ an additional negative radiative forcing due to increased dust loads in the glacial atmosphere (e.g. Claquin et al., 2003) by reducing the total radiative forcing by a maximum of 2.5 W/m^2 during the LGM to test the effects of stronger AMOC weakening (AERO), modulated by the δ^{18}O record based on the reconstructed correlation between dust and δ^{18}O (Winckler et al., 2008, similar to the study of long-term circulation changes in Adloff et al. (2023)). Under this forcing, the AMOC weakens by up to 12 Sv relative to PI during glacial maxima (the model behaviour to this forcing is described more extensively i and water mass age rises to up to 1000 years in the deep North Atlantic as glacial deep water formation now only occurs in the Southern Ocean. In terms of biogeochemical forcings, we ~~added~~ mimicked a terrestrial carbon sink/source ~~which removes~~by removing/~~emits~~ adding 500 PgC during deglaciation/ice age inception ~~(Jeltsch-Thömmes et al., 2019)~~ (LAND Jeltsch-Thömmes et al., 201 and increased the marine phosphate inventory by 30% during the ~~LGM~~glacial maxima by a globally-uniform supply of phosphate into the surface ocean (PO4). The timeseries of both forcings are proportional to δ^{18}O changes, because we assume that both are lagging behind temperature changes due to continental ice-sheets and changing terrestrial environments. Effectively, our nutrient forcing reduces nutrient limitation globally. Rather than simulating the effects of different nutrient inputs in different regions (e.g. iron in the Southern Ocean, phosphate at shelves), we decided to group all these in one simulation with a global forcing because their net effect, increased export production, would be the same in our model, just in different regions. This is the only forcing that we did not apply to the model without interactive sediments because, while nutrients can be added to the surface ocean periodically, there is no simple way of artificially extracting nutrients from the ocean in return. We also reduced the speed of aerobic organic matter remineralization in the ocean by transitioning between the standard, pre-industrial Bern3D particle profile (Martin scaling) during interglacials and a linear profile in the first 2000 m of the water column (REMI, Fig. S9), following the δD record. ~~Finally~~, since we assume that remineralization changes happened synchronously with temperature change. Next, we reduced the PIC:POC rain ratio by ~~30~~33% in the LGM ~~and~~ (PIPO) and similarly modulated the forcing timeseries with the δD record.

~~We performed one 'base' run with orbital and radiative forcing only, one model run for each individual biogeochemical forcing added to the base forcing and combinations of forcings to study non-linear effects of forcing combinations.~~ In addition we performed one run in which we let the model dynamically ~~adjust~~ apply external alkalinity fluxes (in addition to the constant terrestrial solute supply applied in each simulation, see spin-up methodology) to restore the reconstructed atmospheric CO_2 curve (CO2T). In this simulation, the model evaluates the difference between the simulated and reconstructed CO_2 at each time step and adds or removes the marine alkalinity required to cause the necessary compensatory air-sea carbon flux from the surface ocean. Alkalinity changes, e.g. due to changes in shallow carbonate deposition or terrestrial weathering, are an effective

lever for atmospheric CO_2 change (e.g. Brovkin et al., 2007), and this additional run shows the long-term changes in marine biochemistry if ~~these processes were the dominant drivers~~ this was the dominant driver of glacial-interglacial atmospheric CO_2 change. ~~All simulations were started from the pre-industrial spin-up adjusted for MIS 19 radiative forcing. Climate change occurs only in response to the prescribed radiative forcing and not the simulated atmospheric CO_2 concentrations. To this set of 12 primary simulations, we added sensitivity experiments to assess biases induced by our experiment design: 1) We repeated the simulation ALL, including all forcings, with CO_2-sensitive climate to study the impact of the CO_2-climate feedback. 2) We repeated five simulations (REMI, PIPO, BGC, ALL, CO2T) starting from the transiently achieved MIS 15 Earth system state in their primary versions (215 kyr into the simulation) because they showed initial drifts in DIC and isotopes. We discuss the relevance of initial conditions and imbalances of the geologic carbon cycle at the end of the manuscript.~~

Table 1. Forcing scenarios. Simulations are run in two configurations: the standard setup with interactive sediments and a closed-system setup without sediments (except PO4).

ID	Description	LGM-PI amplitude	Modulating proxy
BASE	orbital changes + radiative effect of greenhouse gasses + ice sheet albedo		CO_2, CH_4, $\delta^{18}O$
SOWI	BASE + Wind stress strength over Southern Ocean (>48 °S)	-40%	δD
KGAS	BASE + gas transfer velocity in Southern Ocean	-40%	δD
AERO	BASE + Radiative forcing from dust particles	-2.5 W/m^2	$\delta^{18}O$
PHYS	BASE + all physical forcings combined		
LAND	BASE + land C storage	-500 PgC	$\delta^{18}O$
REMI	BASE + linear glacial remineralization profile in upper 2000m	linear	δD
PIPO	BASE + PIC:POC changes	-0.33	δD
PO4	BASE + marine PO_4 reservoir	+30%	$\delta^{18}O$
BGC	BASE + all biogeochemical forcings combined		
ALL	BASE + all forcings combined		
CO2T	BASE + restoring reconstructed atm. CO_2 concentrations	-90 ppm	CO_2

For the discussion of the simulations, we quantify the factorial effect of the simulated ~~processes~~ forcings on different carbon cycle metrics. In simulation BASE, only the standard forcing is active (see table 1), hence the factorial effect of the standard forcing ~~forcing~~ is equal to the simulated change:

$$fBASE = \text{BASE}$$

In the simulations that combine the standard forcing with one other forcing, the factorial effect of the additional forcing is the difference between the respective simulation and BASE:

$$fFORC = \text{FORC} - fBASE$$

In simulations PHYS, BGC and ALL several forcings are combined. We use these simulations to determine non-linearities by calculating the difference between the results of these simulations and the linear addition of the individual effects of the active forcings:

$$nlPHY\,nlPHYS = \text{PHYS} - (fBASE + fKGAS + fSOWI + fAERO)$$

$$nlBGC = \text{BGC} - (fBASE + fREMI + fPO4 + fPIPO + fLAND)$$

$$nlADD = \text{ALL} - \text{PHY}\,\text{PHYS} - \text{BGC} + \text{BASE}$$

$$nlTOT = nlPHY + nlBGC + nlADD$$

~~The impacts of ocean-sediment interactions and associated weathering-burial fluxes are quantified as differences between simulations with and without sediment module.~~

3 Results

The general response of marine biogeochemistry to the applied forcings has been tested and described in previous studies (e.g. Tschumi et al., 2008, 2011; Menviel and Joos, 2012; Menviel et al., 2012; Jeltsch-Thömmes et al., 2019; Jeltsch-Thömmes and Joos, , here we therefore just provide a brief summary and focus more extensively on their effect on the sediments. A more detailed analysis of the model behaviour under each forcing is provided in the supplementary material.

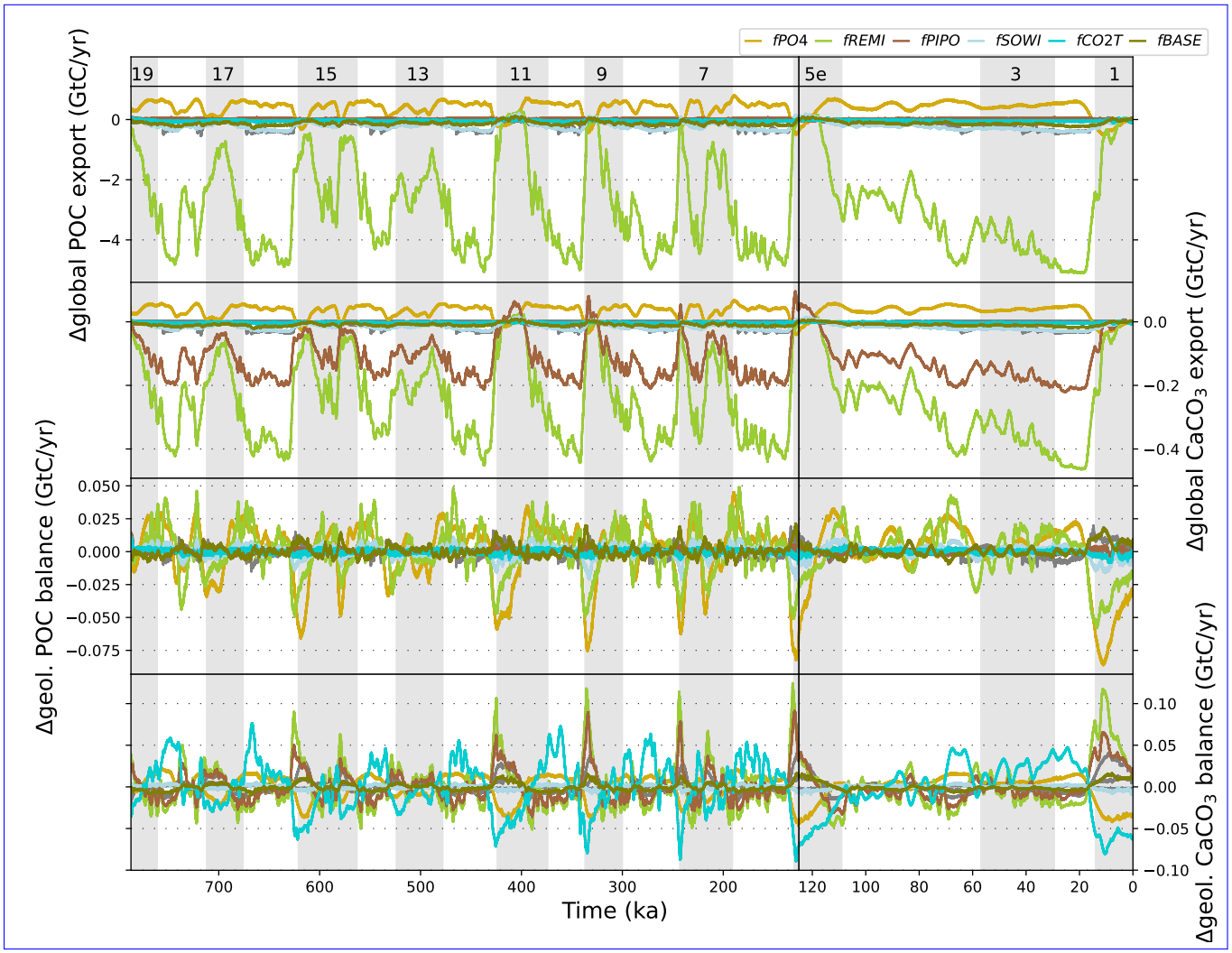

Figure 2. Transient variations of ~~atmospheric CO_2 concentrations as simulated~~ POC and $CaCO_3$ export production and geologic imbalance (i.e. the difference between accumulation of these materials in ~~PHYS, PO4, REMI,~~ marine sediments and ~~LAND~~ the lithosphere minus the constant supply into the surface ocean that mimics terrestrial weathering and ~~reconstructed by Bereiter et al. (2015)~~volcanism in our simulations) due to the applied forcings. Shown ~~is~~ are the ~~deviation from~~ factorial results for each simulation. The results that are explicitly mentioned in the ~~pre-industrial value~~text are shown in colour, the others are shown in gray. Gray shading indicates uneven ~~Marine Isotope stages~~ MIS as indicated at the top of the figure. ~~Dashed lines denote runs without sediment module (not available for PO4)~~See Fig. ~~The same plots~~ S10 for absolute changes in the ~~other~~ simulations~~are shown in S16~~.

~~The simulated amplitudes in CO_2 changes and their timings vary largely between simulations. The effect of dynamic sediments on the simulated atmospheric CO_2 strongly depends on the type of forcing. Interactive sediments have a negligible effect on atmospheric CO_2 changes~~ In our set-up, carbon exchange between the atmosphere, ocean, and sediments reacts to climatic and biogeochemical changes while weathering input fluxes of DIC, alkalinity, and PO_4^{3-} are constant over time. Thus, a carbon flux imbalance arises in our simulations ~~if only physical forcings are considered, but amplify glacial-interglacial~~

~~CO~~in response to the applied forcings (Fig. 2 for factorial results, see Fig. S10 for absolute fluxes). All forcings except $fPO4$ reduce global export production during glacial phases, either due to cooling and expanding sea ice or increased nutrient limitation. In addition to export production, the net C exchange between sediments and the ocean is changed by the applied forcings via changing benthic seawater composition, either through circulation, solubility, or biogeochemical changes. Cooling reduces global sediment accumulation rates of $CaCO_3$ and POC during glacial phases due to the reductions in export production ($fBASE$). In consequence, sequestration of $CaCO_3$ and POC from the reactive sediments (i.e. sedimentary burial) is also reduced in response to these forcings, since it is governed by the sedimentary mass accumulation rate. Instead, reduced marine O_2~~change under biochemical forcings .~~ , due to the deepened remineralization ($fREMI$), increases the preservation of sedimentary POC during glacials. Hence, POC accumulation is higher during glacial than interglacial phases, while the opposite temporal change occurs for $CaCO_3$ accumulation due to reduced $CaCO_3$ export production. Reduced nutrient limitation during glacial phases ($fPO4$) causes more, rather than less, export production during glacial phases. Increased ALK supply in simulation CO2T causes larger sedimentary $CaCO_3$ accumulation during glacial phases and dissolution events during deglaciations.

~~The processes that cause the different model responses to the prescribed forcings have largely been described in other studies (e.g. Tschumi et al., 2008, 2011; Menviel and Joos, 2012; Menviel et al., 2012; Jeltsch-Thömmes et al., 2019; Jeltsch-Thömmes and Joos, ,~~How do the simulated sedimentary changes in our factorial setup compare in magnitude and sign with carbon cycle proxy records?

We focus first on changes in the carbon stored as sedimentary organic and inorganic matter and changes in the benthic carbonate system, then DIC and atmospheric CO_2, before discussing the simulated proxy signals in CO_3^{2-} and ~~are summarised in the SI to our manuscript, including a detailed analysis of the sedimentary changes simulated under the various forcings we tested~~$\delta^{13}C$. Individual proxy records were selected for their resolution or length. This is not an attempt at a comprehensive compilation of proxy records, nor an attempt to understand individual records in detail. Rather we aim to understand why the tested forcings do or do not reproduce prominent spatial or temporal patterns in the proxy records. It is also important to note that our simulations are designed to constrain the potential and plausibility of major contributions of the tested ~~processes~~ forcings to the observed glacial-interglacial atmospheric CO_2 changes, rather than reproducing a full, realistic scenario. ~~In their design, we prescribed the amplitudes and temporal evolution of each simulated process in a simplified way, while their true relative importance for glacial-interglacial carbon cycle changes remains still unknown and might have varied spatially and temporarily.~~ We therefore do not expect that any single simulation presented in our study captures all features of the reconstructed carbon cycle changes over glacial-interglacial cycles. Instead, we investigate the isolated ~~processes~~forcings, which occurred simultaneously in reality, and quantify their effects during eight consecutive glacial cycles. Comparing our results to proxy records, we can identify the dominant processes behind specific patterns in the reconstructions and the remaining challenges in reconciling the many carbon cycle reconstructions that are now available.

4 ~~Comparison with carbon cycle reconstructions~~

~~Summary Model-Data comparison. Shown are the factorial effects of the tested processes and their non-linearites in comparison with reconstructed LGM - Holocene differences in various proxy systems. The direction of each arrow indicates whether a difference is positive (pointing upwards, teal-coloured) or negative (pointing downwards, brown-coloured). The width of the arrows shows the size of the difference relative to the reconstruction in the uppermost row "Data". For POM export and global preformed nutrient concentrations, only qualitative reconstructions exist. Hence, the arrows showing simulated effects are normed by the biggest effect by any simulated process.~~

3.1 Sedimentary burial and CO_3^{2-} concentrations

~~Table 4 provides a summary of the data-consistency of~~ Reconstructions of global POC burial flux changes over the last glacial cycle (Cartapanis et al., 2016) indicate that POC burial was smallest during interglacials, and gradually rose during glacial phases until it peaked during the LGM. $fSOWI$, $fREMI$ and $fPO4$ are the only effects which produce higher POC burial fluxes during glacial maxima than during interglacials (Fig. 2), and the ~~factorial effects of each process we tested for selected carbon cycle proxies, and~~ latter two are the only ones strong enough to overprint the opposite effect due to cooling ($fBASE$, Fig. S10). However, the ~~non-linearities that arise when they are combined. The first row shows the reconstructed direction of LGM- Holocene differences,~~ simulated increase in POC burial already occurs during the glacial inception, such that the highest burial rates persist throughout most of the glacial phase while in the reconstructions they remain close to the interglacial value through MIS4. Reconstructions of global $CaCO_3$ burial changes over the last glacial cycle (Cartapanis et al., 2018) show that burial rates decreased in most ocean basins during glacial inception, while they increased in the Southern Ocean, resulting in only minor glacial-interglacial changes in the global average. Physical forcings (e.g. $fSOWI$ in Fig. 2) do not affect $CaCO_3$ burial rates during glacial inception, consistent with the reconstruction, while $fPO4$ and $fCO2T$ produce burial increases and $fPIPO$ and ~~the next lines show the direction and relative size (compared to the proxy signal) of changes induced by the various tested processes. The last three rows show the direction and relative size of non-linearities caused by three different combinations of the processes above. For many of the considered proxies, these non-linearities are larger than without interactive sediments (not shown) but still small compared to the effect of individual processes, especially when combining only physical processes. For some proxies, the non-linearities are not negligible but still smaller than the biggest effect of an individual process. Hence, in most cases, proxy changes provide a first-order constraint on the plausibility of large changes in individual processes. $fBASE$, the effect of temperature changes due to orbital, albedo and greenhouse gas changes, moves almost all proxy systems in the reconstructed direction (the directions of the arrows match), but almost never to the reconstructed extent (the widths of the arrows do not match). The only exception is strongly reduced export production in the polar Southern Oceanat the LGM, which in our model is predominantly driven by surface cooling and sea ice expansion regardless of which other processes were also changed. The mismatches in amplitudes of $fBASE$ and reconstructed changes show that other processes must have affected the glacial carbon cycle, at least in our model. In the following sections, we expand on these model-data comparisons and discuss atmospheric CO_2, export production, the biological pump, sedimentary fluxes and carbon isotopes in more detail (see also section numbers at the bottom of table 4~~ $fREMI$ produce decreases between MIS5 and MIS3. However, the physical forcings fail to decrease $CaCO_3$ burial rates during MIS3 und MIS2. $fREMI$ and

fPIPO decrease $CaCO_3$ burial during MIS3 and MIS2 but cause much larger burial events in MIS1 than reconstructed (Fig. 2, see also Figs S2, S4, S5, S6, S7).

3.2 ~~Atmospheric CO_2~~

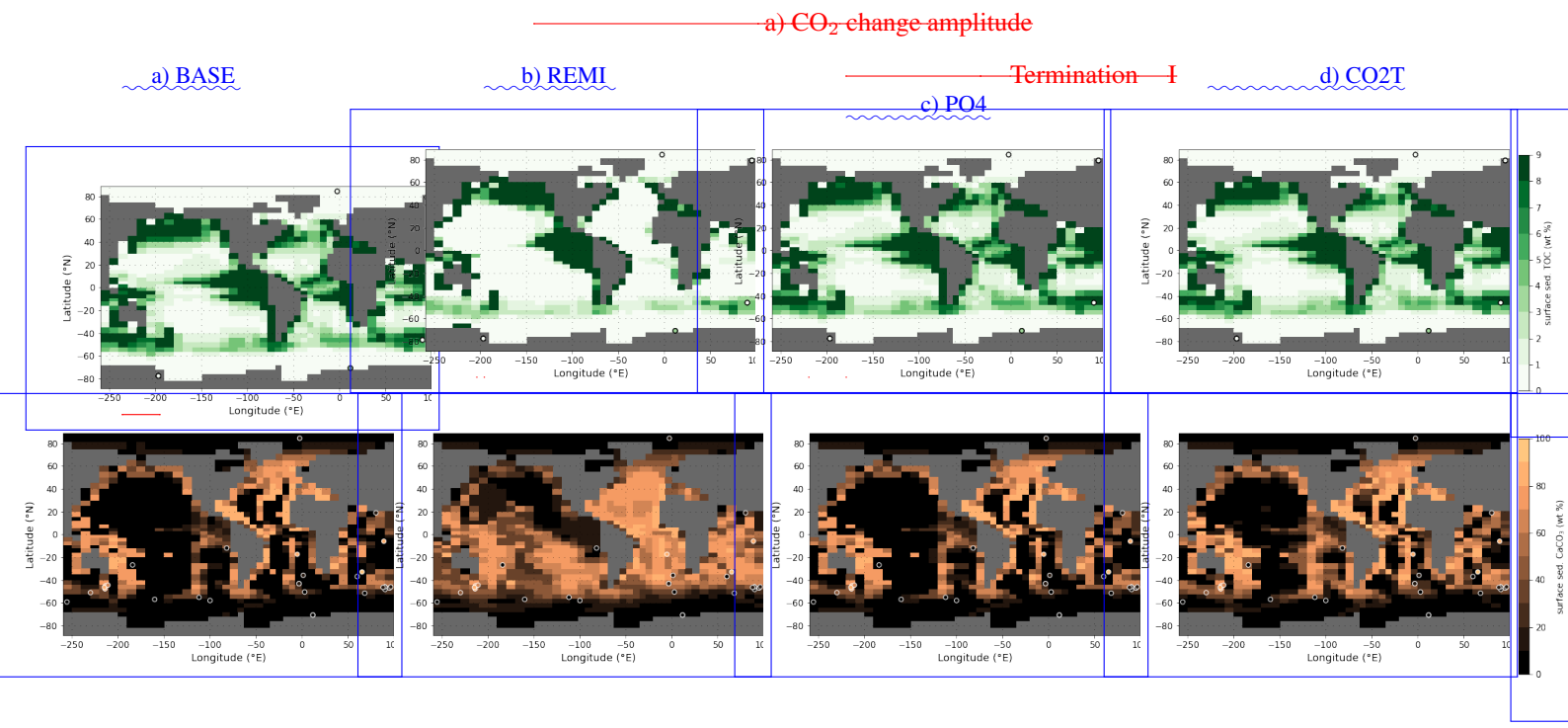

Figure 3. ~~Atmospheric CO_2 changes across deglaciations. a~~Sedimentary POC and $CaCO_3$ fractions during LGM (Cartapanis et al., 2016; Wood et al., 2023) as reconstructed (circles) ~~shows the factorial contributions to the mean glacial-interglacial CO_2 amplitude over the last five glacial terminations~~and in simulations PHYS, ~~as well as the range between their minimum~~ REMI, PO4 and ~~maximum~~CO2T (underlying maps). ~~Light colors indicate results without interactive sediments, full colors indicate results with interactive sediments~~Shown are only data points that fall into the local benthic grid box of the model. The root mean ~~, minimum~~ square errors of simulated and ~~maximum amplitudes over the last five deglaciations in the ice core record (Bereiter et al., 2015)~~ reconstructed values are ~~shown by the black~~ (from left to right): 7.4 %, 3.3 %, 7.4 % and ~~gray horizontal lines. b~~6.4 % for POC (top row) and 33.6 %, 31.5 %, 33.3 % and 34.4 % for $CaCO_3$ (bottom row)~~shows selected factors transiently over the last two terminations~~.

~~By design, CO_2 restoring causes marine carbon uptake and release that shape atmospheric CO_2 in line with observations~~ Most forcings increase the POC content of surface sediments (top 10 cm) during the LGM (Fig. ~~6, S6 sum of fBASE and fCO2T, S16), so here we focus on the CO_2 changes simulated by the other forcings. PO4, REMI and PIPO produce the most consistent CO_2 difference between the LGM and PI with regard to the reconstructions (Fig. 6a). The timing of the lowest CO_2 values occurs during the coldest interval of glacial cycles, the glacial maxima, in all simulations except LAND~~3 top row), the exception being *fREMI*, which decreases POC outside the East Pacific. However, too few reconstructions exist for depths that are consistent with our model bathymetry for a quantitative model-data comparison. For $CaCO_3$, a few more data

points fall within our benthic ocean grid cells. The cooling-related changes ($fBASE$) included in all simulations reproduce a data-consistent carbonate compensation depth (CCD) in most of the Southern Hemisphere extra-tropics but a too high CCD in the tropical South Atlantic and Indian Ocean and a too low CCD off Peru (Fig. 3 bottom row). REMI better captures these tropical CCD changes but produces a too low extra-tropical CCD. These model-data differences indicate that different processes might explain the LGM sedimentary composition in different basins, which is not captured by our globally uniform forcings.

The model has been tuned to the pre-industrial $CaCO_3$ distribution. However, in ~~all simulations CO_2 keeps increasing throughout interglacials when temperature is almost constant. In simulations PO4 and CO2T, this is a consequence of the proxy records used to scale the respective forcing - benthic $\delta^{18}O$ for PO4 and CO_2 for CO2T, which are not constant during interglacials (Fig. **??**)~~ our study late Holocene $CaCO_3$ contents are the result of almost 800 kyr of transient simulation, which result in imbalances of the geologic carbon cycle at the simulation end even though the forcing is that of the Holocene (Table S2). Differences between the dynamically-achieved and observed pre-industrial sedimentary composition add context to the size of the simulated sedimentary fluxes and memory effects. The dynamically-evolved sedimentary POC content is similar across all simulations, while the $CaCO_3$ content exhibits large-scale differences (Fig. S11, S12). Simulations with small sediment perturbations during the glacial cycle (e.g. SOWI, AERO and LAND, Fig. S12) result in $CaCO_3$ contents that are similar to Holocene estimates. In simulations ~~AERO,~~ REMI and PIPO, ~~CO_2 lags the forcing by several thousand years during deglaciations and throughout interglacials (Fig. **??** and **??**). In AERO,~~ the ~~lag is caused by the hysteresis behaviour of AMOC and exists in simulations with and without interactive sediments.In REMIand PIPO, the time lags are caused by weathering-burial imbalances, particularly a large build-up of alkalinity and DIC during~~ large deglacial $CaCO_3$ burial event results in higher sedimentary $CaCO_3$ contents in the late Holocene than measured. Simulation CO2T, on the other hand, has less sedimentary $CaCO_3$ content during the late Holocene than measured. This is the ~~glacial phase which is only gradually reduced by enhanced CaCO~~result of strong dissolution due to forced alkalinity removal from the open ocean during deglaciations, mimicking e.g. coral reef building. It is therefore less likely that sedimentary $CaCO_3$ ~~burial during deglaciation (Fig~~was perturbed to the extent simulated in REMI, PIPO and CO2T. ~~S18). The different correlations between temperature and CO_2 in glacials and interglacials is also a feature of the ice core records (Brovkin et al., 2016), though the timing of peak interglacial CO_2 concentrations and transient features of the atmospheric CO_2 increase during deglaciations in the records is not necessarily reproduced in our idealised simulations with simplified forcings (Fig 6b, right panel). In most simulations, the weathering-burial disequilibrium, which builds up over the glacial phase, amplifies the glacial CO_2 drawdown.~~

~~Difference of the glacial-interglacial atmospheric CO_2 amplitude before and after the MBT in our simulations compared to that in the reconstructed CO_2 record (Bereiter et al., 2015). For the results of the simulations without interactive sediments see Fig. S19~~

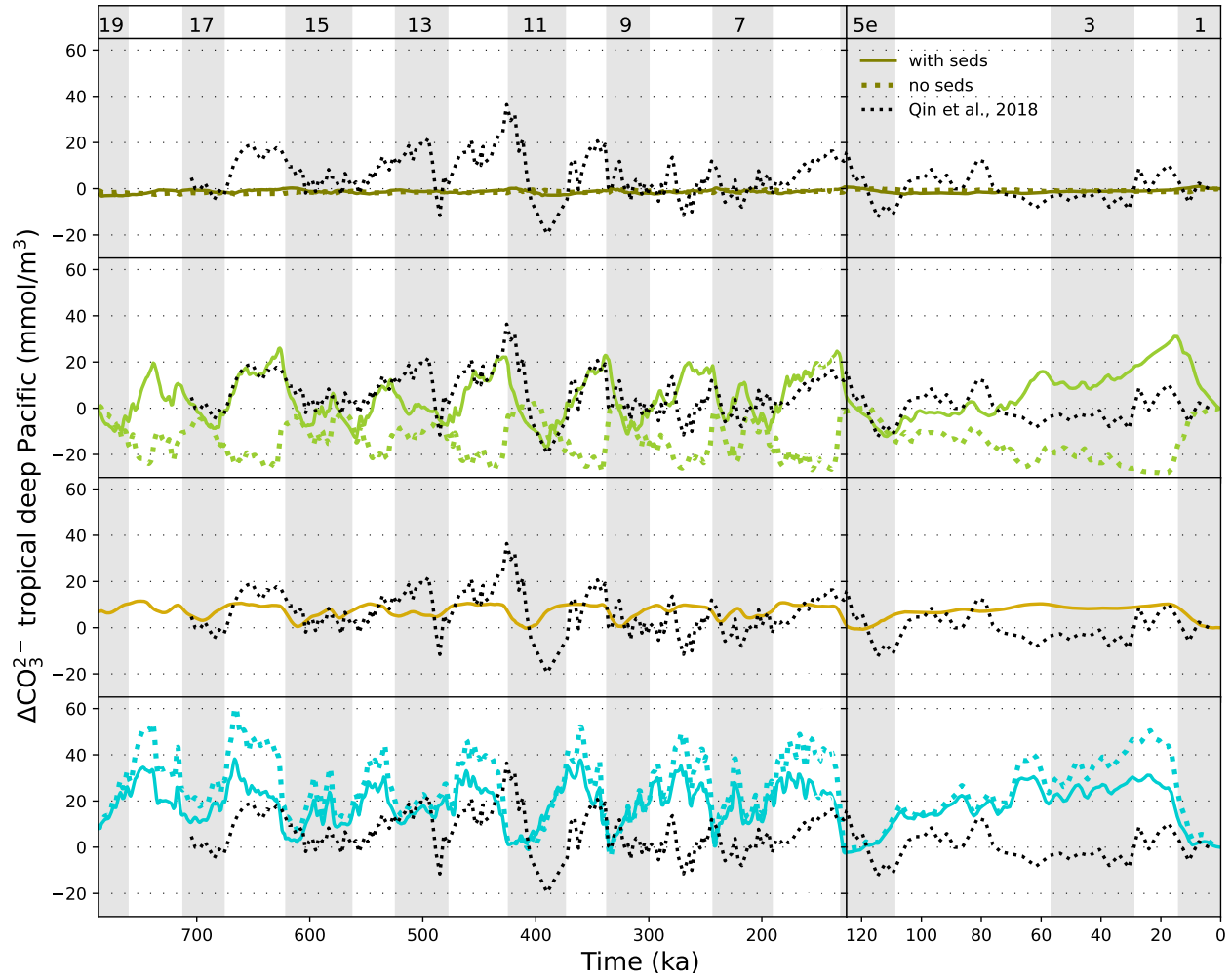

Figure 4. Evolution of CO_3^{2-} in the tropical deep Pacific as simulated for $fBASE$, $fREMI$, $fPO4$ and $fCO2T$ and reconstructed by Qin et al. (2018). The results of the other forcings are shown in Fig. S13.

~~Burial-weathering imbalances also affect the difference between the~~ Next, we address CO_3^{2-} changes. Kerr et al. (2017) found a repeated pattern of low benthic CO_3^{2-} in the tropical Pacific and Indian Ocean during interglacials and high CO_3^{2-} during glacials (difference of 20-55 mmol/m^3) throughout the last 500 kyrs. Qin et al. (2018) found that the same pattern extended over the last 700 kyrs. Physical forcings ($fBASE$, $fKGAS$, $fSOWI$, $fAERO$, $fPHYS$) and $fPO4$ have little effect on deep Pacific CO_3^{2-} over glacial cycles (Fig. 4, S13). Under the biogeochemical forcings ($fREMI$,$fPO4$, $fPIPO$,

$fLAND$), the simulated glacial-interglacial CO_3^{2-} difference ranges from a few mmol/m^3 to 50 mmol/m^3, and is caused by invasion of CO_2 ~~amplitudes of the last five glacial terminations compared to the glacial cycles before. Since maximum temperatures of interglacials were larger during the last four interglacials, the solubility of CO_2 in seawater was lower, contributing to higher atmospheric CO_2 levels. This creates a small direct response to the forced interglacial warming after the MBT under the standard forcing (fBASE, ~5 ppm, Fig. **??**) . Wind-driven circulation~~ into the ocean, ALK redistributions within the ocean, and weathering-burial imbalances due to changes of the carbonate export flux and carbonate compensation (Broecker and Peng, 1987, , Fig. 4 and S13). $fREMI$ and $fCO2T$ cause the largest CO_3^{2-} changes in the deep equatorial Pacific. For the last glacial cycle, these simulated changes are larger than those reconstructed, suggesting that the forcings cause too large ALK re-distributions within the ocean or carbonate compensation during the last glacial cycle. Interestingly, however, during MIS13-MIS11 and the Mid-Brunhes transition, reconstructed CO_3^{2-} changes in the deep equatorial Pacific were larger than during the last glacial cycle (Qin et al., 2018, , Fig. 4). $fCO2T$ and $fREMI$, which produced larger-than-reconstructed CO_3^{2-} changes over the last glacial cycle produced CO_3^{2-} changes more similar to those reconstructed for MIS13-MIS11. The variability of CO_3^{2-} amplitudes between glacial cycles in the record is not reproduced by any of our forcings, but

While the reconstructed deep ocean CO_3^{2-} reservoir in the Pacific was relatively stable over the last deglaciation, a large CO_3^{2-} increase was reconstructed for the deep Atlantic (Qin et al., 2018; Yu et al., 2019). The different sensitivities of deep ocean CO_3^{2-} in the two basins is also apparent in all of our simulations (see examples in Fig. S14 and S15) and is the result of larger circulation and productivity changes in the ~~Southern Ocean (SOWI) have a stronger effect, because in colder interglacials, the deep Pacific remains more isolated than during warm interglacials, preventing the release of an additional 5 ppm in the earlier glacial cycles. Reduced remineralization rates (REMI) and~~ Atlantic than Pacific. However, circulation changes produce lower CO_3^{2-} in the deep sub-polar North Atlantic during the LGM, while reconstructions suggest higher CO_3^{2-} (Yu et al., 2019) . Higher deep Atlantic CO_3^{2-} at the LGM requires increased nutrient supply ~~during colder interglacials have the strongest individual effect on carbon storage differences across glacial cycles, each reducing the glacial-interglacial CO_2 difference by 15 ppm in the early, colder glacial cycles. As already noted in the discussion of absolute CO_2 concentrations, weathering-burial imbalances play a minor role for the simulated physical effects on the glacial-interglacial~~ ($fPO4$), deeper remineralization ($fREMI$) or a net alkalinity input ($fCO2T$). These patterns appear with and without dynamic sediments in our simulations. Sediments mostly affect the amplitude and temporal evolution of deep CO_3^{2-} changes, not their spatial pattern (not shown).

3.2 Atmospheric CO_2

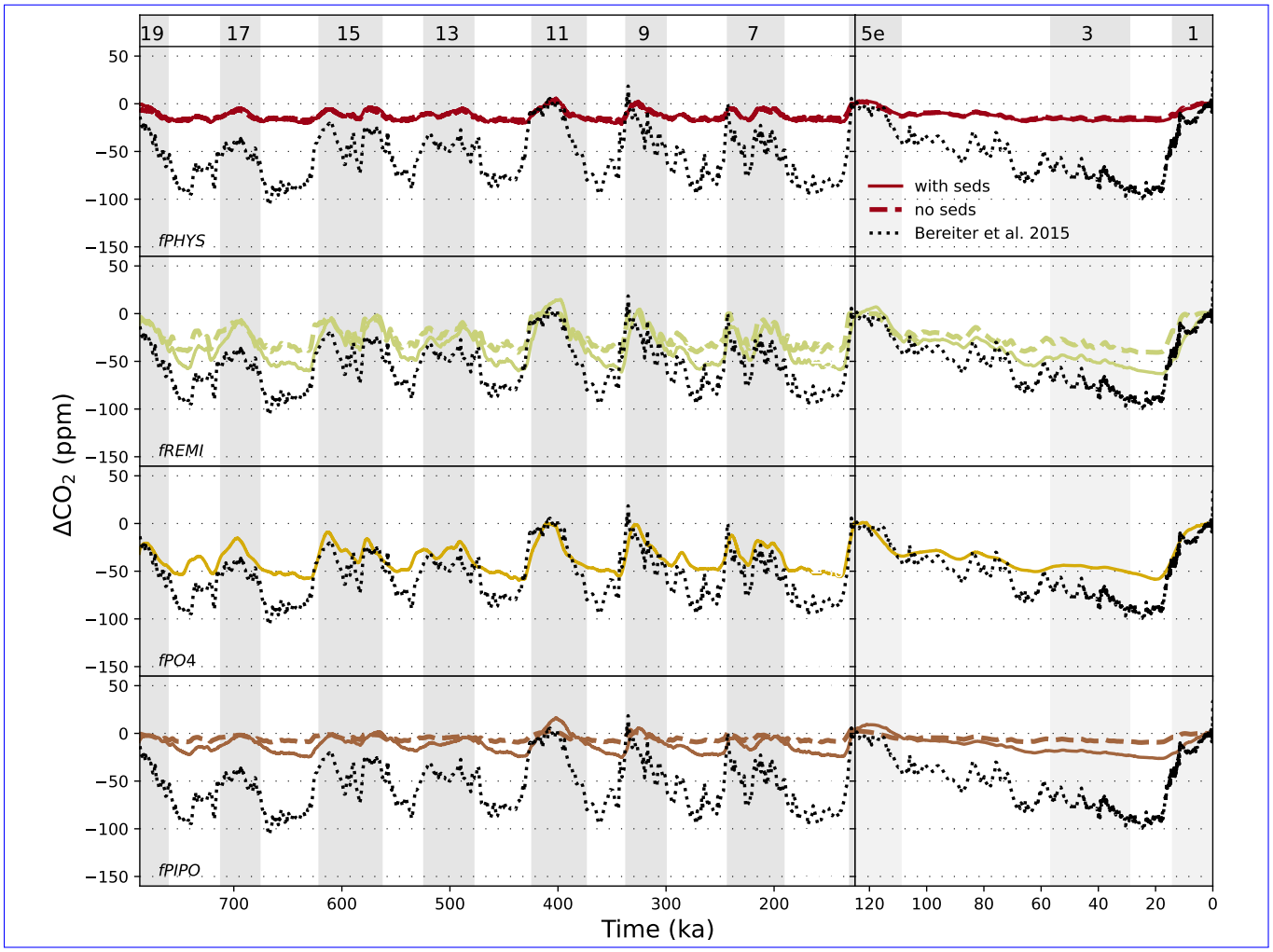

Figure 5. Transient variations of atmospheric CO_2 due to effects $fPHYS$, $fPO4$, $fREMI$, and $fPIPO$ and reconstructed by Bereiter et al. (2015). Shown is the deviation from the pre-industrial value. Gray shading indicates uneven MIS as indicated at the top of the figure. Dashed lines denote runs without sediment module (not available for PO4). The same plots for the other simulations are shown in S16.

Interactive sediments have a negligible effect on atmospheric CO_2 ~~amplitude but amplify the biochemical effects. In fact, only by including interactive sediments does our model simulate a shift in the MBT~~ changes in our simulations with only physical forcings but largely alter glacial-interglacial CO_2 ~~amplitude comparable to the observations~~ change under biogeochemical forcings (Fig. ~~??). In most simulations ,~~ 5). Marine CO_2 uptake and reduced export production in the simulations with physical forcings causes a net dissolution/reduced deposition of sedimentary $CaCO_3$ ~~deposition is reduced~~ during glacials and marine alkalinity and DIC build up as a consequence. A large fraction of the glacial DIC pool is eventually incorporated into $CaCO_3$ and deposited during deglaciations ~~, simultaneously drawing down alkalinity and thus releasing CO_2 to the atmosphere. One effect of interactive sediments is thus the larger of~~ with little effect on outgassing. In simulations with biogeochemcial forcings,

the larger $CaCO_3$ ~~burial and alkalinity draw-down during bigger temperature rises at the onset of warm interglacials, which in our simulations is amplified by changes in PIC:POC (PIPO) and the remineralization profile (REMI)~~perturbations also have a larger effect on sea-air gas exchange. Another effect ~~responsible for the larger CO_2 amplitude changes under biochemical forcings~~ is the reduction of sedimentary organic carbon burial rates during interglacials ~~under~~ in response to increased nutrient supply (~~PO4~~$fPO4$) or a flattened remineralization profile (~~REMI~~$fREMI$) during glacial phases. During deglaciations, sedimentary POC deposited during glacials is remineralized, which raises ~~atmospheric CO_2 in addition to the previously described alkalinity changes. The larger the temperature rise during deglaciation, the more POC is remineralized.~~

~~In summary, most of the simulated processes cause atmospheric CO_2 increases during deglaciations, and the good matches with various features of reconstructed glacial-interglacial CO_2 changes are produced by biochemical changes. Variations of the remineralization profile (simulation REMI) cause the largest deglacial CO_2 change but at a slower pace than reconstructed. Nutrient supply changes in simulation PO4 cause the fastest deglacial CO_2 rise but with a lower amplitude than REMI. All features of the reconstructed CO_2 curve can artifically be achieved by changing external alkalinity fluxes (CO2T). However, the~~ DIC and further reduces ALK, both contributing to enhanced CO_2 ~~changes in these simulations are caused by different mechanisms which also leave traces in the proxy record~~outgassing. We explore the forcing-specific differences in more detail by focusing exemplarily on the last deglaciation.

3.3 ~~Marine DIC and the surface carbonate system~~

~~a) DIC~~ a) CO_2 change b) temporal pattern c) Timing

amplitude

~~Termination I~~ ~~Termination II~~ compared to

CO_2 change forcing

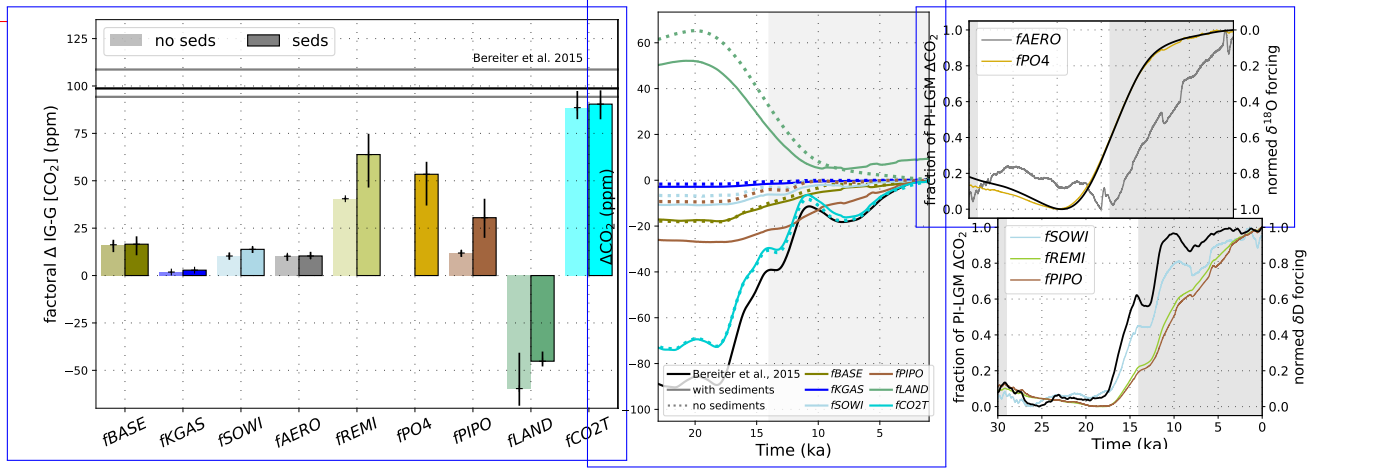

Figure 6. ~~Factorial DIC concentration~~ Effects of individual forcings on deglacial atmospheric CO_2 changes ~~for each process across deglaciations~~compared to reconstructions. ~~In~~ a) ~~,~~shows the factorial ~~contribution of each process~~ contributions to the mean glacial-interglacial CO_2 amplitude over the last five glacial terminations (excluding terminations before the Mid-Brunhes transition), as well as the range between their minimum and maximum. Light ~~colours show the~~ colors indicate results without ~~dynamic~~ interactive sediments, ~~and~~ full ~~colours show the contributions~~ colors indicate results with ~~dynamic~~ interactive sediments. ~~In b)~~The mean, minimum and maximum amplitudes over the ~~absolute temporal DIC evolution across two terminations is~~ last five deglaciations in the ice core record (Bereiter et al., 2015) are shown ~~for selected simulations with~~ by the black and ~~without interactive sediments~~gray horizontal lines. b) shows the factors discussed in the text transiently over the last termination. c) shows time lags between the factors and the respective forcing timeseries.

~~The simulated~~ By design, CO_2 ~~changes are the result of changes in carbon uptake in the surface ocean. All forcings strongly affect air-sea carbon fluxes in the Southern Ocean, by changing SST, sea ice, circulation, producitivity and/or the carbonate system in the surface ocean. It has long been recognised that the Southern Ocean played an important role in glacial-interglacial changes in the partitioning of carbon between atmosphere and ocean (Wenk and Siegenthaler, 1985; Fischer et al., 2010). In addition to changes in the Southern Ocean, in our simulations surface carbonate system shifts in the non-polar oceans are required to achieve glacial-interglacial~~ restoring causes marine carbon uptake that fills the gap between dynamic atmospheric CO_2 changes in BASE and reconstructions (Fig. 6, S6, S16), so here we focus on the other forcings. Biogeochemical forcings produce the largest CO_2 differences ~~that are consistent with reconstructions. In simulations REMI, PO4 and CO2T, which produce the most data-consistent atmospheric CO~~between the LGM and PI with regard to the reconstructions (Fig. 5, 6a). In these simulations, the weathering-burial disequilibrium, which builds up over the glacial phase, amplifies the deglacial CO_2 ~~changes, such carbonate shifts occur: Surface ocean pH increases towards the glacial maximum, which is consistent with reconstructions (Fig. S18, Hönisch and Hemming, 2005; Shao et al., 2019). It is noteworthy that in simulation REMI with interactive sediments, surface ocean pH changes align closely with those in simulation CO2T, in which the model was forced~~

~~to reproduce reconstructed atmospheric~~ rise, particularly in $fREMI$ and $fPIPO$. In both cases, sedimentary accumulation of $CaCO_3$ spikes during deglaciation, due to increased $CaCO_3$ export as the forcings wane (Fig. 2). The corresponding ALK reduction expels more CO_2 ~~changes. This alignment is visible throughout the glaciation up until the onset of the deglaciation, where pH changes in REMI lack behind those in CO2T. During~~ from the surface ocean into the atmosphere. In the case of $fREMI$, this is further enhanced by a reduction in sedimentary POC accumulation during the deglaciation, ~~pH changes in simulation PO4 show the same speed as in CO2T, even though the amplitude is lower. This mirrors our results from the comparison of the simulated~~ which reduces the C loss to the sediments. Under both forcings, the sedimentary processes that amplify the deglacial CO_2 rise also reduce its speed and smooth out transient features of the δD record which are translated into transient atmospheric CO_2 ~~curves, which showed that REMI produced the most data-consistent~~ changes in simulations without interactive sediments (Fig 6). These time lags are caused by the strengthened export production, which counteracts C degassing, and a large build-up of alkalinity and DIC during the glacial phase (amplified by interactive sediments, Fig. S17) which is only gradually reduced by enhanced $CaCO_3$ burial during deglaciations (Fig. S18). If instead export production and sedimentary C accumulation decrease during the deglaciations due to increased nutrient limitation ($fPO4$), the C previously incorporated into biogenic matter is outgassed from the surface ocean and no lag between CO_2 ~~changes during the glaciation but failed to reproduce the quick CO~~rise and the forcing emerges. Weathering-burial imbalances have a smaller effect on circulation-driven deglacial CO_2 ~~release during the deglaciation. The spatial patterns of marine carbon uptake and release in our simulations are thus driven by combinations of physical and chemical processes. The net carbon fluxes into the ocean during glaciation and out of the ocean during deglaciation are roughly of equal magnitude in the Southern Ocean (>40 °C S) as in the rest of~~ degassing ($fSOWI$, $fAERO$), regarding both amplitude and timing. However, CO_2 also lags temperature in $fAERO$ (with and without interactive sediments), due to the hysteresis of the ~~ocean combined, but of opposite sign, under most forcings and with and without interactive sediments~~ AMOC. Enhanced Southern Ocean wind stress ($fSOWI$) is the only forcing in our simulation set that is able to create fast, transient CO_2 releases despite weathering-burial imbalances. In all simulations except LAND, the lowest CO_2 values occur during the coldest interval of glacial cycles, the glacial maxima (Fig. 5, S16). In all simulations in which the deglacial CO_2 rise lags that of temperature, CO_2 keeps rising throughout the Holocene. Only by including interactive sediments does our model simulate a shift in the MBT glacial-interglacial CO_2 amplitude comparable to the observations (Fig. ~~??~~S19, S20).

3.3 Marine DIC and the surface carbonate system

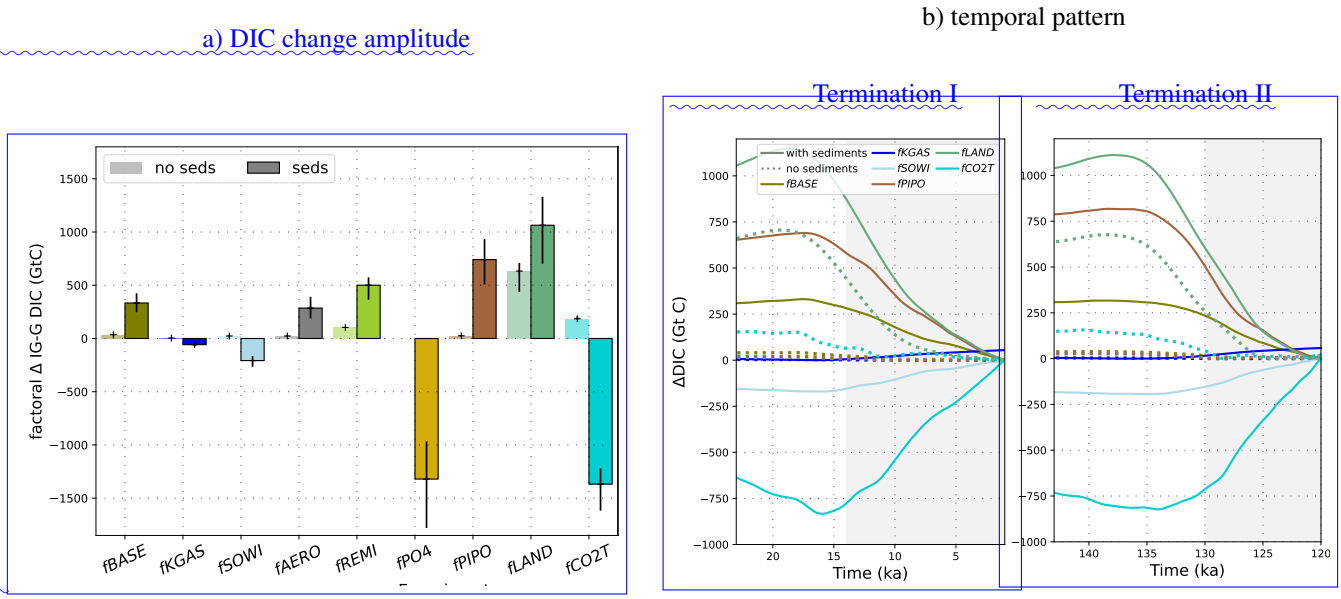

Figure 7. Factorial DIC concentration changes for each forcing over glacial cycles, from the highest or lowest DIC value during the glacial cycle, depending on which occurs earlier, to the other extreme. In a) factorial contribution of each forcing to the mean DIC amplitude over the last five glacial cycles, as well as the range between their minimum and maximum. Light colours show the without dynamic sediments, and full colours show the contributions with dynamic sediments. In b) the factorial contribution of selected forcings to the temporal DIC evolutions across two terminations is shown with and without interactive sediments.

Due to interactive sediments in our simulations, increased uptake or release of carbon in the surface ocean does not linearly correlate with DIC changes because marine carbon storage is also affected by changes in the deposition and dissolution fluxes of particulate carbon at the ocean-sediment interface. Interactive sediments affect marine carbon, alkalinity, and nutrient concentrations in two important ways: Firstly, sediments form a large ~~transient~~ dynamic reservoir which can store and release large amounts of carbon and nutrients for hundreds to tens of thousands of years. Secondly, sedimentary mass accumulation, dissolution, and remineralization rates control ~~lithological~~ sedimentary burial, the only permanent sink for carbon and nutrients in our simulations and the only mechanism ~~to cause imbalances between supply from weathering and sedimentary burial~~by which environmental change can create imbalances with the prescribed constant solute flux from land. Fluxes into and out of the sediments respond to environmental change, in some cases on the timescale of water mass replacement or regional productivity changes. ~~Consequently, the simulated DIC change is much larger than the simulated change in atmospheric carbon under physical and biochemical forcings. In our simulations the ocean inventory changed by 200-1400 GtC and the atmospheric inventory by 1-150 GtC over the last deglaciation. DIC changes differ by a factor of up to 28 between simulations with and without interactive sediments, while~~ Carbon fluxes from the sediments directly affect the ocean, but not the atmosphere, which causes different amplitudes in the simulated DIC and atmospheric CO_2 ~~changes in the atmosphere are maximally four times larger when interactive sediments are considered (Figs 7, S3,~~ changes and different timings of carbon accumulation in ocean and atmosphere. With interactive sediments, $fBASE$, $fAERO$, $fREMI$, $fPIPO$ and $fLAND$ produce highest DIC during

glacial maxima and lowest DIC during interglacials as altered air-sea gas exchange and sediment accumulation result in a net influx of carbon into the ocean during glacial phases. However, while altered air-sea gas exchange still draws down atmospheric CO_2 under $fKGAS$, $fSOWI$ and $fPO4$, larger changes to the sediment fluxes remove carbon from the glacial ocean (Fig. 2) and store excess carbon as carbonate and organic carbon in sediments instead of as DIC in the ocean. Consequently, the lowest DIC occurs during glacial maxima rather than during interglacials under these effects (Fig. S4, S5~~, S7, S23, S25, ??~~). $fCO2T$ alters sedimentary carbonate preservation such that DIC extremes do not occur at the same time as atmospheric CO_2 extremes, but in between, i.e. the DIC maximum occurs during glaciation and the minimum during deglaciation (Fig. S6). Furthermore, the onset of the deglacial CO_2 rise in simulations with sediments does not always coincide with the onset of the deglacial DIC change, as is the case in simulations without sediments. This is simulated e.g. for terminations I and II ~~in LAND and CO2T~~ due to $fLAND$ and $fCO2T$ (Fig. S22), and for terminations I, II, III and IV ~~in PO4 and ALL~~ due to $fPO4$ and $fALL$ (Fig. S21). ~~This suggests that reconstructed DIC changes, e.g., based on radiocarbon (Sarnthein et al., 2013) may be uncertain and do not necessarily imply a comparable CO_2 drawdown from the atmosphere. In simulations PO4 and CO2T, interactive sediments further produces the counter-intuitive result of reduced marine carbon storage during glacial maxima, because in these simulations excess carbon is stored in sediments as carbonate and organic carbon. In the following, we constrain these processesfurther with additional proxy data.~~

3.4 ~~Export production changes during glacial-interglacial cycles~~

~~Export of biogenic matter from the surface ocean exerts a strong control on the carbonate system in the surface ocean and thus the sign and magnitude of the CO_2 flux across the sea-air interface (Volk and Hoffert, 1985). Decreasing temperatures, sea ice expansion, and curtailed nutrient supply due to a weakened circulation during glacials reduce export production in simulations with only physical forcings. In simulation PO4, the prescribed enhanced external nutrient input during glacial phases increases export production, while in simulation REMI, slowing remineralization rates in the surface ocean has the opposite effect by reducing the amount of nutrients in the surface. The lower PIC:POC ratio of simulation PIPO reduces export production of $CaCO_3$.~~

~~a) $fBASE$ $fPHYS$ $fREMI$ $fPIPO$ $fPO4$ $fCO2T$ between the LGM and the PI in simulations BASE, PHYS, REMI, PIPO, PO4 and CO2T with interactive sediments. The filled triangles show the reconstructed sign and qualitative magnitude of change based on Kohfeld et al. (2005): black triangles show reconstructed decreases, white triangles show increases. Big triangles show big reconstructed changes, small triangles show small reconstructed changes.~~

~~Reviewing changes in various productivity proxies, Kohfeld et al. (2005) reconstructed spatial patterns of productivity changes between the Holocene and the LGM. Specifically, they found lower productivity in the polar oceans and increased productivity in the subpolar Southern Ocean and the tropical and subtropical Atlantic during the LGM. The direction of productivity changes in the Southern Ocean and upwelling areas in our simulations align with the reconstructions in most simulations, particularly with additional cooling and circulation slowdown with the physical forcings (Fig **??**). These changes induced by the physical forcing reduce productivity in the polar oceans and, to a lesser extent increase productivity elsewhere as nutrients are redistributed. AMOC weakening reduces productivity in the North Atlantic. Consequently, simulations that~~

contain a strong AMOC weakening (AERO, PHYS) fail to reproduce the reconstructed strong productivity increases in the tropical and North Atlantic. Such a North Atlantic productivity increase is only simulated when AMOC changes are small or external nutrient supply into the North Atlantic is enhanced during glacials (simulation PO4). Increased external nutrient input during glacial phases causes large productivity increases in most of the extrapolar ocean, which is consistent with the reconstructions. The comparison of magnitudes of productivity change between our simulations and reconstructions is more uncertain than comparing the sign of change. Therefore, it must be noted that the standard forcing in BASE also produces small productivity increases in most extrapolar oceans. Yet, the resulting changes in surface ocean carbonate chemistry are far to small to cause data-consistent Across the tested processes, the corresponding ocean DIC inventory changes from glacial to interglacial are -1800–1400 GtC (Fig. 7) while the atmospheric inventory changes by -170–190 GtC (Fig. 6) over the the same period. For individual proceses, DIC changes differ by a factor of up to 28 between simulations with and without interactive sediments, while CO_2 changes , which are better reproduced in simulation PO4. Deepening the mean remineralization depth in simulation REMI produces the biggest mismatch between simulations and reconstructions of export production, although it captures the changes in atmospheric CO_2 well (see previous section). This mismatch indicates that the process behind the simulated carbonate system changes that produced the data-consistent CO_2 changes, large reductions in export production, is not compatible with productivity proxies and did likely not play a dominant role in the real world glacial carbon cycle changesin the atmosphere are maximally four times larger when interactive sediments are considered (Figs 7, 6).

3.4 The efficiency of the soft tissue pump during glacial-interglacial cycles

The interplay between export production and ocean circulation influences the strength of the soft tissue pump, i.e. the degree of nutrient depletion in the euphotic zone and the magnitude of the vertical nutrient and DIC gradients (Volk and Hoffert, 1985) . Two approaches have been developed to quantify the efficiency of the soft tissue pump: nutrient utilization in the surface ocean Sarmiento (2006) and the fraction of regenerated nutrients in the ocean's interior (Ito and Follows, 2005). No direct proxy exists for these metrics across glacial cycles, but several proxies have been used to constrain their evolution indirectly (see reviews in Galbraith and Skinner, 2020; Sigman and Hain, 2024). Nutrient concentrations have been inferred directly from reconstructed δ^{13}C of DIC and dissolved cadmium concentrations based on modern day correlations, and indirectly from export production reconstructions (e.g. Anderson et al., 2002). Hertzberg et al. (2016) inferred the vertical DIC gradient from the reconstructed vertical δ^{13}C gradient, and (Yu et al., 2019) from the reconstructed vertical CO_3^{2-} gradient. These studies suggested that the biological pump was more efficient during the last glacial maximum, i.e. that nutrient utilization was greater and that vertical gradients of DIC were larger in the Southern Ocean, South Pacific and Atlantic, Eastern Equatorial Pacific and North Atlantic. Tools have also been developed to infer regional to global changes in the soft tissue pump efficiency. The deep ocean oxygen concentrations provide constraints on the amount of deep ocean regenerated DIC (Galbraith and Jaccard, 2015) and Vollmer et al. (2022) inferred preformed phosphate concentrations from reconstructed AOU. These studies concluded that regenerated DIC was increased and preformed phosphate decreased in the deep ocean during the last glacial maximum, inferring a net increased efficiency of the global soft tissue pump.

Glacial-Interglacial amplitudes of $PO_{4,reg}$ changes in all simulations. For BASE, the total amplitude is given, for the other simulations, the additional effect of each forcing to the standard forcing in BASE is shown. Error bars indicate the range of the amplitude across the last five deglaciations.

There are thus indirect proxy constraints for an increased efficiency of the soft tissue pump at the last glacial maximum. We set up one simulation, REMI, with reduced remineralization rates during periods of lower δD in the ice core record, i.e. colder climate, which directly increases the soft tissue pump efficiency. As previously discussed, the resulting increased soft tissue pump efficiency in the glacial ocean has a large potential to draw down atmospheric CO_2 and cause the reconstructed accumulation of respired carbon in the glacial ocean, consistent with other modelling studies (e.g. Menviel et al., 2012; Morée et al., 2021) . Despite this large potential to cause CO_2 changes, the soft tissue pump changes in REMI and SOWI do not produce proxy-consistent changes in export production (see above), $\delta^{13}C$, CO_3^{2-} and The magnitude of these DIC changes depends on the forcing strength, which varies between glacial cycles. The lukewarm interglacials of the first 350 kyr of our simulations do not restore the export fluxes and sedimentary $CaCO_3$ burial (see table 4 and the next sections). A scenario of several simultaneously occurring processes with different effects on CO_2 and nutrient concentrations over glacial cycles seems thus more likely than a dominance of soft tissue pump changes. Our simulations also show that a small contribution of soft tissue pump efficiency changes to atmospheric CO_2 changes is not necessarily in contradiction with the proxy record, as processes that alter the total inventories of nutrients and carbon in the ocean can affect nutrient distributions independently of atmospheric CO_2.

With and without interactive sediments, the soft tissue pump efficiency increase in simulation REMI results in increased nutrient utilization in the surface ocean and reduced preformed nutrients in the ocean's interior during glacial phases (Figs **??**, **??**, **??**). Although these metrics by definition do not scale linearly when we consider supply-burial imbalances of phosphate (Fig **??**, **??**), both metrics suggest that the simulated soft tissue pump efficiency increases during glaciation in REMI. However, the simulated accumulation of regenerated nutrients in the deep ocean is smaller with interactive sediments, even though the simulated glacial-interglacial CO_2 changes are larger. Without interactive sediments, the vertical nutrient gradient during glacial phases is steepened primarily because a larger fraction of regenerated phosphate, released from decaying organic matter, accumulates in the ocean's interior. The accumulation of nutrients in the deep ocean is lower in the simulation with interactive sediments because the resulting depletion of O_2 in the deep ocean increases organic carbon burial, and thus phosphate and carbon removal from the ocean. In simulations in which atmospheric CO_2 changes are dominated by processes other than changes in the soft tissue pump efficiency, changing vertical nutrient gradients can also anti-correlate with atmospheric CO_2, even in simulations with a constant marine nutrient inventory and no interactive sediments . For example, this is the case with the standard forcing (BASE) and alkalinity supply changes (CO2T): nutrient utilization and regenerated nutrient concentrations are lower at glacial maxima (Fig. **??**, **??**) because of reduced export production in a colder ocean with increased sea ice cover. In simulation CO2T, marine alkalinity changes have large effects on atmospheric CO_2, while having a marginal effect on marine nutrient distributions (**??**) by changing the strength of the carbonate pump. preservation required to re-balance the geologic carbon cycle, and so marine DIC concentrations are persistently higher during 800-450 ka than at PI. Interglacials of the last

450 kyr of the simulation reduce DIC in the long-term because they are warm and long enough for increased carbon transfer into sediments and sediment burial.

3.4 δ^{13}C in the atmosphere and ocean

a) AERO b) CO2T c) LAND d) PO4

^{13}C over the last recent glacial cycle in various reservoirs. Solid lines are simulations AERO, CO2T, LAND, and PO4. Dotted lines are reconstructions from the Pacific cores ODP 677 and ODP 847, combined and smoothed by Köhler and Bintanja (2008), regional stacks of sediment cores in the North and South Atlantic (Barth et al., 2018), and Talos Dome ice Eggleston et al. (2016) . Results for each individual forcing in an open and closed system are displayed in Fig. **??**, **??**, **??**, **??**, **??**, **??**.

δ^{13}C in the atmosphere and ocean is also affected by weathering-burial imbalances. Ice cores preserve the δ^{13}C signature of atmospheric CO_2 (Friedli et al., 1984), which showed large fluctuations during the last glacial cycle (Fig. 8), such as fluctuations of $\sim$0.5 ‰ during MIS 4 (71-57 ka, Fig. **??**) and during the last deglaciation ($\sim$ 18-8 ka) (Eggleston et al., 2016). They also show a long-term trend of lower atmospheric δ^{13}C during the Eemian than the Holocene (Schneider et al., 2013; Eggleston et al., 2016). None of the forcings that we applied here produce all of the reconstructed features. In our simulations, the Reconstructions of δ^{13}C changes in marine DIC show different trajectories in different ocean basins and water masses (Oliver et al., 2010; Peterson and Lisiecki, 2018). The δ^{13}C signature of marine DIC in a given location and atmospheric CO_2 is influenced by changes of carbon exchange with the ocean (and land in the case of LAND, BGC and ALL) and the spatial pattern of δ^{13}C in the surface oceanprocesses which affect the whole marine carbon reservoir (e.g. changes in the size and composition of marine carbon input or output fluxes), as well as by changes in water mass distribution, export production, and isotopic fractionation during sea-air gas exchange and primary production (Jeltsch-Thömmes et al., 2019; Jeltsch-Thömmes and Joos, 2023 , with any signal diluted by the 4-box land biosphere. With and without interactive sediments, the cooling induced by the standard forcing in simulation BASE leaves atmospheric δ^{13}C virtually invariant except for minor positive excursions of $\sim$0.05 ‰ as the deep ocean is ventilated during deglaciations (Fig. **??**). The largest δ^{13}C variability (up to $\pm$0.5 ‰) is produced by changing organic matter remineralization (REMI) or organic carbon storage (PO4 and LAND). Yet, the gradual trend of reconstructed atmospheric δ^{13}C over the last glacial cycle (+$\sim$0.5 ‰ from inception to LGM) is only achieved in simulation PO4, the forcing with the biggest effect on sedimentary organic carbon storage (Fig. **??**). LAND causes similar long-term changes but of the opposite sign. No simulation captures the large millenial-scale fluctuations in the reconstructions (Fig. 8). Given our smoothed forcing and the absence of freshwater forcings, our simulations do not contain realistic millenial-scale circulation changes, which would likely be required to simulate these fluctuations (Tschumi et al., 2011; Menviel et al., 2015) None of the forcings that we applied here produce all of the reconstructed features. However, unlike in PO4, REMI and LAND, the maximum δ^{13}C change produced by circulation and temperature changes (PHYS) is only of roughly half the amplitude of the δ^{13}C swing during the deglaciation. It is established that a complex combination of processes is required to explain the atmospheric δ^{13}C record (e.g. Menviel et al., 2015) but a simulation over the last glacial period or the deglaciation accurately reproducing the reconstructions has not yet been achieved, and reconciling reconstructed with simulated atmospheric δ^{13}C

~~remains a major challenge for future work~~they show the importance of considering weathering-burial imbalances in their interpretation.

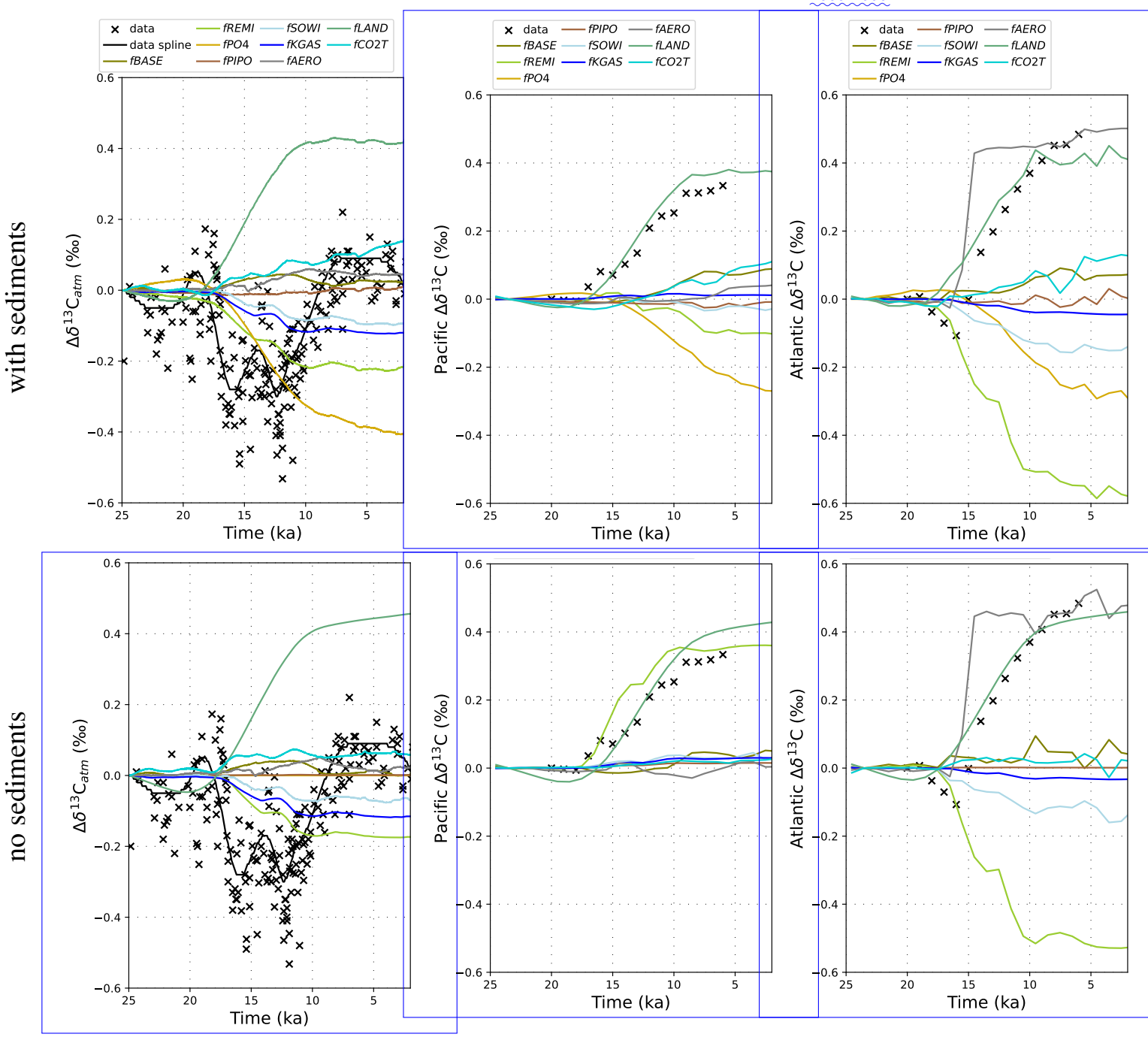

Figure 8. δ^{13}C over the last deglaciation in (a) the atmosphere, (b) ~~intermediate~~ deep Pacific (120–266°E, -35–55°N) and (c) deep ~~Pacific~~ Atlantic (0–65°N) ocean. Lines are ~~from simulations with an open system~~simulation results. Crosses are reconstructions from Schmitt et al. (2012), Eggleston et al. (2016) and Peterson and Lisiecki (2018). All results are shown as differences from 24 ka. Results ~~for~~ with interactive sediments are shown in the ~~closed system~~ top row and results without sediments are ~~displayed~~ shown in Fig. ~~??~~the bottom row.

The Fig. 8 shows the factorial effects of the different forcings on atmospheric and marine δ^{13}C signature of marine DIC in a given location is influenced by processes which affect the whole marine carbon reservoir (e.g. changes in the size and composition of marine carbon input or output fluxes), as well as by changes in water mass distribution and isotopic fractionation during sea-air gas exchange and primary production, which change the isotopic composition of local DIC (Jeltsch-Thömmes et al., 2019; Jeltsch-Thömmes and Joos, 2023). Changes to the whole marine carbon reservoir are the dominant cause of DIC changes in LAND and CO2T. In simulation LANDC across the last deglaciation in comparison to the reconstructed isotopic shifts in these reservoirs. Under $fLAND$, δ^{13}C changes are driven by the simulated release of isotopically light land carbon (-24 ‰) during glacial inceptions and throughout the glacial, resulting in δ^{13}C minima in all reservoirs during glacial maxima and large δ^{13}C increases during deglaciation in response to land carbon uptake, with and without interactive sediments (Fig. **??**, 8). Equally a This whole ocean shift is the dominant signal in $\delta^{13}C_{DIC}$ decrease during the second half of the glacial phase, albeit of lower magnitude, occurred in simulation CO2T, driven by lower CO_2 and a consequent shift in fractionation that causes increased incorporation of isotopically heavy carbon into biogenic export and burial and therefore removal of isotopically heavy carbon from the ocean (Fig. S6). Compared to LAND and CO2T, deep ocean δ^{13}C changes were inverted in simulations REMI and PO4: deep ocean δ^{13}C increased from glacial inception towards the glacial maximum records of the deep Pacific. In simulations without interactive sediments, $fREMI$ also causes a similar shift in the deep Pacific, yet the shift is of opposite sign in simulations with interactive sediments due to the negative geologic POC balance during the deglaciation (Fig. **??**, **??**)as more POC is buried, removing isotopically light C from the system. In these simulations, during terminations (and in simulation PO4 also during interglacials), a decrease of δ^{13}C is simulated in all dynamic carbon reservoirs as $CaCO_3$ burial peaks temporarily and POC burial fluxes return to inter-glacial levels (Jeltsch-Thömmes et al., 2019). In addition, reduced POC fluxes to the sediments and increased ventilation of the deep ocean result in remineralization events of previously deposited sedimentary organic matter. While these tendencies of deep ocean δ^{13}C occur globally in simulation PO4, they are restricted to the Atlantic, particularly the North Atlantic, in simulation REMI.

Because the sensitivities of 2). $fPO4$ has a similar isotopic effect on the ocean as $fREMI$ with sediments because it also leads to the release of sedimentary organic carbon during the deglaciation. Since the processes that affect $\delta^{13}C_{CO_2}$ and $\delta^{13}C_{DIC}$ are different, and $\delta^{13}C_{DIC}$ varies between ocean basins, the forcings which best reproduce reconstructed evolution of δ^{13}C changes also vary between atmosphere and ocean, and specific water masses . In the North Atlantic, nutrient input (PO4) and deepening of the remineralization depth (REMI) result in δ^{13}C changes at intermediate depth that are similar to observations (green curve in Fig. **??** and Fig. **??**). Yet, under these forcings deep ocean δ^{13}C outside the North Atlantic does not evolve as reconstructed. Deep ocean δ^{13}C in the Pacific and South Atlantic are best reproduced by alkalinity nudging (CO2T) and land carbon release (LAND, blue and yellow lines in Fig. **??**). LAND and CO2T are also the only simulations with a persistent δ^{13}C increase in the deep and abyssal Pacific during the last deglaciation, with LAND roughly reproducing the reconstructed amplitude (Fig. 8). The δ^{13}C record of the deep North Atlantic is best reproduced by additional radiative cooling in simulation AERO, due to the resulting AMOC shoaling (purple curve in Fig. **??**)(Oliver et al., 2010). This indicates that different processes were likely the dominant controls on δ^{13}C regionally, even if they were not necessarily the dominant drivers of atmospheric CO_2. In our simulations, the simulated δ^{13}C at intermediate depth in the North Atlantic is

most data-consistent in PO4, followed by AERO, the latter of which also reproduces the reconstructed changes in the deep Atlantic. δ^{13}C at intermediate depth in the North Atlantic might thus have been dominated by changing export fluxes and circulation changes, while the latter dominated δ^{13}C The impact of interactive sediments also varies between water masses. For example, in the deep North Atlantic. In the deep Pacific and South Atlantic, Pacific accumulation of isotopically light δ^{13}C as in simulation LAND likely dominated in the deep Pacific and South Atlantic. None of our simulations show lower marine benthic δ^{13}C during the Eemian than during the Holocene, as reconstructed from marine sediments (Bengtson et al., 2021) and which may be linked to changes in weathering fluxes not considered here.

3.5 Sedimentary burial and CO_3^{2-} concentrations

Changes in the simulated sedimentary burial fluxes result in net transfers of up to 2000 PgC between the carbon pools of the ocean and sediments throughout a glacial cycle, while the net transfer between the ocean and atmosphere is roughly 200 PgC, and between the terrestrial biosphere and atmosphere on the order of 500-1000 PgC (Jeltsch-Thömmes et al., 2019). The carbon cycle impact of glacial cycles was thus likely larger in the ocean than in the atmosphere (Roth et al., 2014; Buchanan et al., 2016) , due to changes in sedimentary carbon storage. How realistic are the simulated fluxes?

a) POC burial Simulated and reconstructed (Cartapanis et al., 2016, 2018) relative changes of global POC and $CaCO_3$ burial changes over the last glacial cycle. Gray shading indicates odd isotope stages (MIS5e, MIS3 and MIS1).

Reconstructions of global POC burial flux changes over the last glacial cycle (Cartapanis et al., 2016) found that POC burial was smallest during interglacials, and gradually rose during glacial phases until it peaked during the LGM *fLAND* likely dominated (Fig. 8b) but must have over-compensated the sediment-enhanced isotopic effects of *fREMI* and *fPO4*, and cannot explain the reconstructed CO_2 rise (Fig. **??**a, see also simulated and reconstructed POC burial rates across the last glacial cycle in Figs S2, S4, S5, S6, S7). Simulations REMI and PO4 are the only single-forcing simulations which produce higher POC burial fluxes during glacial maxima than during interglacials. However, in these simulations, the simulated increase in POC burial already occurs during inception, such that the highest burial rates persist throughout most of the glacial phase while in the reconstructions they remain below the Holocene value until MIS2. PO4 also roughly reproduces the magnitude of POC burial changes during the last deglaciation but fails to produce the reconstructed low POC burial rates at the end of the Eemian. The large reconstructed POC burial reduction after the Eemian is only simulated when all biochemical forcings are combined (BGC), and also then is not sustained into MIS4 as indicated by the reconstructions. The sedimentary record indicates that the glacial increase in POC burial occurred predominantly in the Southern Ocean (Cartapanis et al., 2016). In 6). In the deep North Atlantic, the model, surface ocean cooling and sea ice expansion reduce export production in the Southern Ocean during glacial inceptions, which reduces burial rates. External nutrient supply to the glacial Southern Ocean increases the flux of organic particles to the sediments relative to the other forcings and can counteract the climate-driven productivity reductions. Simulation PO4 is thus the simulation which most closely aligns with the geographic pattern of reconstructed POC burial changes during glacial inceptions. In REMI, POC burial remains unchanged in the Southern Ocean and instead increased on continental margins in the Pacific and Indian Oceans. In either case, we have to recall that in our simulations the forcings are

simplified to be globally uniform, which might affect the spatial pattern of simulated burial changes. During deglaciations, the reconstructions show a strong decrease of POC burial in the Southern ocean, while most other ocean areas see burial increases during deglaciations. The latter are captured in most simulations, and are a response to surface ocean warming and enhanced upwelling of nutrients that previously accumulated in the deep ocean during the glacial, but the changes in the Southern Ocean are again best reproduced in simulation PO4.

Reconstructions of global $CaCO_3$ burial changes magnitude of the $\delta^{13}C$ shift can also be reproduced by additional radiative cooling and the resulting AMOC shoaling due to $fAERO$ (Fig. 8c) and the simulated isotopic shifts are less affected by interactive sediments.

In the atmosphere, the largest $\delta^{13}C$ variability (up to ± 0.5 ‰) is also produced by $fLAND$, with and without interactive sediments, and by $fREMI$ and $fPO4$ in simulations with interactive sediments. In fact, the gradual trend of reconstructed atmospheric $\delta^{13}C$ over the last glacial cycle (Cartapanis et al., 2018) show that burial rates decreased in most ocean basins during glacial inception , while they increased in the Southern Ocean, resulting in only minor glacial-interglacial changes in the global average. Physical forcings result in roughly constant $CaCO_3$ burial rates during glacial inception, as suggested by the reconstruction, while simulations PO4 and CO2T display burial increases and all other simulations decreases between MIS5 and MIS3. The simulations of physical forcings also reproduces decreased $CaCO_3$ burial rates starting in MIS4, though at a smaller amplitude than reconstructed (+$\sim$0.5 ‰ from inception to LGM) is only achieved in $fPO4$, the forcing with the biggest effect on sedimentary organic carbon storage (Fig. **??**b), while biochemical forcings produce much larger changes and mostly inreased burial. The error in amplitude under biochemical forcings is particularly large during terminations (see also Figs S2, S4, S5, S6, S7). However, biochemical forcings produce more data-consistent spatial patterns of $CaCO_3$ burial changes . Simulations PO4 and CO2T are the only setups which produced the reconstructed amplified $CaCO_3$ burial in the Southern Ocean between MIS5 and MIS3 (Cartapanis et al., 2018). In PO4, burial rates increase due to increased productivity, and in CO2T due to higher sedimentary preservation in the open ocean (e.g. due to less deposition on shelves or more alkalinity input from weathering). In addition, burial rates continue to rise through the LGM in the Southern Ocean in both simulations , while the reconstructions show that burial rates decreased from MIS 3. It is possible that constraining nutrient supply to the Southern Ocean, e.g. by assuming that meteoric iron fertilization was the dominant nutrient forcing, could change the spatial pattern and result in more data-consistent burial changes during glacial inceptions. The reconstructed burial rate decline between MIS 3 and the LGM, which is missing in PO4, would then require that one of the other forcings became dominant over changes in nutrient supply. In our simulations , the other forcings all caused Southern Ocean $CaCO_3$ burial rates to reach a minimum during the LGM, consistent with the reconstructions2). $fLAND$ causes similar long-term changes but of the opposite sign. No simulation captures the large millennial-scale fluctuations in the reconstructions (Fig. 8). Given our smoothed forcing and the absence of freshwater forcings, our simulations do not contain realistic millennial-scale circulation changes, which would likely be required to simulate these fluctuations (Tschumi et al., 2011; Schmitt et al., 2012; Menviel et al., 2015). It is well-established that a complex combination of processes is required to explain the atmospheric $\delta^{13}C$ record (e.g. Menviel et al., 2015) but a simulation over the last glacial period or the deglaciation accurately reproducing the reconstructions has not yet been achieved, and reconciling reconstructed with simulated atmospheric $\delta^{13}C$ remains a major challenge for future work. However, our

simulations show that interactive sediments change the δ^{13}C signals of Earth system changes on deglacial time scales and need to be considered in such future work, despite challenges associated with model spin-up as discussed next.

3.5 Long isotopic drifts due to weathering-burial imbalances

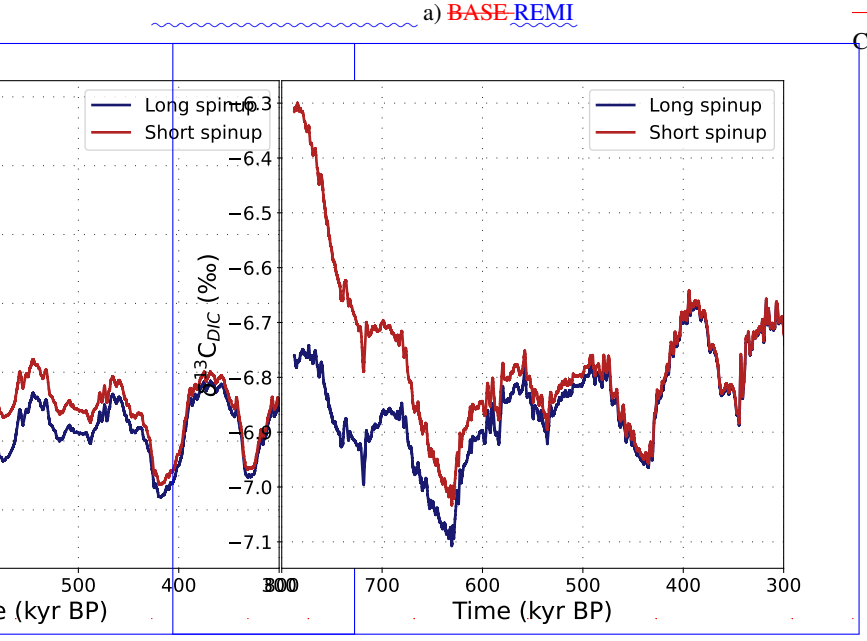

Figure 9. ~~Sedimentary $CaCO_3$ fraction during the late Holocene (top row Cartapanis et al., 2018) and LGM (bottom row Wood et al., 2023) as reconstructed (circles) and~~ Comparison of simulated atmospheric δ^{13}C in simulations ~~BASE~~REMI and CO2T when started from a 'short spinup', ~~PHYS~~i.e. a 70 kyr PI spinup followed by a 2 kyr adjustment to MIS19 conditions, ~~BGC~~ and ~~CO2T (underlying maps)~~a 'long spinup', i.e. the short spinup plus 215 kyr of transiently simulated MIS19-MIS15.

~~Model-data comparison for the $CaCO_3$ content of surface sediments is more challenging because of the simplified assumption of globally uniform detrial fluxes to the sediment and the coarse model resolution which does not resolve sea mounts and steep slopes. Yet, large-scale resemblance or mismatch of simulated and reconstructed sedimentary $CaCO_3$ fraction can still offer some constraint on the reasonability of the simulated processes. For the LGM, the simulated distribution of sedimentary $CaCO_3$ under the standard forcing (BASE) shows good agreement with the reconstructions by Wood et al. (2023) in most ocean basins~~

An important technical lesson of our simulations is that the long adjustment timescale in the geologic carbon cycle also presents an initialization problem, especially for carbon isotopes (Jeltsch-Thömmes and Joos, 2023). We started our experiments from MIS19, which was a colder interglacial than the the Holocene, and Holocene conditions were not reached during the lukewarm interglacials of the first 400 kyr of the simulations. In simulations with interactive sediments, the initial imbalance between weathering inputs derived from the pre-industrial spin-up and burial fluxes adjusting to the colder lukewarm interglacials and glacial states caused δ^{13}C drifts during the first glacial cycles (Fig. ~~3). The low $CaCO_3$ content at the North Pacific~~

margins is better simulated in REMI with slower remineralization rates in the surface ocean. Yet, no simulation reproduces the reconstructed low $CaCO_3$ content in the North Atlantic and high $CaCO_3$ content in the equatorial Pacific. The model has been tuned to the pre-industrial $CaCO_3$ distribution, however, in our study late Holocene $CaCO_3$ contents are the result of almost 800 kyr of transient simulation. The model-data match for the Holocene is relatively good for simulations with small sediment perturbations during the glacial cycle, especially simulations BASE, KGAS, SOWI, AERO and LAND, but also PO4 which does not produce a $CaCO_3$ burial spike during deglaciations. In simulations REMIand PIPO, however, $CaCO_3$ burial rates have not yet stabilised by the end of 9). Consequently, the simulations after the large $CaCO_3$ burial event during the last deglaciation, resulting in much higher sedimentary $CaCO_3$ contents in the Holocene than reconstructed. Simulation CO2T, on the other side, has less sedimentary $CaCO_3$ content during the Holocene than reconstructed. This is the result of strong dissolution due to forced alkalinity removal from the ocean during deglaciations.

Evolution of CO_3^{2-} in the tropical deep Pacific as simulated in simulations BASE, PHYS, BGC and ALL and reconstructed by Qin et al. (2018). The results of the other forcings are shown in Fig. S13.

Comparing our simulation results to reconstructed CO_3^{2-} changes is another test of how realistic the simulated carbonate systemchanges during glacial cycles are. Kerr et al. (2017) found a repeated pattern of low benthic CO_3^{2-} in the tropical Pacific and Indian Ocean during interglacials and high CO_3^{2-} during glacials (difference of 20-55 mmol/m^3) across the last 500 kyrs. Qin et al. (2018) found that the same pattern extended over the last 700 kyrs. In our simulations with purely physical forcings (BASE, KGAS, SOWI, AERO, PHYS) and PO4simulated glacial-interglacial $\delta^{13}C$ signal over this period is altered by the long-term adjustment of the geologic carbon cycle. We addressed this issue by transiently simulating two full glacial cycles before starting the experiments. The magnitude of the initial imbalance in the geologic carbon cycle, and hence isotopic drift, depended on the simulated forcing and was largest in simulations REMI, CO_3^{2-} is almost constant over glacial cycles (Fig. 4, S13). In PIPO, LAND, REMI and PIPO and CO2Tthe simulated CO_3^{2-} changes are closer to the reconstructed magnitude. CO_3^{2-} maxima during glacial maxima are present in all simulations with interactive sediments, the glacial-interglacial difference ranging from a few mmol/m^3 to 110 mmol/m^3, and is caused by invasion of CO_2 into the ocean and weathering-burial imbalances due to changes of the carbonate export flux and sediment dissolution (Fig. 4 and S13). In simulations without interactive sediments, this glacial CO_3^{2-} maximum is not simulated in PIPO, REMI and LAND. Importantly, the drift is a result of perturbing the sediment-weathering balance. The drift can therefore not be corrected for with a control simulation without forcing, because it only appears in the perturbed system. Instead, to avoid a drift, the experiment needs to start from an isotopically balanced geologic carbon cycle, which most commonly will require a long spin-up with a fully-coupled, open system, ideally over several glacial cycles especially when simulating large changes of the biological pump or marine carbonate system. We suggest that the size of the transient imbalance of the geologic carbon cycle, and thus the length of the required spin-up, could be minimized by balancing the geologic carbon cycle not for an interglacial state but for the mean burial fluxes over a full glacial cycle.

a) without sediments b) with sediments

4 Discussion

During the last deglaciation, reconstructions of CO_3^{2-} of The data references are provided at the deep equatorial Pacific showed only small variability, which is solely simulated with purely physical forcings or in simulations without interactive sediments (Fig. **??**). The offset from the reconstructed glacial values and the large changes during the deglaciation suggest that all applied changes to nutrient supply (PO4) and remineralization (REMI) cause too large weathering-burial imbalances of alkalinity. While net alkalinity removal from the ocean during deglaciation (e.g. by shallow deposition, coral reef growth or strongly reduced weathering inputs) can cause widespread dissolution which might diminish excess accumulation of $CaCO_3$ (see above), it cannot offset the strong CO_3^{2-} decrease which is not part of the reconstructions but caused by bottom of the applied nutrient and remineralization forcings table.

Insterestingly, during MIS13-MIS11 and the Mid-Brunhes transition, reconstructed CO_3^{2-} changes in the deep equatorial Pacific were much larger than during the last glacial cycle (Fig. 4). Such variability of CO_3^{2-} amplitude between glacial cycles is not reproduced by any of our simulations, but simulations CO2T and REMI, which produced larger-than-reconstructed CO_3^{2-} changes over the last glacial cycle produced CO_3^{2-} changes more similar to those reconstruced for MIS13-MIS11The direction of each arrow indicates whether a difference is positive (pointing upwards, teal-coloured) or negative (pointing downwards, brown-coloured).

a) $fBASE$ Selected factorial effects on simulated LGM-PI differences in deep CO_3^{2-} (3500 m depth). The width of the arrows shows the size of the difference relative to the reconstruction in the uppermost row "Data". For POM export only qualitative reconstructions exist. Hence, the arrows showing simulated effects are normed by the biggest effect of any forcing.

During the last deglaciation, reconstructions of CO_3^{2-} of The data references are provided at the deep equatorial Pacific showed only small variability, which is solely simulated with purely physical forcings or in simulations without interactive sediments (Fig. **??**). The offset from the reconstructed glacial values and the large changes during the deglaciation suggest that all applied changes to nutrient supply (PO4) and remineralization (REMI) cause too large weathering-burial imbalances of alkalinity. While net alkalinity removal from the ocean during deglaciation (e.g. by shallow deposition, coral reef growth or strongly reduced weathering inputs) can cause widespread dissolution which might diminish excess accumulation of $CaCO_3$ (see above), it cannot offset the strong CO_3^{2-} decrease which is not part of the reconstructions but caused by bottom of the applied nutrient and remineralization forcings table.

Insterestingly, during MIS13-MIS11 and the Mid-Brunhes transition, reconstructed CO_3^{2-} changes in the deep equatorial Pacific were much larger than during the last glacial cycle (Fig. 4). Such variability of CO_3^{2-} amplitude between glacial cycles is not reproduced by any of our simulations, but simulations CO2T and REMI, which produced larger-than-reconstructed CO_3^{2-} changes over the last glacial cycle produced CO_3^{2-} changes more similar to those reconstruced for MIS13-MIS11The direction of each arrow indicates whether a difference is positive (pointing upwards, teal-coloured) or negative (pointing downwards, brown-coloured).

a) $fBASE$ Selected factorial effects on simulated LGM-PI differences in deep CO_3^{2-} (3500 m depth). The width of the arrows shows the size of the difference relative to the reconstruction in the uppermost row "Data". For POM export only qualitative reconstructions exist. Hence, the arrows showing simulated effects are normed by the biggest effect of any forcing.

Table 2. Comparison Quantified metrics of simulated the carbon cycle according to reconstructions and reconstructed (Yu et al., 2013) CO_3^{2-} changes model responses in our set of simulations with sediments. Shown are the deep factorial effects of the tested forcings and their non-linearites in comparison with reconstructed differences (3500 mLGM minus Holocene) West Equatorial Pacific with over the last deglaciation (specific times of the comparisons vary slightly by proxy record, depending on temporal resolution and without dynamic sedimentsrecord length, and are indicated in the table header) in various proxy systems.

During the last deglaciation, reconstructions of CO_3^{2-} of The data references are provided at the deep equatorial Pacific showed only small variability, which is solely simulated with purely physical forcings or in simulations without interactive sediments (Fig. **??**). The offset from the reconstructed glacial values and the large changes during the deglaciation suggest that all applied changes to nutrient supply (PO4) and remineralization (REMI) cause too large weathering-burial imbalances of alkalinity. While net alkalinity removal from the ocean during deglaciation (e.g. by shallow deposition, coral reef growth or strongly reduced weathering inputs) can cause widespread dissolution which might diminish excess accumulation of $CaCO_3$ (see above), it cannot offset the strong CO_3^{2-} decrease which is not part of the reconstructions but caused by bottom of the applied nutrient and remineralization forcings table.

Insterestingly, during MIS13-MIS11 and the Mid-Brunhes transition, reconstructed CO_3^{2-} changes in the deep equatorial Pacific were much larger than during the last glacial cycle (Fig. 4). Such variability of CO_3^{2-} amplitude between glacial cycles is not reproduced by any of our

~~While the reconstructed deep ocean CO_3^{2-} reservoir in the Pacific was relatively stable over the last deglaciation, a large CO_3^{2-} increase was reconstructed for~~ Table 4 provides an overview of different proxy signals that are produced in by our factorial forcings, and the non-linearities that arise when they are combined, with interactive sediments over the last deglaciation. The first row shows the reconstructed direction of LGM - Holocene differences, and the next lines show the direction and relative size (compared to the proxy signal) of changes induced by the various tested forcings. The last four rows show the direction and relative size of non-linearities caused by three different combinations of the forcings above. For many of the considered proxies, the ~~deep Atlantic Qin et al. (2018); Yu et al. (2019). The different sensitivities of deep ocean CO_3^{2-} in~~ signals are strongly amplified by the dynamic weathering-burial imbalances, and also the non-linearities are larger with than without interactive sediments. However, the ~~two basins is also apparent in all of our simulations (see examples in Fig. ?? and S15) and is the result of larger circulation and productivity changes in the Atlantic than Pacific. However, circulation changesproduce lower CO_3^{2-} in the deep subpolar North Atlantic during the LGM, while reconstructions suggest higher CO_3^{2-} (Yu et al., 2019). Higher deep Atlantic CO_3^{2-} at the LGM requires increased nutrient supply (PO4), deeper remineralization (REMI) or a net alkalinity input (CO2T). These patterns appear with and without dynamic sediments in our simulations. Sediments mostly affect the amplitude and temporal evolution of deep CO_3^{2-} changes, not their spatial pattern (not shown).~~

4.1 ~~Imbalances of the geologic carbon cycle~~

non-linearities are still small compared to the effect of individual biogeochemcial forcings, and for some proxies of similar size as the effect of physical forcings. Hence, in most cases, proxy changes provide a first-order constraint on the plausibility of large changes in individual processes. $fBASE$, the effect of temperature changes due to orbital, albedo and greenhouse gas changes, moves almost all proxy systems in the reconstructed direction (the directions of the arrows match), but almost never to the reconstructed extent (the widths of the arrows do not match). It is only sufficient to explain strongly reduced export production in the polar Southern Ocean at the LGM, which in our model is predominantly driven by surface cooling and sea ice expansion regardless of which other processes also occurred.

~~The previous model-data comparison showed that weathering-burial imbalances increase the potential of many forcings to draw down CO_2 during glacial periods and buffer carbon cycle changes during deglaciations.~~ We identified two processes ~~which are most effective at raising~~ by which weathering-burial imbalances most effectively raise atmospheric CO_2 during deglaciations in our simulations: Alkalinity removal and organic carbon remineralization. ~~In simulations PIPO, REMI, BGC and ALL~~ Under $fPIPO$ and $fREMI$ the combination of high alkalinity at the end of glacial phases and increased $CaCO_3$ export production during deglaciation causes large transient $CaCO_3$ deposition events in the open ocean (Fig. ~~S25~~2) which remove the excess glacial alkalinity and thus drive a large but slow continuous CO_2 rise compared to the reconstruction. The marine DIC and alkalinity that built up over the previous glacial phase are too large to be removed instantly, and the resulting large deposition of $CaCO_3$ during the deglaciation persists far into the interglacial. In consequence, these ~~simulations~~ forcings produce poorer model-data matches for Holocene $CaCO_3$ ~~and marine δ^{13}C distributions than the initial PI spinup (see Fig. ??,??)~~. We also showed that the resulting δ^{13}C and $[CO_3^{2-}]$ ~~changes~~ signals in the deep Pacific are not consistent with reconstructions. ~~In CO2T, alkalinity removal is forced~~ $fCO2T$ shows the effect of forced alkalinity removal during galciations

to reproduce the reconstructed atmospheric CO_2 record, and can serve to study the effect of alkalinity removal through means other than deep ocean $CaCO_3$ burial (e.g. shallow deposition, coral reef growth, reduced terrestrial input) on other proxy systems. ~~In this simulation,~~ This forcing causes deep ocean $CaCO_3$ dissolution ~~occurs during the deglaciation and marine DIC increases, resulting in more proxy-consistent~~ and increasing marine DIC during the deglaciation, moving $\delta^{13}C$ ~~changes~~ in the deep Pacific ~~but still~~ in the proxy-consistent direction but still producing a large mismatch in $[CO_3^{2-}]$. ~~Alternatively, in simulation PO4, the~~ $fPO4$ results in a deglacial CO_2 rise ~~is largely caused by~~ due to a reduction in export production and increased remineralization of sedimentary organic matter which accumulated during the previous glacial period under reduced benthic O_2 concentrations. The resulting CO_2 increase is of similar amplitude as that ~~in simulation REMI~~ due to $fREMI$ but happens faster, more consistent with the reconstruction. In addition, deep Pacific $[CO_3^{2-}]$ is less perturbed by this ~~process than in REMI or CO2T~~effect than by $fREMI$ or $fCO2T$, yet deep ocean $\delta^{13}C$ is shifted in the wrong direction.

~~There are several ways, however, in which the amplitude or regional pattern of the simulated changes might be biased by our experiment design. Firstly, by design our forcings are smooth in time and spatially uniform, which is a stark simplification. For example, the PO4 forcing ties nutrient supply to the $\delta^{18}O$ record. The correlation between dust (iron source to the open ocean) concentrations in the EPICA Dome C ice core and benthic $\delta^{18}O$ is of first order only and varies over the glacial cycle (Winckler et al., 2008). Several macro- and micronutrients were likely supplied to varying parts of the glacial ocean (Broecker, 1982b; Martin, 1990; Pollock, 1997; Deutsch et al., 2004) and while dust flux changes seem to correlate globally (Kukla et al., 1990; Winckler et al., 2008), the timings and rates of other nutrient fluxes might in reality have varied temporally and spatially. Similarly, our other forcings might change more slowly over the deglaciation than the real processes they represent.~~

~~Another simplification in our experiment design is that the majority of our simulations assume temporally constant carbon inputs although in reality these fluxes are climate sensitive (Munhoven, 2002). It is unlikely that removing this simplification could resolve the bias in simulated global carbon fluxes and reservoir size changes because it is estimated that global weathering rate changes during glacial cycles were small despite large local variability, possibly because they canceled out in the global mean (Jones et al., 2002; Von Blanckenburg et al., 2015; Frings, 2019; Börker et al., 2020). It was estimated that glacial-interglacial weathering flux changes altered atmospheric CO_2 by a maximum of 20 ppm (Köhler and Munhoven, 2020). Yet, the resulting $\delta^{13}C$ perturbation could be larger because a global balance in carbon flux changes does not imply a balance in carbon isotope fluxes (Jeltsch-Thömmes and Joos, 2023). Additionally, there might have been non-linear changes in isotopic input fluxes during the simulated time period.~~

~~Finally, the imbalance between weathering and burial fluxes is also shaped by the sedimentation rate. In our simulations, sedimentation rates vary due to changes in biogenic export, yet accumulation of non-biogenic material remained constant. This omission, however, does not seem to be the source of large errors. In a sensitivity experiment, we prescribed step-wise 30% increases and decreases of the non-biogenic flux in the PI steady state, which had only marginal effects on atmospheric CO_2, DIC and sedimentary accumulation of biogenic particles (Fig. S1).~~

~~Regardless of which process or combination of processes we simulated, no simulation reached a weathering-burial equilibrium by the late Holocene. It seems likely that carbon burial in marine sediments was still adjusting to interglacial conditions at the~~

beginning of the industrial revolution. This is also indicated by the reconstructed changes in global sedimentary burial rates over the last glacial cycle, which suggest that burial fluxes changed throughout the Eemian and the current interglacial and only find apparent balances during the longer glacial phases (Fig S3, Cartapanis et al., 2016, 2018).

a) REMI b) CO2T Comparison of simulated atmospheric $\delta^{13}C$ in simulations REMI and CO2T when started from a 'short spinup', i.e. a 50 kyr PI spinup followed by a 2 kyr adjustment to MIS19 conditions, and a 'long spinup', i.e. the short spinup plus 215 kyr of transiently simulated MIS19-MIS15.

On a technical note, the long adjustment timescale in the geologic carbon cycle also presented an initialization problem, especially for carbon isotopes (Jeltsch-Thömmes and Joos, 2023). We started our experiments from MIS19, which was a colder interglacial than the the Holocene, and Holocene conditions were not reached during the lukewarm interglacials of the first 400 kyr of the simulations. In simulations with interactive sediments, the initial imbalance between weathering inputs derived from the pre-industrial spin-up and burial fluxes adjusting to the colder lukewarm interglacials and glacial states caused $\delta^{13}C$ drifts during the first glacial cycles (Fig. 9). Consequently, the simulated glacial-interglacial $\delta^{13}C$ signal over this period is altered by the long-term adjustment of the geologic carbon cycle. We addressed this issue by transiently simulating two full glacial cycles before starting the experiments. The magnitude of the initial imbalance in the geologic carbon cycle, and hence isotopic drift, depended on the simulated forcing and was largest in simulations REMI, PIPO and CO2T. Importantly, the drift is a result of perturbing the sediment-weathering balance. The drift can therefore not be corrected for with a control simulation without forcing, because it only appears in the perturbed system. Instead, to avoid a drift, the experiment needs to start from an isotopically balanced geologic carbon cycle, which most commonly will require a long spin-up with a fully-coupled, open system, ideally over several glacial cycles especially when simulating large changes of the biological pump or marine carbonate system. We suggest that the size of the transient imbalance of the geologic carbon cycle, and thus the length of the required spin-up, could be minimized by balancing the geologic carbon cycle not for an interglacial state but the mean burial fluxes over a full glacial cycleFuture work will have to test which combinations of these processes are most consistent with the wide range of available proxy data.

5 Discussion

It is well established that cooling and circulation changes altered sea-air gas exchange and increased deep ocean carbon storage by isolating it from the surface during glacial phases (e.g. Brovkin et al., 2007). Combined, these effects contribute to changes in atmospheric CO_2 in our simulations that are comparable to Brovkin et al. (2012) (26 ppm compared to 30 ppm). Our simulations also capture some transient features of of sea-air gas exchange variability over the last glacial cycle that have been simulated by Brovkin et al. (2012). For example, we found a brief atmospheric CO_2 increase between 110 and 90 ka due to circulation changes, but only in simulations in which AMOC has already weakened substantially by this point, i.e. those with feedbacks that amplify orbitally-driven cooling (e.g. increased aerosol load). Brovkin et al. (2012) showed that a higher vertical diffusivity in the Southern Ocean increases the sensitivity of the sea-air CO_2 flux to sea ice changes. Raising the vertical diffusivity of ice-free areas by an order of magnitude in their model resulted in an additional CO_2 draw-down of 10 ppm during

~~inception due to Southern Ocean cooling. We did not test the effect of such change in our simulations, but reducing the piston velocity in the Southern Ocean by up to 40 % in simulation KGAS caused an additional CO_2 draw-down of only ~2 ppm.~~

Isolating the deep Pacific through ~~increased~~ reduced Southern Ocean wind forcing (~~simulation SOWI~~effect $fSOWI$) caused a glacial CO_2 decline by ~13 ppm, the biggest CO_2 draw-down on top of the effect orbital cooling ($fBASE$) of any isolated physical forcing that we tested. Tschumi et al. (2011) showed that this effect also has the potential to cause larger CO_2 draw-down with sedimentary amplification than simulated here. The idealised, strong reductions in wind speeds over the Southern Ocean prescribed by Tschumi et al. (2011) as a tuning knob for producing old deep ocean waters are unrealistic, but other processes could have contributed to increased isolation of the deep Pacific. Bouttes et al. (2011) showed that during glacial stages enhanced brine rejection during sea ice formation can isolate abyssal waters and cause atmospheric CO_2 and $\delta^{13}C$ changes that are similar to those reconstructed. Enhanced brine rejection could thus have provided an additional physical process that increased the glacial marine carbon storage. The strength of this process, however, is only poorly constrained, and Ganopolski and Brovkin (2017) showed that, at a sufficient strength to significantly affect deep ocean carbon storage, this process creates bigger $\Delta^{14}C$ anomalies in the deep ocean than reconstructed. Following ~~(Menviel et al., 2011)~~Menviel et al. (2011), they also argue that the timing of increased sea ice formation and atmospheric CO_2 changes during the last deglaciation (Roberts et al., 2016) are not entirely consistent with a strong control of brine formation rates on marine carbon storage.

In further agreement with other modelling studies, e.g. Buchanan et al. (2016) and Morée et al. (2021), we find that changing the efficiency of the biological pumps ($fREMI$) is an efficient mechanism to achieve glacial-interglacial atmospheric CO_2 changes similar to those reconstructed from ice cores~~and to reproduce the reconstructed decreased preformed nutrient concentrations during glacial phases (Ito and Follows, 2005; Vollmer et al., 2022)~~. However, because of its large effects on deep Pacific $[CO_3^{2-}]$ and $CaCO_3$ accumulation during deglaciation it was unlikely the dominant carbon cycle change over the last glacial cycle. ~~Several biochemical forcings in addition to reduced remineralization in the surface ocean (REMI) substantially reduce atmospheric CO_2, especially increased nutrient and alkalinity supply (PO4, CO2T). The low glacial DIC in the former simulations also shows that CO_2 removal from the atmosphere in theory does not need to result in increased DIC in the ocean. Instead, these biochemical forcings cause sedimentary changes that can store large amounts of carbon in inorganic and organic sedimentary matter.~~

A relevant role of marine sediments, particularly sedimentary $CaCO_3$, in glacial-interglacial carbon cycle dynamics has long been discussed (e.g. Broecker, 1982b; Broecker and Peng, 1987; Opdyke and Walker, 1992; Archer and Maier-Reimer, 1994; Raven and Falkowski, 1999) and shown in numerical experiments of differing physical and ~~biochemical~~ biogeochemical complexities (Ridgwell et al., 2003; Joos et al., 2004; Tschumi et al., 2011; Menviel et al., 2012; Roth et al., 2014; Wallmann et al., 2016; Ganopolski and Brovkin, 2017; Jeltsch-Thömmes et al., 2019; Köhler and Munhoven, 2020; Stein et al., 2020; Kobayashi et al., 2021). In agreement with other studies (e.g. Ganopolski and Brovkin, 2017; Köhler and Munhoven, 2020), we find that changing marine alkalinity can produce large CO_2 changes. Organic carbon storage is less often considered in modelling studies, although it also showed significant changes across the last glacial cycle (Cartapanis et al., 2016). Out of the ~~processes~~ forcings we tested, ~~increased nutrient supply~~ reduced nutrient limitation during glacial phases (~~simulation PO4~~ $fPO4$) produces temporal and regional organic carbon deposition changes that were most consistent with the reconstruc-

tions. In this simulation, marine sediments turn into a strong carbon sink during cold phases. The simulated increased organic carbon deposition during glacial phases reproduces the reconstructed long-term trends in atmospheric and surface ocean $\delta^{13}C$ during glacials, but ~~fails to simulate~~ is not sufficient in isolation to reproduce the reconstructed deep ocean $\delta^{13}C$ changes in the Pacific and Atlantic. Thus, while sedimentary organic carbon burial could have provided a carbon sink during glacial phases, it must have been ~~small enough or be compensated by other isotopic forcings to not influence~~ operating alongside other processes to allow for the reconstructed benthic $\delta^{13}C$ evolution. Interestingly, ~~our simulations with increased~~ processes that increase organic carbon burial during glacial phases ($fPO4$, $fREMI$) show that some of the deposited organic carbon can be returned to the ocean during deglaciations with a large potential to contribute to a fast post-glacial rise in atmospheric CO_2. In addition to carbon, nutrients are also removed from the ocean when organic matter is buried (Roth et al., 2014). Tschumi et al. (2011) demonstrated in their steady state experiments that increased organic nutrient burial enhances nutrient limitation on export production and reduces $CaCO_3$ export, which increases surface alkalinity and amplifies the CO_2 drawdown caused by the ~~removal~~ increased burial of organic carbon. ~~In simulation REMI~~Under $fREMI$, this process operates transiently. Given the reconstructed increased organic carbon burial rates during glacial maxima, this could have been a relevant process over the last glacial cycles, though it might have been reduced in its efficiency ~~due to~~ by reductions in the PIC:POC of export production during glacial phases (Dymond and Lyle, 1985; Sigman and Boyle, 2000). Finally, sedimentary organic carbon oxidation can also regulate marine alkalinity by affecting sedimentary $CaCO_3$ dissolution (Emerson and Bender, 1981; Sigman and Boyle, 2000)~~. The only simulation in our set which shows increased alkalinity fluxes out of the sediments~~ , but this effect is not directly quantified in our setup. However, we can assess that increased sedimentary organic matter remineralization on a global scale during glacial phases ~~is LAND, in which terrestrial carbon release causes sedimentary dissolution. In all others, especially those which reproduce the reconstructed increase of~~ does not occur due to any of our tested forcings. On the contrary, the effects ($fPO4$,$fREMI$) that increase organic carbon burial during glacial maxima, a prominent feature of the reconstructions, decrease globally-averaged sedimentary remineralization rates ~~decrease~~ during glacial times. ~~Thus, remineralization-driven sedimentary dissolution does not contribute to the glacial~~

A close relationship between DIC and $\Delta^{14}C$(DIC) is found in modern deep ocean waters and this relationship has been used to reconstruct past DIC changes from radiocarbon reconstructions (Sarnthein et al., 2013). Sedimentary carbon fluxes can de-couple deep ocean $\Delta^{14}C$ from DIC (Dinauer et al., 2020) and change DIC without altering sea-air carbon transfer, meaning that DIC changes do not necessarily imply a comparable CO_2 ~~draw-down in our simulations.~~ change in the atmosphere. In all of our simulations with interactive sediments, the DIC inventory change over a glacial cycles is larger than the simultaneous atmospheric CO_2 inventory perturbation because of changes in carbon reservoirs in sediments and weathering-burial imbalances. ~~In some~~ Changes in the simulated sedimentary burial fluxes result in net transfers of up to 2000 PgC between the carbon pools of the ocean and sediments throughout a glacial cycle, while the net loss of atmospheric C to reproduce the reconstructed glacial CO_2 is roughly 200 PgC (Sigman and Boyle, 2000; Yu et al., 2010), and the net loss of terrestrial C is on the order of 500-1000 PgC (Jeltsch-Thömmes et al., 2019). The carbon cycle impact of glacial cycles was thus likely larger in the ocean than in the atmosphere (Roth et al., 2014; Buchanan et al., 2016), due to changes in sedimentary carbon storage. In some of our simulations, large DIC changes are produced by big ~~sedimentary~~

~~changes during glacials which cannot be restored during~~ sustained weathering-burial imbalances during glacials that cannot be compensated during the relatively short deglaciations and cause interglacial carbonate preservation patterns that are not consistent with observations (Fig. S11, S12). While this suggests that such a scenario is unrealistic, it does not generically preclude the possibility of large transient weathering-burial imbalances. Testing a wider range of forcing magnitudes and combinations with the same model but different set-up, ~~Morée et al. (2021)~~ Jeltsch-Thömmes et al. (2019) (the DIC results of which are published in the Appendix of Morée et al. (2021)) found a larger DIC change between the pre-industrial and LGM than simulated here (3900±550 GtC compared to a maximum of 1100±300 GtC in Fig. 7) that is consistent with carbonate system proxy constraints. Combinations of the tested forcings thus allow for larger transient weathering-burial imbalances than produced by our simulation ensemble that can still be reconciled with carbonate system proxies. Some of the tested forcings also show lower glacial than inter-glacial DIC ($fPO4$, $fCO2T$) showing that CO_2 removal from the atmosphere in theory does not need to result in increased DIC in the ocean. Instead, these biogeochemical forcings cause sedimentary changes that can store large amounts of carbon in inorganic and organic sedimentary matter. Kemppinen et al. (2019) and Jeltsch-Thömmes et al. (2019) previously showed and discussed the possibility of a negative glacial DIC anomaly due to increased sedimentary storage. As found by Jeltsch-Thömmes et al. (2019), organic carbon burial extensive enough to cause a negative glacial DIC anomaly as due to $fPO4$, produces large $\delta^{13}C$ signals of opposite sign than reconstructed, and thus seem unlikely. In the study by Jeltsch-Thömmes et al. (2019), a negative glacial DIC anomaly due to alkalinity-driven $CaCO_3$ accumulation is also inconsistent with the proxy record of the last 25 kyr. Consistently, we find that reconstructed deep Pacific [CO_3^{2-}] changes make a large-scale alkalinity-driven ($fCO2T$) glacial $CaCO_3$ accumulation, which reduces atmospheric CO_2 while also reducing DIC, unlikely because it causes larger deep Pacific [CO_3^{2-}] changes than reconstructed over the last deglaciation (Table 4). The isotopic signal of such large $CaCO_3$ deposition, however, is smaller than that of POC burial changes and could more likely be overprinted by other processes (e.g. terrestrial carbon release and export production changes) to yield proxy-consistent evolutions (Table 4).

~~Regardless of the dominant carbon cycle change, like previous studies~~ It has long been suggested that sedimentary imbalances also contributed to the reconstructed interglacial sedimentary changes and CO_2 rises after deglaciations (Broecker et al., 1999; Ridgwell et a . Consistently we find that CO_2 degassing from the ocean persisted throughout deglaciations and into interglacials (e.g. Brovkin et al., 2012), and that the carbon cycle does not reach a new equilibrium before the next glacial inception (e.g. supply-burial imbalances in the late Holocene in Table S2). In our simulations AMOC hysteresis, sedimentary changes and ~~,~~delayed temperature responses, e.g. due to ice ~~shields (~~sheets (mimicked by scaling most forcings to the $\delta^{18}O$ record), introduce memory effects which buffer deglacial carbon cycle reorganizations and cause continued CO_2 rise throughout interglacials. For example, in PO4, BGC and ALL, the simulations which best align with the reconstructed glacial-interglacial organic carbon burial changes, not all glacial organic matter is remineralised and carbonate dissolution continued throughout the interglacials. ~~It has long been suggested that sedimentary imbalances contributed to the observed interglacial sedimentary changes and CO_2 rises (Broecker et al., 1999; Ridgwell et al., 2003; Joos et al., 2004; Broecker and Stocker, 2006; Elsig et al., 2009; Menviel et al., 2012; Brovk~~

5 Conclusions

In response to different simulated carbon cycle forcings over the repeated glacial-interglacial cycles of the past 780 kyr in the Bern3D model, we found large sedimentary changes which substantially alter marine carbon and nutrient concentrations and spatial distributions. Our simulations show that ~~biochemical~~ biogeochemical forcings are required to perturb the sediments sufficiently to reproduce reconstructed burial changes and CO_3^{2-} variations, yet ~~other processes~~ compensating processes (e.g. shallow carbonate deposition) must have operated to reduce the buffering impact of this perturbation on the deglacial carbon cycle re-organization in order to match the speed of the associated carbon release. Our set of factorial simulations further leads to the following conclusions:

Firstly, ocean-sediment interactions and related weathering-burial imbalances, including fluxes of nutrients, alkalinity, organic and inorganic carbon, tend to amplify glacial-interglacial CO_2 change.

Secondly, ~~changes in the ocean inventory of DIC do not scale with changes in~~ the relationship between marine DIC and atmospheric CO_2 ~~but are~~ changes is not linear across the different forcings and strongly influenced by sediment fluxes. For example, the potential addition of phosphate from exposed continental shelves causes ~~not only~~ a decrease in atmospheric CO_2 ~~but also in ocean carbon inventory~~and marine DIC by increasing sedimentary carbon storage. Factorial simulations yield ~~an average DIC change~~ changes in the ocean DIC inventory between -1340 to +1400 GtC and in the atmospheric CO_2 ~~changes between -45 and 80 ppm (~~inventory between -96 and 180 GtC (-45 and 80 ppm) over the last five deglaciations in response to individual prescribed physical and biogeochemical forcings. This suggests that approaches utilizing the relationship between radiocarbon and DIC from modern data to reconstruct the ocean's glacial DIC inventory and the postulated corresponding CO_2 change from glacial radiocarbon data may be biased.

Thirdly, ocean-sediment interactions strongly impact the evolution of important carbon cycle parameters such as $\delta^{13}C(DIC)$ and $\delta^{13}C_{CO_2}$, $CO_3^{=}$, export production, $CaCO_3$ and POM burial fluxes, preformed and remineralized nutrient concentrations, and oxygen. The interpretation of the proxy records without consideration of weathering-burial imbalances and ocean-sediment interactions for both organic and inorganic carbon may lead to erroneous conclusions.

We also showed that the long timescales of ocean-sediment interactions and the weathering-burial cycle pose substantial challenges for model spin ~~ups~~ up because imbalances in the geologic carbon cycle can cause isotopic drifts at the beginning of simulations and which are not present in a control run. Depending on the initial isotopic imbalance, it takes up to 200 kyr for the drift to subside and the signal of the applied forcing to dominate the simulated transient $\delta^{13}C$ changes. Further studies are needed to test whether $\delta^{13}C$ can be spun up in more computationally-expensive models by combining them with lower-complexity models. In the absence of such a spin up strategy, open system simulations of glacial $\delta^{13}C$ are likely strongly affected by these initial drifts.

Data availability. All simulation output necessary to produce the figures in this manuscript are available at https://doi.org/10.5281/zenodo.11385608

Author contributions. FP and AJT designed the simulations. AJT ran the simulations. MA processed the model output and drafted the manuscript. MA, AJT, FP, FJ and TFS interpreted the results and edited the manuscript.

Competing interests. The authors declare that they have no conflict of interest.

Acknowledgements. This research has been supported by the Schweizerischer Nationalfonds zur Förderung der Wissenschaftlichen Forschung (grant nos. 200020-200511 and 200020-200492) and Horizon 2020 (grant nos. 101023443 and 40 820970).

References

Adloff, M., Pöppelmeier, F., Jeltsch-Thömmes, A., Stocker, T. F., and Joos, F. (2023). Multiple thermal AMOC thresholds in the intermediate complexity model Bern3D. *Climate of the Past Discussions*, 2023:1–24.

Anderson, R. F., Chase, Z., Fleisher, M. Q., and Sachs, J. (2002). The Southern Ocean's biological pump during the last glacial maximum. *Deep Sea Research Part II: Topical Studies in Oceanography*, 49(9-10):1909–1938.

Archer, D. and Maier-Reimer, E. (1994). Effect of deep-sea sedimentary calcite preservation on atmospheric CO_2 concentration. *Nature*, 367(6460):260–263.

Barth, A. M., Clark, P. U., Bill, N. S., He, F., and Pisias, N. G. (2018). Climate evolution across the Mid-Brunhes transition. *Climate of the Past*, 14(12):2071–2087.

Battaglia, G. and Joos, F. (2018). Marine N_2O emissions from nitrification and denitrification constrained by modern observations and projected in multimillennial global warming simulations. *Global Biogeochemical Cycles*, 32(1):92–121.

Bengtson, S. A., Menviel, L. C., Meissner, K. J., Missiaen, L., Peterson, C. D., Lisiecki, L. E., and Joos, F. (2021). Lower oceanic $\delta^{13}C$ during the last interglacial period compared to the Holocene. *Climate of the Past*, 17(1):507–528.

Bereiter, B., Eggleston, S., Schmitt, J., Nehrbass-Ahles, C., Stocker, T. F., Fischer, H., Kipfstuhl, S., and Chappellaz, J. (2015). Revision of the EPICA Dome C CO_2 record from 800 to 600 kyr before present. *Geophysical Research Letters*, 42(2):542–549.

Berger, A. (1978). Long-term variations of caloric insolation resulting from the Earth's orbital elements. *Quaternary research*, 9(2):139–167.

Berger, A. and Loutre, M.-F. (1991). Insolation values for the climate of the last 10 million years. *Quaternary science reviews*, 10(4):297–317.

Börker, J., Hartmann, J., Amann, T., Romero-Mujalli, G., Moosdorf, N., and Jenkins, C. (2020). Chemical weathering of loess and its contribution to global alkalinity fluxes to the coastal zone during the Last Glacial Maximum, Mid-Holocene, and Present. *Geochemistry, Geophysics, Geosystems*, 21(7):e2020GC008922.

Bouttes, N., Paillard, D., and Roche, D. (2010). Impact of brine-induced stratification on the glacial carbon cycle. *Climate of the Past*, 6(5):575–589.

Bouttes, N., Paillard, D., Roche, D. M., Brovkin, V., and Bopp, L. (2011). Last Glacial Maximum CO_2 and $\delta^{13}C$ successfully reconciled. *Geophysical Research Letters*, 38(2).

Broecker, W. S. (1982a). Glacial to interglacial changes in ocean chemistry. *Progress in Oceanography*, 11(2):151–197.

Broecker, W. S. (1982b). Ocean chemistry during glacial time. *Geochimica et cosmochimica acta*, 46(10):1689–1705.

Broecker, W. S., Clark, E., McCorkle, D. C., Peng, T.-H., Hajdas, I., and Bonani, G. (1999). Evidence for a reduction in the carbonate ion content of the deep sea during the course of the Holocene. *Paleoceanography*, 14(6):744–752.

Broecker, W. S. and Peng, T.-H. (1987). The role of $CaCO_3$ compensation in the glacial to interglacial atmospheric CO_2 change. *Global Biogeochemical Cycles*, 1(1):15–29.

Broecker, W. S. and Stocker, T. F. (2006). The Holocene CO_2 rise: Anthropogenic or natural? *Eos, Transactions American Geophysical Union*, 87(3):27–27.

Brovkin, V., Brücher, T., Kleinen, T., Zaehle, S., Joos, F., Roth, R., Spahni, R., Schmitt, J., Fischer, H., Leuenberger, M., et al. (2016). Comparative carbon cycle dynamics of the present and last interglacial. *Quaternary Science Reviews*, 137:15–32.

Brovkin, V., Ganopolski, A., Archer, D., and Munhoven, G. (2012). Glacial CO_2 cycle as a succession of key physical and biogeochemical processes. *Climate of the Past*, 8(1):251–264.

Brovkin, V., Ganopolski, A., Archer, D., and Rahmstorf, S. (2007). Lowering of glacial atmospheric CO_2 in response to changes in oceanic circulation and marine biogeochemistry. *Paleoceanography*, 22(4).

Buchanan, P. J., Matear, R. J., Lenton, A., Phipps, S. J., Chase, Z., and Etheridge, D. M. (2016). The simulated climate of the Last Glacial Maximum and insights into the global marine carbon cycle. *Climate of the Past*, 12(12):2271–2295.

Cartapanis, O., Bianchi, D., Jaccard, S. L., and Galbraith, E. D. (2016). Global pulses of organic carbon burial in deep-sea sediments during glacial maxima. *Nature communications*, 7(1):10796.

Cartapanis, O., Galbraith, E. D., Bianchi, D., and Jaccard, S. L. (2018). Carbon burial in deep-sea sediment and implications for oceanic inventories of carbon and alkalinity over the last glacial cycle. *Climate of the Past*, 14(11):1819–1850.

Claquin, T., Roelandt, C., Kohfeld, K., Harrison, S., Tegen, I., Prentice, I., Balkanski, Y., Bergametti, G., Hansson, M., Mahowald, N., et al. (2003). Radiative forcing of climate by ice-age atmospheric dust. *Climate Dynamics*, 20(2):193–202.

Deutsch, C., Sigman, D. M., Thunell, R. C., Meckler, A. N., and Haug, G. H. (2004). Isotopic constraints on glacial/interglacial changes in the oceanic nitrogen budget. *Global Biogeochemical Cycles*, 18(4).

Dinauer, A., Adolphi, F., and Joos, F. (2020). Mysteriously high Δ^{14}C of the glacial atmosphere: influence of 14 C production and carbon cycle changes. *Climate of the Past*, 16(4):1159–1185.

Dymond, J. and Lyle, M. (1985). Flux comparisons between sediments and sediment traps in the eastern tropical Pacific: Implications for atmospheric C02 variations during the Pleistocene 1. *Limnology and Oceanography*, 30(4):699–712.

Edwards, N. R., Willmott, A. J., and Killworth, P. D. (1998). On the role of topography and wind stress on the stability of the thermohaline circulation. *Journal of physical oceanography*, 28(5):756–778.

Eggleston, S., Schmitt, J., Bereiter, B., Schneider, R., and Fischer, H. (2016). Evolution of the stable carbon isotope composition of atmospheric CO_2 over the last glacial cycle. *Paleoceanography*, 31(3):434–452.

Elsig, J., Schmitt, J., Leuenberger, D., Schneider, R., Eyer, M., Leuenberger, M., Joos, F., Fischer, H., and Stocker, T. F. (2009). Stable isotope constraints on Holocene carbon cycle changes from an Antarctic ice core. *Nature*, 461(7263):507–510.

Emerson, S. and Bender, M. (1981). Carbon fluxes at the sediment-water interface of the deep-sea: calcium carbonate preservation.

Etminan, M., Myhre, G., Highwood, E. J., and Shine, K. P. (2016). Radiative forcing of carbon dioxide, methane, and nitrous oxide: A significant revision of the methane radiative forcing. *Geophysical Research Letters*, 43(24):12–614.

Fischer, H., Schmitt, J., Lüthi, D., Stocker, T. F., Tschumi, T., Parekh, P., Joos, F., Köhler, P., Völker, C., Gersonde, R., et al. (2010). The role of Southern Ocean processes in orbital and millennial CO_2 variations–A synthesis. *Quaternary Science Reviews*, 29(1-2):193–205.

Friedli, H., Moor, E., Oeschger, H., Siegenthaler, U., and Stauffer, B. (1984). $^{13}C/^{12}C$ ratios in CO_2 extracted from Antarctic ice. *Geophysical research letters*, 11(11):1145–1148.

Frings, P. J. (2019). Palaeoweathering: how do weathering rates vary with climate? *Elements: An International Magazine of Mineralogy, Geochemistry, and Petrology*, 15(4):259–265.

Galbraith, E. D. and Jaccard, S. L. (2015). Deglacial weakening of the oceanic soft tissue pump: global constraints from sedimentary nitrogen isotopes and oxygenation proxies. *Quaternary Science Reviews*, 109:38–48.

Galbraith, E. D. and Skinner, L. C. (2020). The biological pump during the Last Glacial Maximum. *Annual Review of Marine Science*, 12:559–586.

Ganopolski, A. and Brovkin, V. (2017). Simulation of climate, ice sheets and CO_2 evolution during the last four glacial cycles with an Earth system model of intermediate complexity. *Climate of the Past*, 13(12):1695–1716.

Griffies, S. M. (1998). The Gent–McWilliams skew flux. *Journal of Physical Oceanography*, 28(5):831–841.

Hayes, C. T., Costa, K. M., Anderson, R. F., Calvo, E., Chase, Z., Demina, L. L., Dutay, J.-C., German, C. R., Heimbürger-Boavida, L.-E., Jaccard, S. L., et al. (2021). Global ocean sediment composition and burial flux in the deep sea. *Global biogeochemical cycles*, 35(4):e2020GB006769.

Heinze, C., Maier-Reimer, E., Winguth, A. M., and Archer, D. (1999). A global oceanic sediment model for long-term climate studies. *Global Biogeochemical Cycles*, 13(1):221–250.

Hertzberg, J. E., Lund, D. C., Schmittner, A., and Skrivanek, A. L. (2016). Evidence for a biological pump driver of atmospheric CO_2 rise during Heinrich Stadial 1. *Geophysical Research Letters*, 43(23):12–242.

Hönisch, B. and Hemming, N. G. (2005). Surface ocean pH response to variations in pCO_2 through two full glacial cycles. *Earth and Planetary Science Letters*, 236(1-2):305–314.

Ito, T. and Follows, M. J. (2005). Preformed phosphate, soft tissue pump and atmospheric CO_2. *Journal of Marine Research*, 63(4):813–839.

Jeltsch-Thömmes, A., Battaglia, G., Cartapanis, O., Jaccard, S. L., and Joos, F. (2019). Low terrestrial carbon storage at the Last Glacial Maximum: constraints from multi-proxy data. *Climate of the Past*, 15(2):849–879.

Jeltsch-Thömmes, A. and Joos, F. (2020). Modeling the evolution of pulse-like perturbations in atmospheric carbon and carbon isotopes: The role of weathering–sedimentation imbalances. *Climate of the Past*, 16(2):423–451.

Jeltsch-Thömmes, A. and Joos, F. (2023). Carbon Cycle Responses to Changes in Weathering and the Long-Term Fate of Stable Carbon Isotopes. *Paleoceanography and paleoclimatology*, 38(2):e2022PA004577.

Jones, I. W., Munhoven, G., Tranter, M., Huybrechts, P., and Sharp, M. J. (2002). Modelled glacial and non-glacial HCO_3^-, Si and Ge fluxes since the LGM: little potential for impact on atmospheric CO2 concentrations and a potential proxy of continental chemical erosion, the marine Ge/Si ratio. *Global and Planetary Change*, 33(1-2):139–153.

Joos, F., Gerber, S., Prentice, I., Otto-Bliesner, B. L., and Valdes, P. J. (2004). Transient simulations of Holocene atmospheric carbon dioxide and terrestrial carbon since the Last Glacial Maximum. *Global Biogeochemical Cycles*, 18(2).

Joos, F. and Spahni, R. (2008). Rates of change in natural and anthropogenic radiative forcing over the past 20,000 years. *Proceedings of the National Academy of Sciences*, 105(5):1425–1430.

Jouzel, J., Masson-Delmotte, V., Cattani, O., Dreyfus, G., Falourd, S., Hoffmann, G., Minster, B., Nouet, J., Barnola, J., Chappellaz, J., et al. (2007). EPICA Dome C ice core 800kyr deuterium data and temperature estimates. *IGBP PAGES/World Data Center for Paleoclimatology data contribution series*, 91.

Kalnay, E., Kanamitsu, M., Kistler, R., Collins, W., Deaven, D., Gandin, L., Iredell, M., Saha, S., White, G., Woollen, J., et al. (1996). The NCEP/NCAR 40-year reanalysis project. *Bulletin of the American meteorological Society*, 77(3):437–472.

Kemppinen, K., Holden, P. B., Edwards, N. R., Ridgwell, A., and Friend, A. D. (2019). Coupled climate–carbon cycle simulation of the Last Glacial Maximum atmospheric CO_2 decrease using a large ensemble of modern plausible parameter sets. *Climate of the Past*, 15(3):1039–1062.

Kerr, J., Rickaby, R., Yu, J., Elderfield, H., and Sadekov, A. Y. (2017). The effect of ocean alkalinity and carbon transfer on deep-sea carbonate ion concentration during the past five glacial cycles. *Earth and Planetary Science Letters*, 471:42–53.

Kobayashi, H., Oka, A., Yamamoto, A., and Abe-Ouchi, A. (2021). Glacial carbon cycle changes by Southern Ocean processes with sedimentary amplification. *Science Advances*, 7(35):eabg7723.

Kohfeld, K. E., Quere, C. L., Harrison, S. P., and Anderson, R. F. (2005). Role of marine biology in glacial-interglacial CO_2 cycles. *Science*, 308(5718):74–78.

Kohfeld, K. E. and Ridgwell, A. (2009). Glacial-interglacial variability in atmospheric CO_2. *Surface ocean-lower atmosphere processes*, 187:251–286.

Köhler, P. and Bintanja, R. (2008). The carbon cycle during the mid Pleistocene transition: The Southern Ocean decoupling hypothesis. *Climate of the Past*, 4(4):311–332.

Köhler, P. and Munhoven, G. (2020). Late Pleistocene carbon cycle revisited by considering solid Earth processes. *Paleoceanography and Paleoclimatology*, 35(12):e2020PA004020.

Krakauer, N. Y., Randerson, J. T., Primeau, F. W., Gruber, N., and Menemenlis, D. (2006). Carbon isotope evidence for the latitudinal distribution and wind speed dependence of the air–sea gas transfer velocity. *Tellus B: Chemical and Physical Meteorology*, 58(5):390–417.

Kukla, G., An, Z., Melice, J., Gavin, J., and Xiao, J. (1990). Magnetic susceptibility record of Chinese loess. *Earth and Environmental Science Transactions of the Royal Society of Edinburgh*, 81(4):263–288.

Lindgren, A., Hugelius, G., and Kuhry, P. (2018). Extensive loss of past permafrost carbon but a net accumulation into present-day soils. *Nature*, 560(7717):219–222.

Lisiecki, L. E. and Raymo, M. E. (2005). A Pliocene-Pleistocene stack of 57 globally distributed benthic δ18O records. *Paleoceanography*, 20(1).

Loulergue, L., Schilt, A., Spahni, R., Masson-Delmotte, V., Blunier, T., Lemieux, B., Barnola, J.-M., Raynaud, D., Stocker, T. F., and Chappellaz, J. (2008). Orbital and millennial-scale features of atmospheric CH4 over the past 800,000 years. *Nature*, 453(7193):383–386.

Lüthi, D., Le Floch, M., Bereiter, B., Blunier, T., Barnola, J.-M., Siegenthaler, U., Raynaud, D., Jouzel, J., Fischer, H., Kawamura, K., et al. (2008). High-resolution carbon dioxide concentration record 650,000–800,000 years before present. *nature*, 453(7193):379–382.

Martin, J. H. (1990). Glacial-interglacial CO_2 change: The iron hypothesis. *Paleoceanography*, 5(1):1–13.

Menviel, L. and Joos, F. (2012). Toward explaining the Holocene carbon dioxide and carbon isotope records: Results from transient ocean carbon cycle-climate simulations. *Paleoceanography*, 27(1).

Menviel, L., Joos, F., and Ritz, S. (2012). Simulating atmospheric CO_2, ^{13}C and the marine carbon cycle during the Last Glacial–Interglacial cycle: possible role for a deepening of the mean remineralization depth and an increase in the oceanic nutrient inventory. *Quaternary Science Reviews*, 56:46–68.

Menviel, L., Mouchet, A., Meissner, K. J., Joos, F., and England, M. H. (2015). Impact of oceanic circulation changes on atmospheric $\delta^{13}CO_2$. *Global Biogeochemical Cycles*, 29(11):1944–1961.

Menviel, L., Timmermann, A., Timm, O. E., and Mouchet, A. (2011). Deconstructing the Last Glacial termination: the role of millennial and orbital-scale forcings. *Quaternary Science Reviews*, 30(9-10):1155–1172.

Morée, A. L., Schwinger, J., Ninnemann, U. S., Jeltsch-Thömmes, A., Bethke, I., and Heinze, C. (2021). Evaluating the biological pump efficiency of the Last Glacial Maximum ocean using $\delta^{13}C$. *Climate of the Past*, 17(2):753–774.

Müller, S., Joos, F., Edwards, N., and Stocker, T. (2006). Water mass distribution and ventilation time scales in a cost-efficient, three-dimensional ocean model. *Journal of Climate*, 19(21):5479–5499.

Müller, S. A., Joos, F., Plattner, G.-K., Edwards, N. R., and Stocker, T. F. (2008). Modeled natural and excess radiocarbon: Sensitivities to the gas exchange formulation and ocean transport strength. *Global Biogeochemical Cycles*, 22(3).

Munhoven, G. (2002). Glacial–interglacial changes of continental weathering: estimates of the related CO_2 and HCO_3^- flux variations and their uncertainties. *Global and Planetary Change*, 33(1-2):155–176.

Najjar, R., Orr, J., Sabine, C., and Joos, F. (1999). Biotic-HowTo. *Internal OCMIP Report, LSCE/CEA Saclay, Gifsur-Yvette, France*.

Oliver, K. I., Hoogakker, B. A., Crowhurst, S., Henderson, G., Rickaby, R. E., Edwards, N., and Elderfield, H. (2010). A synthesis of marine sediment core δ^{13}C data over the last 150 000 years. *Climate of the Past*, 6(5):645–673.

Opdyke, B. N. and Walker, J. C. (1992). Return of the coral reef hypothesis: Basin to shelf partitioning of $CaCO_3$ and its effect on atmospheric CO_2. *Geology*, 20(8):733–736.

Orr, J. and Epitalon, J.-M. (2015). Improved routines to model the ocean carbonate system: mocsy 2.0. *Geoscientific Model Development*, 8(3):485–499.

Orr, J., Najjar, R., Sabine, C., and Joos, F. (1999). Abiotic-HowTo. *Internal OCMIP Report, LSCE/CEA Saclay, Gifsur-Yvette, France*, 1999.

Orr, J. C., Najjar, R. G., Aumont, O., Bopp, L., Bullister, J. L., Danabasoglu, G., Doney, S. C., Dunne, J. P., Dutay, J.-C., Graven, H., et al. (2017). Biogeochemical protocols and diagnostics for the CMIP6 Ocean Model Intercomparison Project (OMIP). *Geoscientific Model Development*, 10(6):2169–2199.

Parekh, P., Joos, F., and Müller, S. A. (2008). A modeling assessment of the interplay between aeolian iron fluxes and iron-binding ligands in controlling carbon dioxide fluctuations during Antarctic warm events. *Paleoceanography*, 23(4).

Peterson, C. D. and Lisiecki, L. E. (2018). Deglacial carbon cycle changes observed in a compilation of 127 benthic δ^{13}C time series (20–6 ka). *Climate of the Past*, 14(8):1229–1252.

Petit, J.-R., Jouzel, J., Raynaud, D., Barkov, N. I., Barnola, J.-M., Basile, I., Bender, M., Chappellaz, J., Davis, M., Delaygue, G., et al. (1999). Climate and atmospheric history of the past 420,000 years from the Vostok ice core, Antarctica. *Nature*, 399(6735):429–436.

Pollock, D. E. (1997). The role of diatoms, dissolved silicate and Antarctic glaciation in glacial/interglacial climatic change: a hypothesis. *Global and Planetary Change*, 14(3-4):113–125.

Pöppelmeier, F., Jeltsch-Thömmes, A., Lippold, J., Joos, F., and Stocker, T. F. (2023). Multi-proxy constraints on Atlantic circulation dynamics since the last ice age. *Nature geoscience*, 16(4):349–356.

Pöppelmeier, F., Scheen, J., Jeltsch-Thömmes, A., and Stocker, T. F. (2020). Simulated stability of the AMOC during the Last Glacial Maximum under realistic boundary conditions. *Climate of the Past Discussions*, 2020:1–28.

Qin, B., Li, T., Xiong, Z., Algeo, T., and Jia, Q. (2018). Deep-Water Carbonate Ion Concentrations in the Western Tropical Pacific Since the Mid-Pleistocene: A Major Perturbation During the Mid-Brunhes. *Journal of Geophysical Research: Oceans*, 123(9):6876–6892.

Raven, J. A. and Falkowski, P. G. (1999). Oceanic sinks for atmospheric CO_2. *Plant, Cell & Environment*, 22(6):741–755.

Ridgwell, A. J., Watson, A. J., Maslin, M. A., and Kaplan, J. O. (2003). Implications of coral reef buildup for the controls on atmospheric CO_2 since the Last Glacial Maximum. *Paleoceanography*, 18(4).

Roberts, J., Gottschalk, J., Skinner, L. C., Peck, V. L., Kender, S., Elderfield, H., Waelbroeck, C., Vázquez Riveiros, N., and Hodell, D. A. (2016). Evolution of South Atlantic density and chemical stratification across the last deglaciation. *Proceedings of the National Academy of Sciences*, 113(3):514–519.

Roth, R., Ritz, S., and Joos, F. (2014). Burial-nutrient feedbacks amplify the sensitivity of atmospheric carbon dioxide to changes in organic matter remineralisation. *Earth System Dynamics*, 5(2):321–343.

Sarmiento, J. L. (2006). *Ocean biogeochemical dynamics*. Princeton university press.

Sarnthein, M., Schneider, B., and Grootes, P. M. (2013). Peak glacial ^{14}C ventilation ages suggest major draw-down of carbon into the abyssal ocean. *Climate of the Past*, 9(6):2595–2614.

Schmitt, J., Schneider, R., Elsig, J., Leuenberger, D., Lourantou, A., Chappellaz, J., Köhler, P., Joos, F., Stocker, T. F., Leuenberger, M., et al. (2012). Carbon isotope constraints on the deglacial CO_2 rise from ice cores. *Science*, 336(6082):711–714.

Schmittner, A. (2003). Southern Ocean sea ice and radiocarbon ages of glacial bottom waters. *Earth and Planetary Science Letters*, 213(1-2):53–62.

Schmittner, Andreas Galbraith, E. D. (2008). Glacial greenhouse-gas fluctuations controlled by ocean circulation changes. *Nature*, 546.

Schneider, R., Schmitt, J., Köhler, P., Joos, F., and Fischer, H. (2013). A reconstruction of atmospheric carbon dioxide and its stable carbon isotopic composition from the penultimate glacial maximum to the last glacial inception. *Climate of the Past*, 9(6):2507–2523.

Shackleton, N. J. (2000). The 100,000-year ice-age cycle identified and found to lag temperature, carbon dioxide, and orbital eccentricity. *Science*, 289(5486):1897–1902.

Shao, J., Stott, L. D., Gray, W. R., Greenop, R., Pecher, I., Neil, H. L., Coffin, R. B., Davy, B., and Rae, J. W. (2019). Atmosphere-ocean CO_2 exchange across the last deglaciation from the boron isotope proxy. *Paleoceanography and Paleoclimatology*, 34(10):1650–1670.

Siegenthaler, U., Stocker, T. F., Monnin, E., Luthi, D., Schwander, J., Stauffer, B., Raynaud, D., Barnola, J.-M., Fischer, H., Masson-Delmotte, V., et al. (2005). Stable carbon cycle climate relationship during the Late Pleistocene. *Science*, 310(5752):1313–1317.

Sigman, D. M. and Boyle, E. A. (2000). Glacial/interglacial variations in atmospheric carbon dioxide. *Nature*, 407(6806):859–869.

Sigman, D. M. and Hain, M. P. (2024). Ocean oxygen, preformed nutrients, and the cause of the lower carbon dioxide concentration in the atmosphere of the last glacial maximum. *Paleoceanography and Paleoclimatology*, 39(1):e2023PA004775.

Sigman, D. M., Hain, M. P., and Haug, G. H. (2010). The polar ocean and glacial cycles in atmospheric CO_2 concentration. *Nature*, 466(7302):47–55.

Smith, H. J., Fischer, H., Wahlen, M., Mastroianni, D., and Deck, B. (1999). Dual modes of the carbon cycle since the Last Glacial Maximum. *Nature*, 400(6741):248–250.

Stein, K., Timmermann, A., Kwon, E. Y., and Friedrich, T. (2020). Timing and magnitude of Southern Ocean sea ice/carbon cycle feedbacks. *Proceedings of the National Academy of Sciences*, 117(9):4498–4504.

Stephens, B. B. and Keeling, R. F. (2000). The influence of Antarctic sea ice on glacial–interglacial CO_2 variations. *Nature*, 404(6774):171–174.

Tschumi, T., Joos, F., Gehlen, M., and Heinze, C. (2011). Deep ocean ventilation, carbon isotopes, marine sedimentation and the deglacial CO_2 rise. *Climate of the Past*, 7(3):771–800.

Tschumi, T., Joos, F., and Parekh, P. (2008). How important are Southern Hemisphere wind changes for low glacial carbon dioxide? A model study. *Paleoceanography*, 23(4).

Volk, T. and Hoffert, M. I. (1985). Ocean carbon pumps: Analysis of relative strengths and efficiencies in ocean-driven atmospheric CO_2 changes. *The carbon cycle and atmospheric CO2: Natural variations Archean to present*, 32:99–110.

Vollmer, T., Ito, T., and Lynch-Stieglitz, J. (2022). Proxy-Based Preformed Phosphate Estimates Point to Increased Biological Pump Efficiency as Primary Cause of Last Glacial Maximum CO_2 Drawdown. *Paleoceanography and Paleoclimatology*, 37(11):e2021PA004339.

Von Blanckenburg, F., Bouchez, J., Ibarra, D. E., and Maher, K. (2015). Stable runoff and weathering fluxes into the oceans over Quaternary climate cycles. *Nature Geoscience*, 8(7):538–542.

Wallmann, K., Schneider, B., and Sarnthein, M. (2016). Effects of eustatic sea-level change, ocean dynamics, and nutrient utilization on atmospheric pCO_2 and seawater composition over the last 130 000 years: a model study. *Climate of the Past*, 12(2):339–375.

Wanninkhof, R. (2014). Relationship between wind speed and gas exchange over the ocean revisited. *Limnology and Oceanography: Methods*, 12(6):351–362.

Weiss, R. (1974). Carbon dioxide in water and seawater: the solubility of a non-ideal gas. *Marine chemistry*, 2(3):203–215.

Wenk, T. and Siegenthaler, U. (1985). The high-latitude ocean as a control of atmospheric CO_2. *The carbon cycle and atmospheric CO2: natural variations Archean to present*, 32:185–194.

Willeit, M., Ganopolski, A., Calov, R., and Brovkin, V. (2019). Mid-Pleistocene transition in glacial cycles explained by declining CO_2 and regolith removal. *Science Advances*, 5(4):eaav7337.

Winckler, G., Anderson, R. F., Fleisher, M. Q., McGee, D., and Mahowald, N. (2008). Covariant glacial-interglacial dust fluxes in the equatorial Pacific and Antarctica. *science*, 320(5872):93–96.

Wood, M., Hayes, C. T., and Paytan, A. (2023). Global Quaternary Carbonate Burial: Proxy-and Model-Based Reconstructions and Persisting Uncertainties. *Annual review of marine science*, 15:277–302.

Yu, J., Anderson, R. F., Jin, Z., Rae, J. W., Opdyke, B. N., and Eggins, S. M. (2013). Responses of the deep ocean carbonate system to carbon reorganization during the Last Glacial–interglacial cycle. *Quaternary Science Reviews*, 76:39–52.

Yu, J., Menviel, L., Jin, Z., Thornalley, D., Foster, G. L., Rohling, E., McCave, I., McManus, J., Dai, Y., Ren, H., et al. (2019). More efficient North Atlantic carbon pump during the last glacial maximum. *Nature communications*, 10(1):2170.

Yu, Z., Loisel, J., Brosseau, D. P., Beilman, D. W., and Hunt, S. J. (2010). Global peatland dynamics since the last glacial maximum. *Geophysical research letters*, 37(13).

~~Ocean circulation changes~~Model limitations

~~The ocean circulation changes in all experiments due to the prescribed changes in insolation, radiative forcings from greenhouse gasses and land albedo. These forcings result in cyclic transitions between interglacial and glacial circulation states. The glacial states show a reduction of the Atlantic Meridional Overturning Circulation (AMOC) by up to 4.5 Sv and an increase of the shallow overturning cell in the equatorial Pacific north of the Equator of up to 1 Sv compared to the PI (Fig S8). Accordingly, water mass ages increase below 2000 m in the North Atlantic and decrease in the South Atlantic and Pacific during glacials. With additional wind stress reductions in the Southern Ocean (SO, <40°S, simulation SOWI), the South Pacific downwelling is strengthened by up to 1.5 Sv locally in glacials, and the AMOC strength further reduced by up to 1 Sv. The increased stratification in~~ There are several ways in which the amplitude or regional pattern of the simulated changes might be biased by our experiment design. Firstly, by design our forcings are smooth in time and spatially uniform, which is a stark simplification. For example, the PO4 forcing ties nutrient supply to the δ^{18}O record. The correlation between dust (iron source to the ~~SO reduces upwelling and increases the water mass age throughout the Pacific and South Atlantic by up to 150 years. The slower AMOC also results in ~100 yr older waters below 2000 m in the North Atlantic. If instead of the wind stress the glacial radiative forcing is further reduced (by 2.5 Wm^{-2}, simulation AERO), AMOC weakens in all glacials by up to 12 Sv relative to PI during the glacial maxima (the model behaviour to this forcing is described more extensively in Adloff et al., 2023). The Pacific circulation is much less affected, showing only a small decrease (up to 1 Sv) in the Pacific Meridional Overturning Circulation (PMOC, here evaluated at 30degS). As a result of the AMOC collapse, the Atlantic water mass age increase caused by the standard forcing is amplified, with an aging of up to 1000 years in the deep North Atlantic as glacial deep water formation now only occurs in~~ open ocean) concentrations in the EPICA Dome C ice core and benthic δ^{18}O is of first order only and varies over the glacial cycle (Winckler et al., 2008). Several macro- and micronutrients were likely supplied to varying parts of the glacial ocean (Broecker, 1982b; Martin, 1990; Pollock, 1997; Deutsch et al., 2004) and while dust flux changes seem to correlate globally (Kukla et al., 1990; Winckler et al., 2008), the ~~Southern Ocean~~timings and rates of other nutrient fluxes might in reality have varied temporally and spatially. Similarly, our other forcings might change more slowly over the deglaciation than the real processes they mimick.

Another simplification in our experiment design is that the majority of our simulations assume temporally constant terrestrial solute inputs although in reality these fluxes are climate sensitive (Munhoven, 2002). It is unlikely that removing this simplification would substantially alter the simulated global carbon fluxes and reservoir size changes because it is estimated that global weathering rate changes during glacial cycles were small despite large local variability, possibly because they canceled out in the global mean (Jones et al., 2002; Von Blanckenburg et al., 2015; Frings, 2019; Börker et al., 2020). It was estimated that glacial-interglacial weathering flux changes altered atmospheric CO_2 by a maximum of 20 ppm (Köhler and Munhoven, 2020) . Yet, the resulting δ^{13}C perturbation could be larger because a global balance in carbon flux changes does not imply a balance in carbon isotope fluxes (Jeltsch-Thömmes and Joos, 2023). Additionally, there might have been non-linear changes in isotopic input fluxes during the simulated time period.

~~These circulation changes are largest in MIS 16a, 6a and 2, when the respective forcings are strongest, and also appear in interglacials that were colder than the PI , although at much smaller amplitude~~

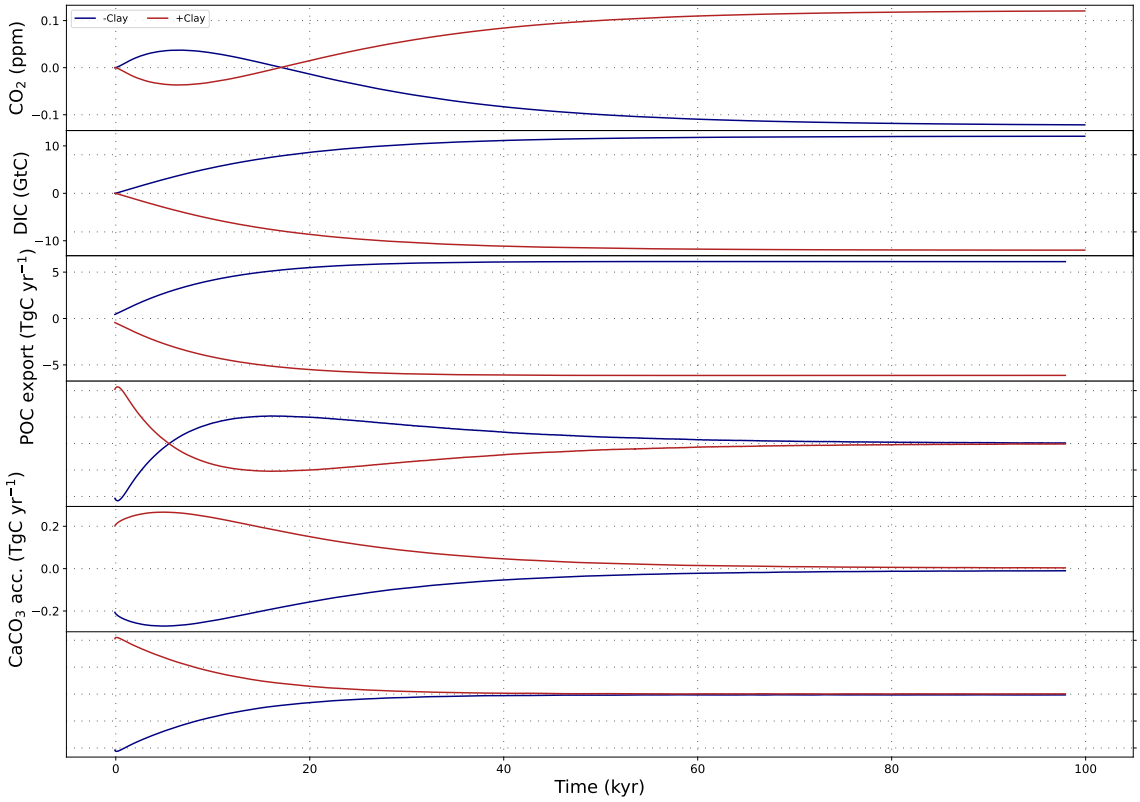

Figure S1. The effect of step changes of plus or minus 30% of the prescribed clay flux on atmospheric CO_2 concentrations, DIC and carbon fluxes over 100 kyr.

Finally, the imbalance between weathering and burial fluxes is also shaped by the sedimentation rate. In our simulations, sedimentation rates vary due to changes in biogenic export, yet accumulation of non-biogenic material was kept constant. This omission, however, is not a large error source, given that a separately prescribed step-wise 30% increase and decrease of the non-biogenic flux in the PI steady state had only marginal effects on atmospheric CO_2, DIC and sedimentary accumulation of biogenic particles (Fig. S1).

Effects of orbital, insolation and albedo changes on carbon fluxes

In the following, we examine the underlying glacial-interglacial carbon cycle changes and the effect of interactive sediments under each forcing. First we focus on the standard forcing, before discussing the effects of additional forcings.

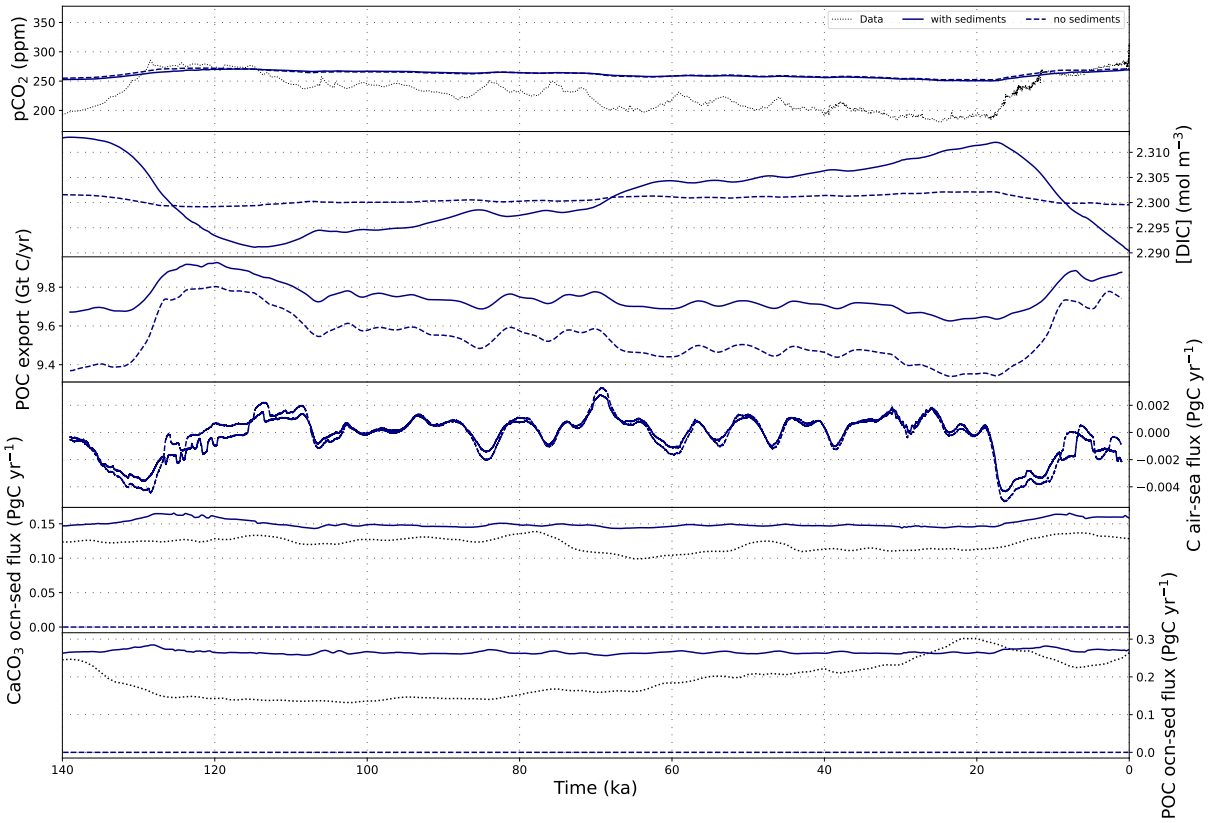

Figure S2. Atmospheric CO_2 concentrations, DIC and carbon fluxes over the most recent full glacial cyle in simulation BASE with and without dynamic sediments.

The dynamic circulation and climate affect the partitioning of carbon between the interactive carbon reservoirs in the model (atmosphere, ocean, reactive sediments and lithosphere). The applied forcings vary the CO_2 concentration gradient between air and seawater by modifying CO_2 solubility and surface ocean DIC and alkalinity concentrations. Without dynamic sediments (Fig S2), carbon in response moves between the atmosphere, the marine DIC and, to a lesser extent, DOC reservoirs in the ocean. With the standard forcing, CO_2 and O_2 solubilities increase during glacial phases because of the cooling surface ocean, leading to a steady marine uptake of carbon and oxygen from the atmosphere from peak interglacial through to the glacial maximum. The cooling reduces deep water formation rates in the North Atlantic and increases deep water formation in the Southern Ocean. These circulation changes increase the marine uptake of CO_2 while expanding sea ice prevents outgassing of marine CO_2 in the Southern Ocean. ~~Circulation changes also redistribute dissolved nutrients. Polar export production declines due to the amplified cooling in polar oceans and expanding sea ice, causing an overall productivity~~ Overall POC and $CaCO_3$ export fluxes decrease during glaciation despite increased primary productivity in mid-latitudes and sub-tropics due to ~~the circulation-driven reduction of nutrient transport into the polar oceans. In~~ reduced export production in the high latitudes, ~~POC and $CaCO_3$ export fluxes decrease,~~ predominantly due to sea ice growth, in places also because of reduced nutrient supply and

lower temperatures. These export fluxes changes, particularly in the Southern Ocean, alter phosphate cycling: In interglacial states, high export fluxes effectively transfer phosphate from the photic zone to the intermediate ocean, where most exported POC is remineralized. Upwelling of intermediate water masses returns phosphate to the surface ocean. In glacial states, less of the phosphate upwelling in the Southern Ocean is incorporated into POC and exported to intermediate ocean depths. Instead, it is downwelled and incorporated into bottom waters. In consequence, the glacial deep ocean is enriched in preformed phosphate, while phosphate concentrations at intermediate depth decrease due to climate-driven export reduction. In the surface, reduced upwelling of nutrients and reduced nutrient uptake result in almost no net change of nutrient concentrations. During deglaciation, surface and deep waters warm and upwelling as well as export fluxes are restored. Hence, decreases in atmospheric CO_2 concentration during the onsets of glaciations are directly mirrored by increases in marine DIC and decreases in marine DOC, and the inverse occurs during deglaciation.

When interactive sediments are included in the simulations, export production and ocean chemistry changes ~~also~~ alter sediment burial and dissolution fluxes, resulting in more than 10x larger DIC fluctuations over a glacial cycle than in the ~~previous,~~ closed system. Changes in net sea-air gas exchange across the glacial cycle ($\sim$0.007 PgC/yr) are smaller than changes in each POC and $CaCO_3$ burial rates ($\sim$0.02 PgC/yr). $CaCO_3$ burial is predominantly driven by productivity changes and peaks during interglacials. In glacials, $CaCO_3$ burial is reduced below areas with reduced euphotic zone $CaCO_3$ export, e.g. in the high latitudes, but additionally where $CaCO_3$ becomes unstable due lower temperatures or reduced pH due to increased sedimentary POC oxydation rates. The standard forcing is not sufficient to cause wide-spread O_2 depletion in the glacial deep ocean, hence under the standard forcing POC burial rates are driven by export production rates, with less/more burial in areas with reduced/increased POC export production, respectively. The exception is the upwelling zone in the Equatorial East Pacific and parts of the Indian Ocean, where increased POC export depletes benthic and sediment pore water O_2 during glacial phases. During deglaciations, sea ice recedes, ocean ventilation increases and the surface and intermediate oceans warm, fostering increased primary productivity. While productivity and POC burial increase quickly in the subpolar regions, POC burial rates in the Eastern Equatorial Pacific respond more slowly to the warming: Long turnover timescales of pore water O_2 in sediments and remineralisation of previously deposited POC delay the return of interglacial POC remineralisation rates relative to export rates from the surface ocean. Therefore, deglaciations are marked by faster productivity increases in the surface ocean than sedimentary POC remineralisation. This results in a 'sweet spot' during glacial terminations, when tropical POC burial is still higher than in the interglacial while extratropical POC export and burial has already recovered to interglacial levels, particularly during the last 400 kyr which show larger glacial-interglacial temperature contrasts and faster warming rates during deglaciations. This 'sweet spot' causes the maximum of global POC burial to occur during deglaciation, before the full interglacial.

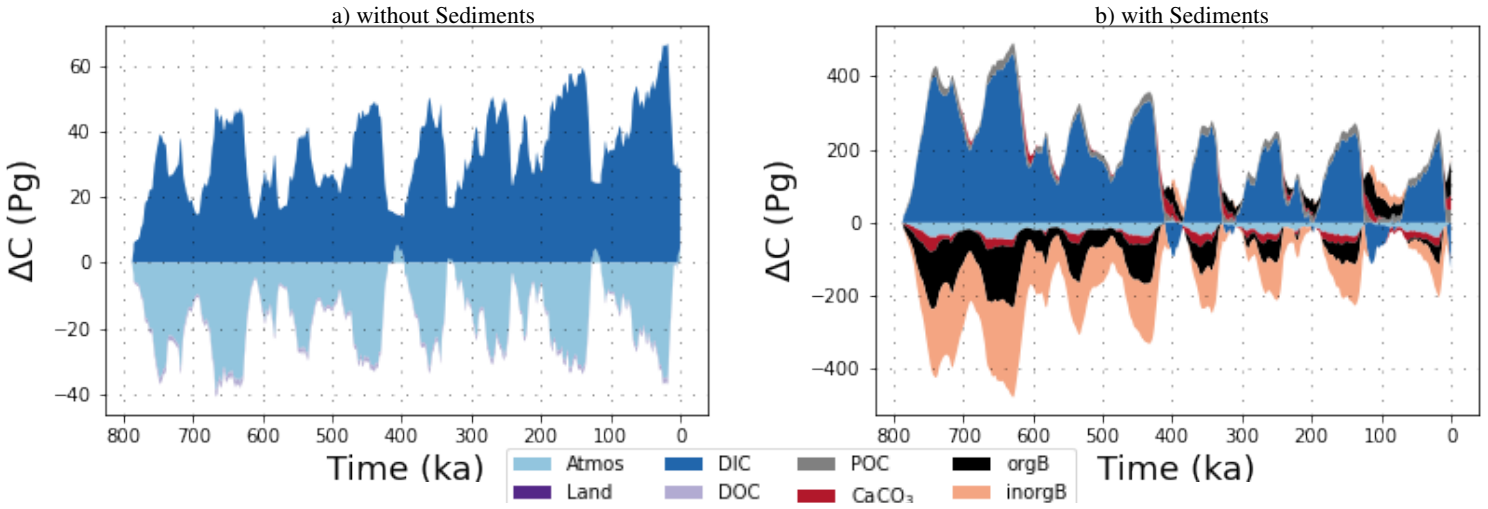

Figure S3. Transient carbon reservoir size changes across the last 780kyr as simulated in simulations with the standard (orbital, radiation and albedo) forcings in simulation BASE with and without dynamic marine sediments. Shown are the size changes of atmospheric, terrestrial, marine (DIC and DOC), sedimentary (POC and $CaCO_3$) and lithospheric (organic and inorganic) carbon storage. Note that the y-axis scale is an order of magnitude larger in b) than in a).

Introducing sediments (and a constant weathering flux) also changes carbon cycle dynamics over multiple glacial cycles. Fig S3 shows the transient changes in the simulated carbon reservoirs in simulation BASE over the entire simulated time period. In our set-up, carbon exchange between the atmosphere, ocean and sediments reacts to climatic and ~~biochemical~~ biogeochemical changes while weathering input fluxes of DIC, alkalinity and PO_4^{3-} are constant over time. A carbon flux imbalance arises during glacial phases in this open system. Under purely physical forcings, export fluxes from the photic zone decrease during glacial phases. Despite locally increased sedimentary POC preservation, global sediment accumulation rates decrease. In consequence, ~~transfer~~ sequestration of $CaCO_3$ and POC from the reactive sediments ~~to the lithosphere~~ (i.e. sediment burial) is reduced as well, since it is governed by the mass accumulation rate. The carbon which would have otherwise been buried instead accumulates as DIC in the ocean. Acceleration of sediment mass accumulation rates during glacial terminations increases ~~the carbon transfer into the lithosphere~~sediment burial, which reduces marine DIC. The strength of these carbon cycle responses depends on the forcing strength, which varies between glacial cycles. The lukewarm interglacials of the first 350 kyr of our simulations do not restore the export fluxes and sedimentary $CaCO_3$ preservation required to re-balance the geologic carbon cycle, and so marine DIC concentrations are persistently higher during 800-450ka than at PI. Interglacials of the last 450kyr of the simulation reduce DIC in the long-term because they are warm and long enough for increased carbon transfer into sediments and ~~the lithosphere~~sediment burial.

Effects of additional forcings and Earth system changes on carbon fluxes

The previously described carbon cycle changes vary when further forcings and Earth system changes are applied.

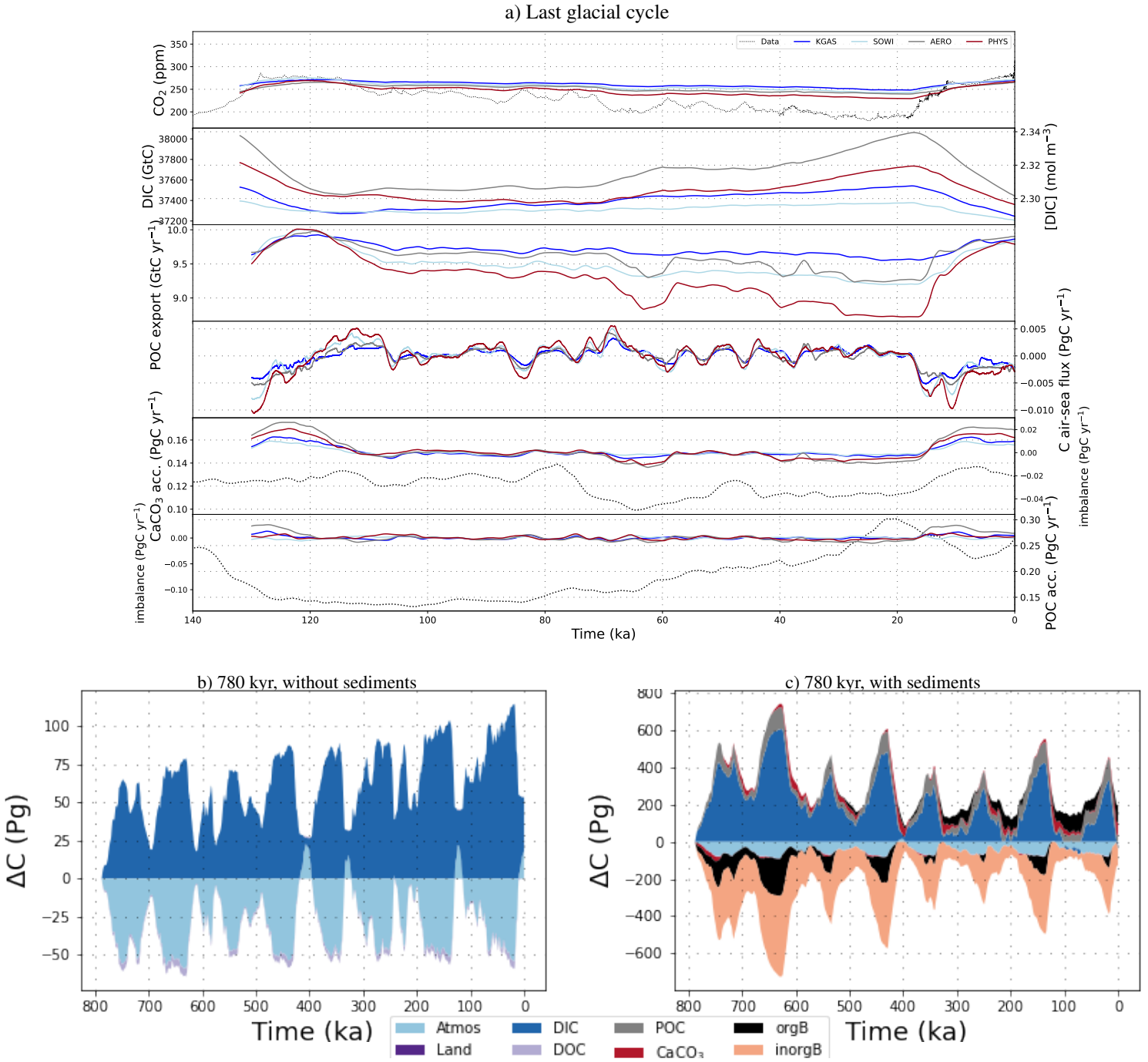

Figure S4. a) Atmospheric CO_2 concentrations, DIC and carbon fluxes over the most recent full glacial cyle in simulations with additional physical forcings in an open system. b) Transient carbon reservoir size changes across the last 780 kyr as simulated with all additional physical forcings combined in a closed system and c) in an open system. Shown are the size changes of atmospheric, terrestrial, marine (DIC and DOC), sedimentary (POC and $CaCO_3$) and lithospheric (organic and inorganic) carbon storage. Reservoir changes for individual forcings are displayed in Fig S23. Flux timeseries for simulations in a closed system are displayed in Fig S24.

Additional physical forcings result in roughly 1.5x larger carbon fluxes (Fig. S4), partially by amplifying the processes under the standard forcing and partially by introducing additional ones. Additional reduction of wind stress in the Southern Ocean (simulation SOWI) leads to a stronger isolation of deep Pacific water masses, reducing benthic oxygen levels~~and pH and increasing the carbon content of the glacial deep Pacific~~. With dynamic sediments, more organic matter and $CaCO_3$ reaching the sediments is preserved due to the reduced oxygen concentrations, particularly in Pacific upwelling zones. This results in a larger net removal of nutrients and carbon from the ocean during glacial times which would have otherwise been released at intermediate depth. In consequence, wind stress forcing over the Southern Ocean reduces the carbon content of Pacific deep water when dynamic sediments are considered, despite an increase in water mass age. The re-ventilation of the deep Pacific during glacial termination leads to rising benthic oxygen concentrations. Due to the lower storage of dissolved nutrients and carbon in the glacial deep ocean, the potential to upwell nutrients during deglaciation is reduced, suppressing the spike in POC burial during terminations seen under the standard forcing and reducing PIC burial during these transition phases.

Reducing the transfer velocity of CO_2 in the Southern Ocean during glacials (simulation KGAS) also reduces CO_2 outgassing in the Southern Ocean which increases DIC in the deep Pacific but leaves ocean circulation unaffected, which reduces its global impact and, unlike the wind forcing, does not trap nutrients in the deep Pacific.

The AMOC slow-down in simulations with an additional reduction of incoming radiation during glacial phases and especially glacial maxima (e.g. via aerosol dimming, simulation AERO) creates an old, nutrient-rich and O_2-poor bottom water mass in the glacial Atlantic. Unlike with a vigorous AMOC, nutrients are not returned as quickly to the surface Atlantic but accumulate in the deep. The additional cooling combined with reduced nutrient supply reduces POC and $CaCO_3$ export in the Atlantic. In the North, where sea ice extent is increased and temperatures drop the most, they cease entirely. Globally, the additional cooling increases CO_2 and O_2 solubility. Overall these effects increase glacial carbon storage in the deep ocean. With dynamic sediments, the reduced $CaCO_3$ export in the North Atlantic raises the local lysocline, causing dissolution and increased marine DIC concentrations. The sudden shift in water masses when AMOC resumes during deglaciation amplifies the spike in burial rates observed under the standard forcing.

The different carbon and nutrient fluxes under these forcings change the total carbon and nutrient inventories in simulations with an open system, resulting in different DIC and nutrient concentrations at the start of the last glacial cycle and at the end of the runs.

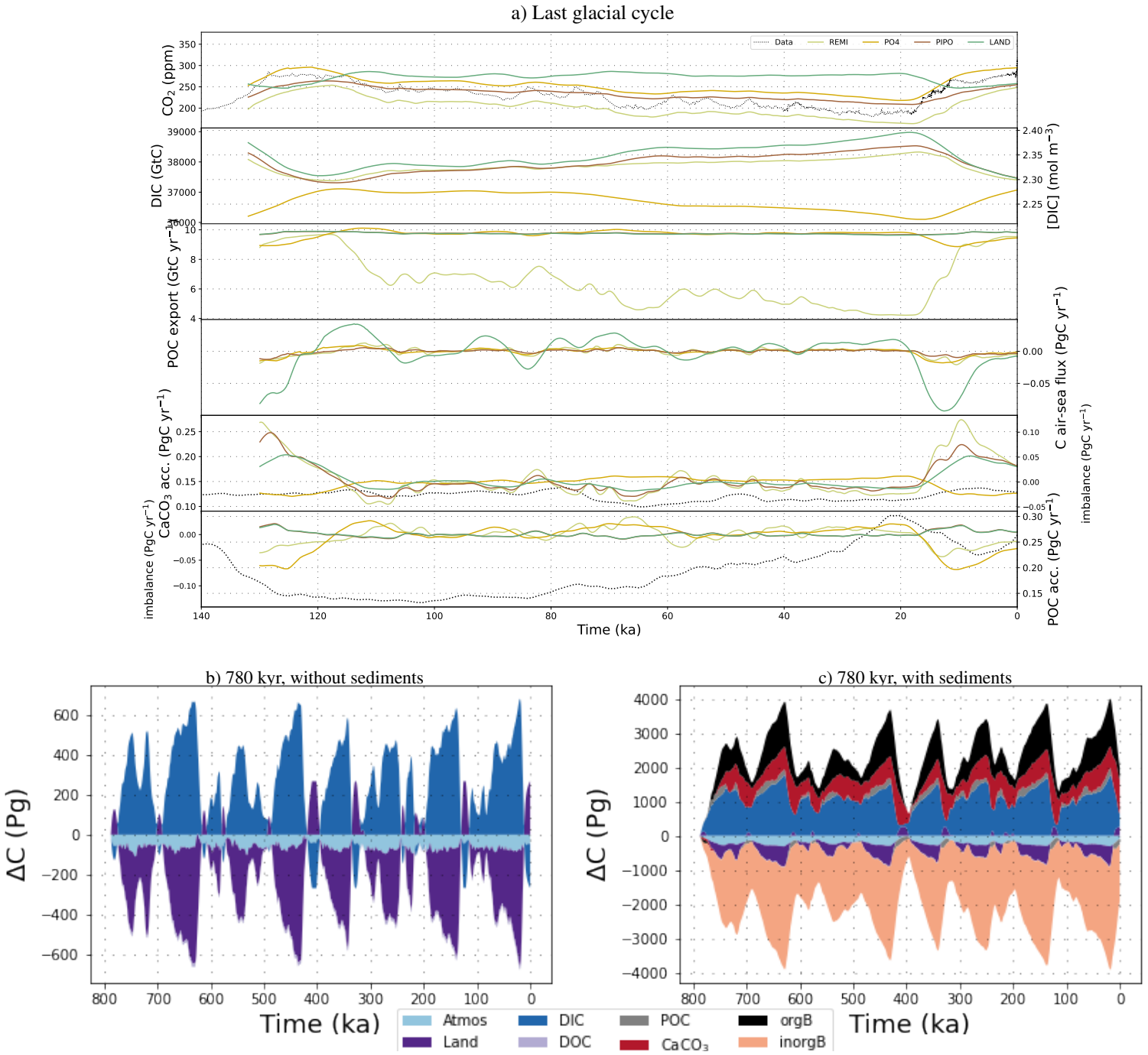

Figure S5. a) Atmospheric CO_2 concentrations, DIC and carbon fluxes over the most recent full glacial cyle in simulations with additional ~~biochemical~~ biogeochemical forcings in an open system. b) Transient carbon reservoir size changes across the last 780 kyr as simulated with all additional ~~biochemical~~ biogeochemical forcings combined in a closed system and c) in an open system. Shown are the size changes of atmospheric, terrestrial, marine (DIC and DOC), sedimentary (POC and $CaCO_3$) and lithospheric (organic and inorganic) carbon storage. Reservoir changes for individual forcings are displayed in Fig S25 and **??**. Flux timeseries for simulations in a closed system are displayed in Fig **??**.

~~Biochemical~~ Biogeochemical forcings affect carbon transfer primarily through the biological pump and the size of the terrestrial carbon sink. Nutrient inputs during glacial phases in simulation PO4 increase POC and $CaCO_3$ export, and sedimentary burial rates through increased sedimentary mass accumulation and lower O_2 concentrations in the deep ocean (Fig S5). During glacial termination, the prescribed nutrient supply to the surface ocean stops before the deep ocean is fully re-ventilated and the nutrients that accumulated in intermediate and deep water masses have returned to the surface. This delay results in low nutrient concentrations in the surface ocean, a transient drop in POC export, and consequentially burial fluxes. The reduced carbon burial raises DIC and increases the net carbon transfer from surface waters to the atmosphere during deglaciation. In consequence, when nutrients are added to a glacial ocean with responsive sediments, glacial phases become the dominant periods of organic and inorganic C ~~transfer to the lithosphere~~sediment burial, reducing the accumulation of marine DIC and increasing the marine uptake of atmospheric CO_2 during glacial phases. This simulation PO4 yields the temporal CO_2 evolution which most closely resembles reconstructions from ice cores.

Reducing the PIC:POC ratio of export production during glacial phases (simulation PIPO) increases alkalinity in the surface ocean which enhances marine carbon uptake from the atmosphere, resulting in an additional CO_2 drawdown of up to $\sim$10ppm without sediments. This effect is enhanced by 20ppm when dynamic sediments are considered. When the export production is tilted towards organic matter production in an ocean with interactive sediments, reduced $CaCO_3$ export during inceptions and glacial periods translate into reduced $CaCO_3$ burial rates. This leads to a shoaling of the carbonate compensation depth, a build-up of alkalinity in the ocean and increased carbon transfer from the atmosphere to the ocean. The reduced sedimentary carbonate accumulation reduces the total mass flux to the sediments. On extratropical continental slopes, the reduced mass accumulation slows organic carbon burial, retaining more nutrients in the ocean and decreasing O_2 concentrations through continued remineralization instead. On continental slopes under upwelling areas with high productivity, the reduced O_2 expands the O_2 minimum zones, an effect which outweighs the local reduction of carbonate export and results in higher POC burial rates despite less carbonate deposition. Restoration of the interglacial PIC:POC ratio during deglaciation then enhances sedimentary carbonate deposition in benthic waters with higher pH and larger O_2 minimum zones than under the standard forcing, increasing the temporal spikes in carbonate and POC burial. Reduced glacial PIC:POC increases $CaCO_3$ burial events during glacial terminations.

Lowering the remineralization depth of organic matter in the glacial water column (simulation REMI) leads to a net carbon and nutrient transfer from the surface ocean to intermediate and deep water masses, where more O_2 is consumed. Without dynamic sediments, the increased DIC concentrations in the deep ocean increases the carbon storage of the glacial ocean. In addition, the reduced dissolution of POC in the upper water column during glacials increases surface ocean pH and CO_2 uptake by the ocean. With dynamic sediments, the resulting reduction in deep ocean O_2 concentration increases POC preservation in sediments below high productivity zones, e.g. tropical continental margins and upwelling areas. Where the larger flux of POC reaching the sediments is not preserved, it is remineralized, reducing the stability of sedimentary $CaCO_3$. Glacial inceptions are then characterized by increased POC and POP fluxes into the sediments and reduced $CaCO_3$ burial. During glacial terminations, POC is increasingly remineralized at shallower depth again, leading to reduced POC fluxes into the deep ocean and POC burial compared to the glacial phase. Surface ocean pH decreases and C is returned to the atmosphere. Compared to the standard

forcing, lowering the remineralization depth thus shifts the timing of maximal POC burial rates from the interglacial to the glacial and amplifies the transient spike in $CaCO_3$ burial as increased nutrient supply during glacials does, but it also increases sedimentary $CaCO_3$ dissolution during glacial phases.

Land carbon release to the atmosphere during glacial phases (simulation LAND) invades and acidifies the ocean due to increased atmospheric concentrations, growing the marine DIC reservoir during glacials with and without dynamic sediments, resulting in the biggest glacial marine DIC reservoirs across our simulations. When interactive sediments are considered, this marine carbon uptake reduces $CaCO_3$ preservation and leads to a shoaling of the lysocline. During termination, as the external carbon addition subsides, the ocean vents carbon back into the atmosphere, transiently allowing for increased $CaCO_3$ burial.

The previous paragraphs show that varying biogenic particle production in the surface ocean is only a relevant control on marine carbon storage changes when interactive sediments are simulated. Instead, lowering the main remineralization depth (simulation REMI) and adding terrestrial carbon release during glaciation (simulation LAND) strongly influence marine carbon storage with and without dynamic sediments. Without dynamic sediments, they double the marine carbon uptake during glacial periods. When including interactive sediments, all ~~biochemical~~ biogeochemical forcings have substantially larger effects on the carbon cycle than physical changes, with 5-10x larger carbon fluxes than under the standard forcing (Fig S5).

CO_2 restoring and non-linear effects of combined forcings on carbon fluxes

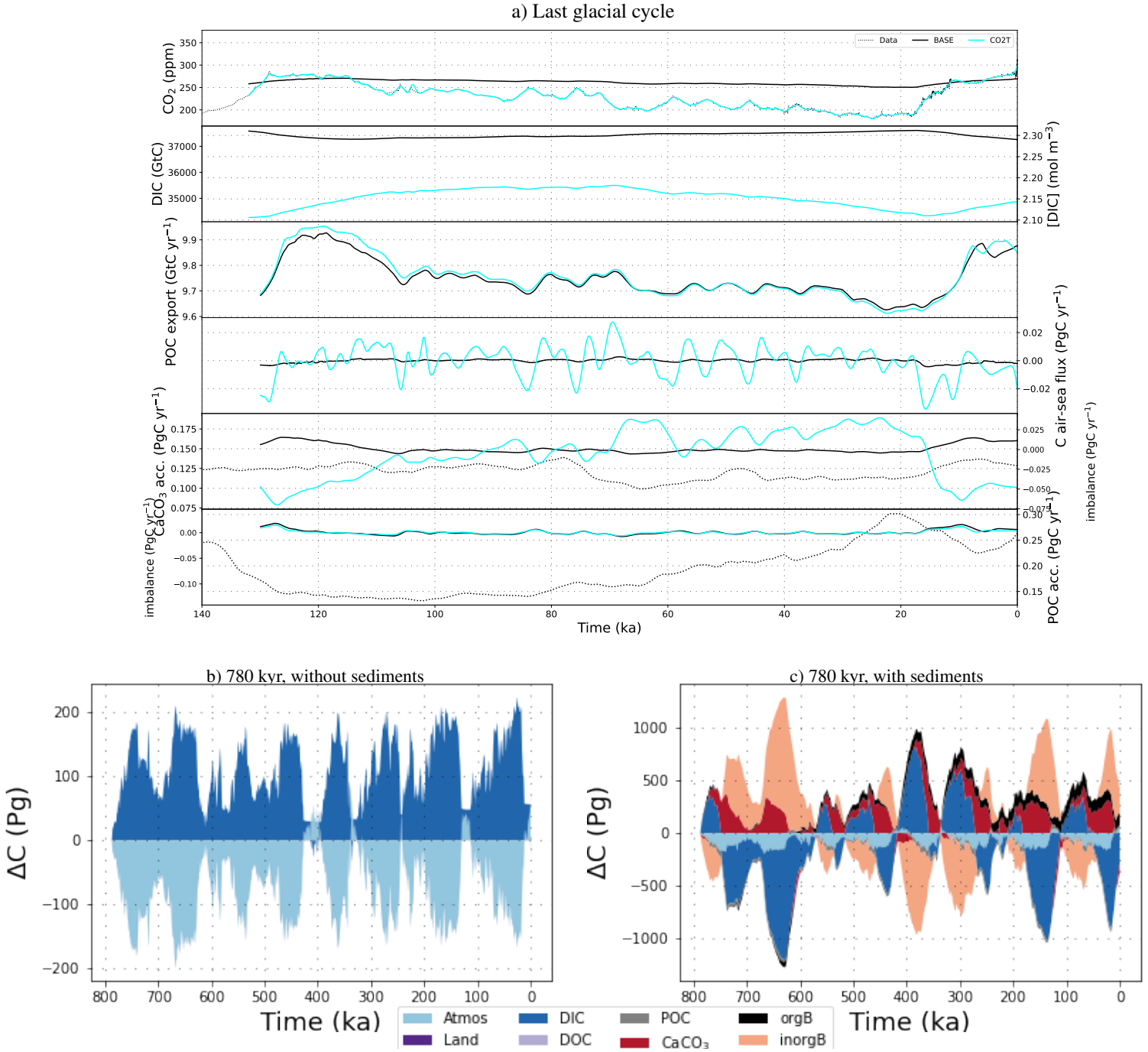

Figure S6. a) Atmospheric CO_2 concentrations, DIC and carbon fluxes over the most recent full glacial cyle in simulations BASE and CO2T in an open system. b) Transient carbon reservoir size changes across the last 780 kyr as simulated with alkalinity nudging in a closed system and c) in an open system. Shown are the size changes of atmospheric, terrestrial, marine (DIC and DOC), sedimentary (POC and $CaCO_3$) and lithospheric (organic and inorganic) carbon storage.

By design, the applied alkalinity nudging causes marine carbon uptake and release that shape atmospheric CO_2 in line with observations (Fig S6). As a consequence, the surface ocean is more alkaline in glacial times and more acidic during terminations than in the standard forcing, enabling increased marine carbon uptake. In simulations with dynamic sediments, $CaCO_3$ burial during cold phases is increased but the burial spike during terminations suppressed.

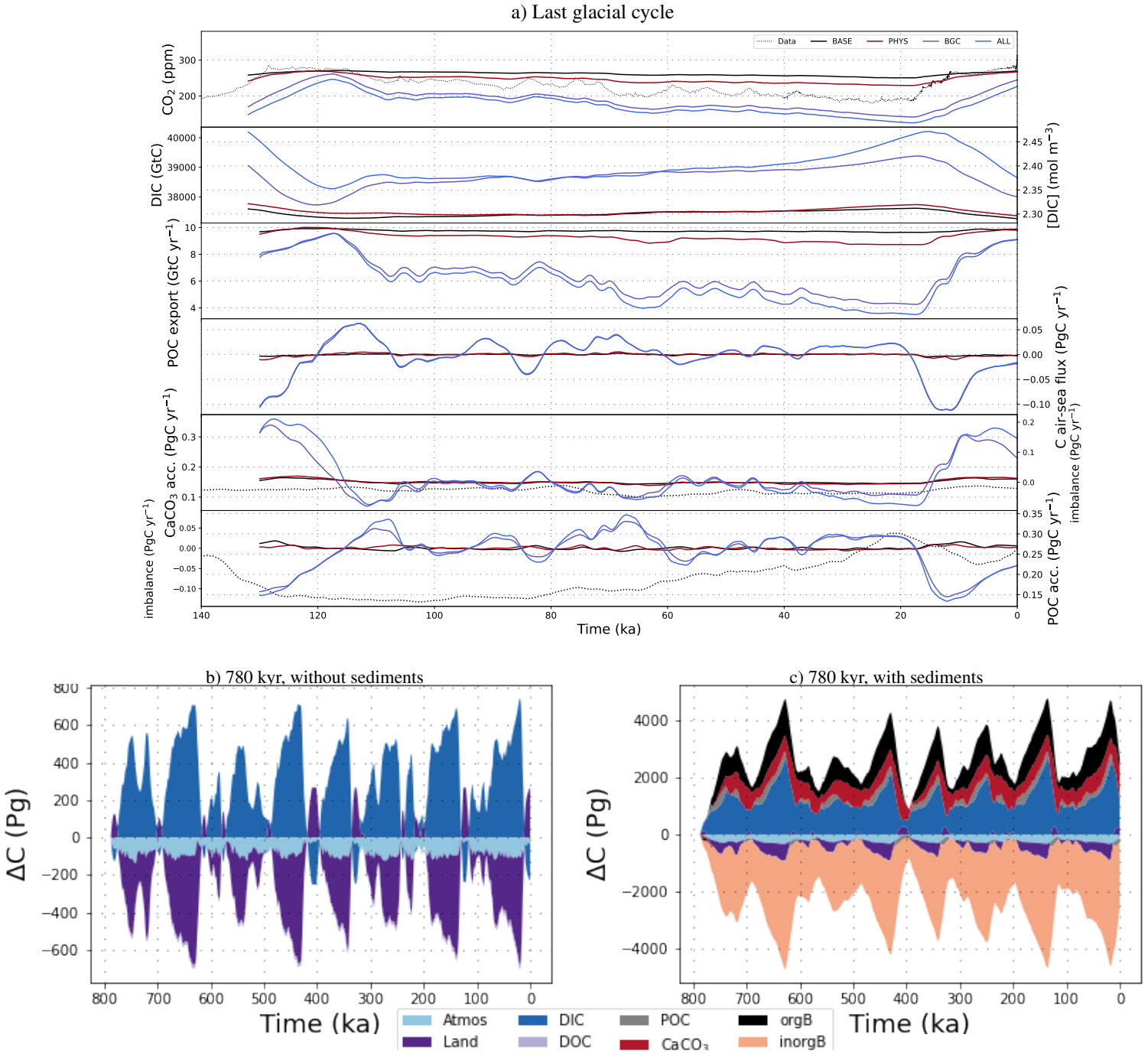

Figure S7. a) Atmospheric CO_2 concentrations, DIC and carbon fluxes over the most recent full glacial cyle in simulations with different combinations of additional forcings in an open system. b) Transient carbon reservoir size changes across the last 780 kyr as simulated with all additional forcings combined in a closed system and c) in an open system. Shown are the size changes of atmospheric, terrestrial, marine (DIC and DOC), sedimentary (POC and $CaCO_3$) and lithospheric (organic and inorganic) carbon storage. Flux timeseries for simulations in a closed system are displayed in Fig **??**.

The three tested physical forcings combine almost linearly in their effect on atmospheric CO_2. Circulation change is dominated by radiation reductions, with strong AMOC weakening during glacials and some reduction of the PMOC, but less than in simulation SOWI because of increased sea ice cover in the Southern Ocean which limits the effect of wind stress changes. In consequence, the glacial deep ocean holds more nutrients when all forcings are combined: it has a large Atlantic reservoir due to sluggish overturning and a larger Pacific reservoir than in SOWI due to less organic carbon burial. During deglaciation, the release of these nutrients back into the surface ocean creates a larger productivity spike than when the forcings are applied individually, reducing marine $[O_2]$ further but causing only a minimal temporary reduction of <5 ppm in atmospheric CO_2 (Fig. S7). In simulations with interactive sediments, additional radiative forcing (AERO) and Southern Ocean wind forcing (SOWI) shift sedimentary $CaCO_3$ and POC accumulation rates in opposite directions. Yet, their effects on nutrient, temperature and oxygen distributions are almost additive.

While physical effects on carbon concentrations combine almost linearly, the combination of ~~biochemical~~ biogeochemical forcings is non-linear because they directly alter production and dissolution patterns in opposing ways. Acidification of benthic water masses through external nutrient (PO4) and carbon (LAND) supply during glacials counteracts the benthic pH increase under a deepened remineralisation depth (REMI). When all ~~biochemical~~ biogeochemical forcings are combined, net $CaCO_3$ fluxes into marine sediments are reduced during glacial maxima and increased during terminations, but the burial peak is delayed. ~~Biochemical~~ Biogeochemical forcings dominate the carbon cycle response when all forcings are combined, except for the North Atlantic where circulation changes cause the biggest perturbation. The magnitude of the non-linearities that occur when all forcings are combined is similar to the combined effect of only the physical forcings.

~~Climate feedback effects~~

~~Atmospheric CO_2 concentrations, DIC and carbon fluxes over the most recent full glacial cyle in simulations with all additional forcings combined in an open system, with and without climate feedback.~~

~~All simulations described so far were run with prescribed radiative forcing, i.e. without the radiative effect of simulated CO_2 changes. The benefit of this setup is that the climatic changes in the simulations are comparable, allowing to distinguish the carbon cycle effects of temperature change from the other physical and biochemical changes we simulated. At the same time, however, this simplified setup creates a bias by neglecting the climate feedback of carbon cycle changes. To assess the effect of this bias in the prescribed carbon cycle dynamics, we reran simulation ALL, which contains all tested forcings, with the carbon cycle climate feedback (ALL-Clim). The prescribed forcings in simulation ALL result in a glacial-interglacial CO_2 change that is 30% larger than in observations, but with absolute CO_2 values mostly below those reconstructed. Including the radiative effect of this CO_2 offset results in up to 2.5° colder glacial maxima. Simulation AERO showed that cooling has only limited effects on the carbon cycle. The additional cooling increases marine CO_2 uptake and reduces primary productivity, and consequently the amount of $CaCO_3$ and POC reaching the sediments, during glacial phases. The climate response to the simulated carbon cycle changes thus causes a net C and nutrient transfer into the ocean, increasing the peak glacial-interglacial atmospheric CO_2 difference by 10 ppm.~~

Additional Figures

~~a) BASE, KGAS, SOWI, AERO~~

Table S1. Prescribed constant solute input into the surface ocean to balance steady-state interglacial sedimentary burial fluxes.

	~~b) PIPO, BGC, ALL, CO2T~~ DIC (GtC/yr)	ALK (Tmol eq/yr)	PO_4^{3-} (Tmol P/yr)	SiO (Tmol Si/yr)	$DI^{13}C$
heightBASE	0.414	21.61	0.19	4.52	

~~Transient variations of atmospheric CO_2 concentrations as simulated in the simulations not shown in Fig. 5 in the main text, and as reconstructed by Bereiter et al. (2015). Shown is the deviation from the respective pre-industrial value.~~

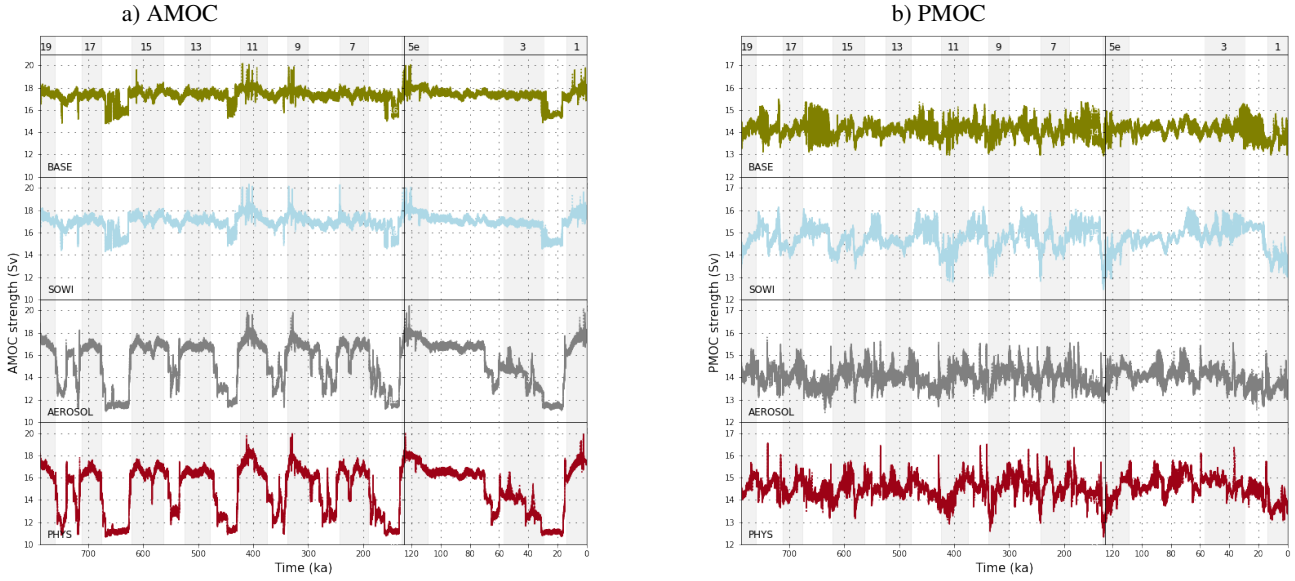

Figure S8. Transient variations of AMOC and PMOC strengths in simulations with different physcial forcings.

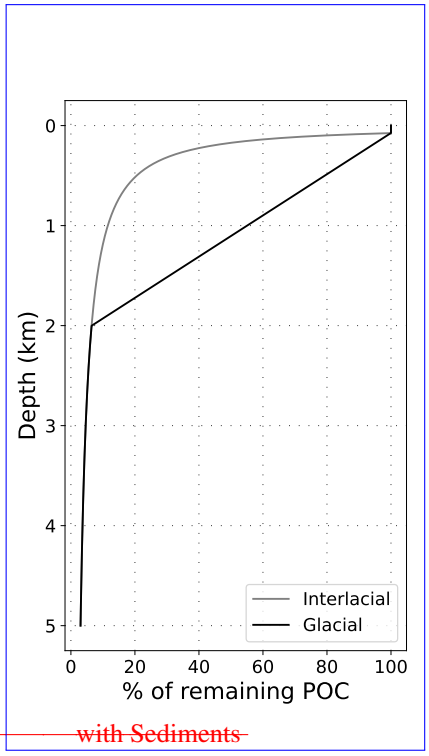

~~without Sediments~~ ~~with Sediments~~

Figure S9. Comparison of the interglacial and glacial end-members of the prescribed remineralization profiles.

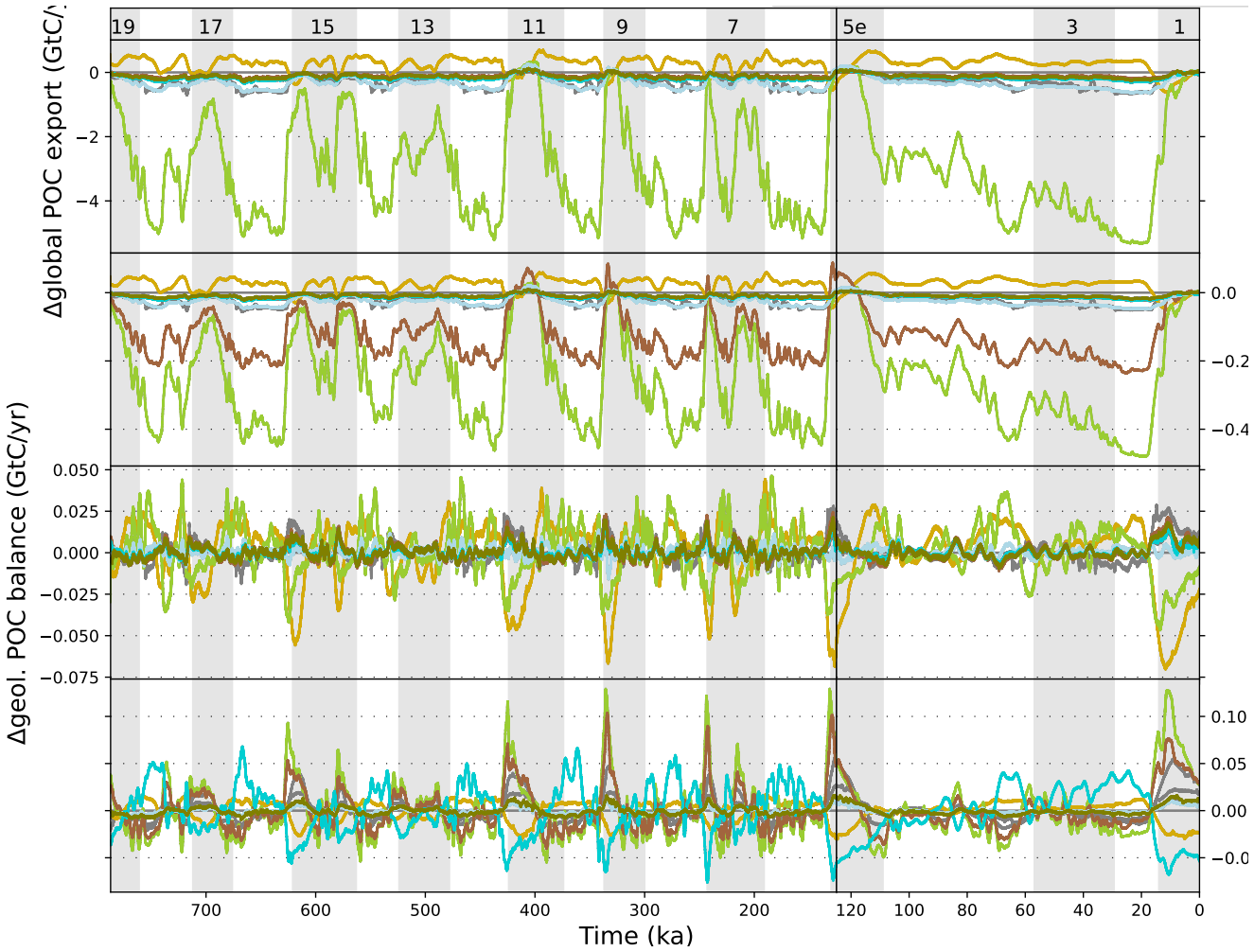

Figure S10. Transient variations of POC and $CaCO_3$ export production and geologic imbalance (i.e. the difference between accumulation of these materials in marine sediments and the constant supply into the surface ocean that mimics terrestrial weathering in our simulations) due to the applied forcings. Shown are the absolute results for each simulation. The results that are explicitly mentioned in the text are shown in colour, the others are shown in gray. Gray shading indicates uneven MIS as indicated at the top of the figure.

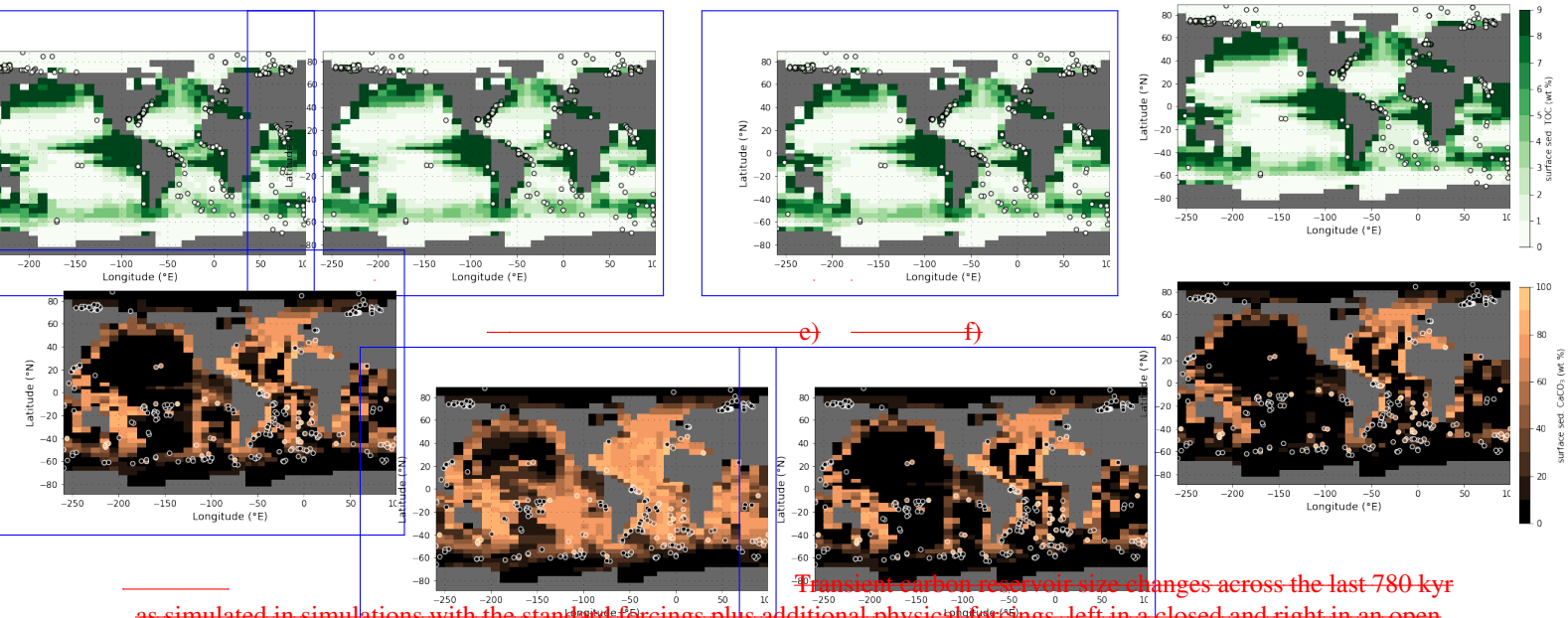

~~Transient carbon reservoir size changes across the last 780 kyr as simulated in simulations with the standard forcings plus additional physical forcings, left in a closed and right in an open system. Shown are the size changes of atmospheric, terrestrial, marine (DIC and DOC), sedimentary (POC and $CaCO_3$) and lithospheric (organic and inorganic) carbon storage.~~

Figure S11. ~~Atmospheric CO_2 concentrations, DIC~~ Sedimentary POC and ~~carbon fluxes over~~ $CaCO_3$ fractions during the ~~most recent full glacial cycle~~ late Holocene (Hayes et al., 2021) as reconstructed (circles) and in simulations ~~with additional physical forcings~~ PHYS, REMI, PO4 and ~~without dynamic sediments~~CO2T (underlying maps). Shown are only data points that fall into the local benthic grid box of the model. The root mean square errors of simulated and reconstructed values are (from left to right): 7.6 %, 7.0 %, 7.6 % and 8.2 % for POC (top row) and 27.5 %, 25.7 %, 29.4 % and 31.4 % for $CaCO_3$ (bottom row).

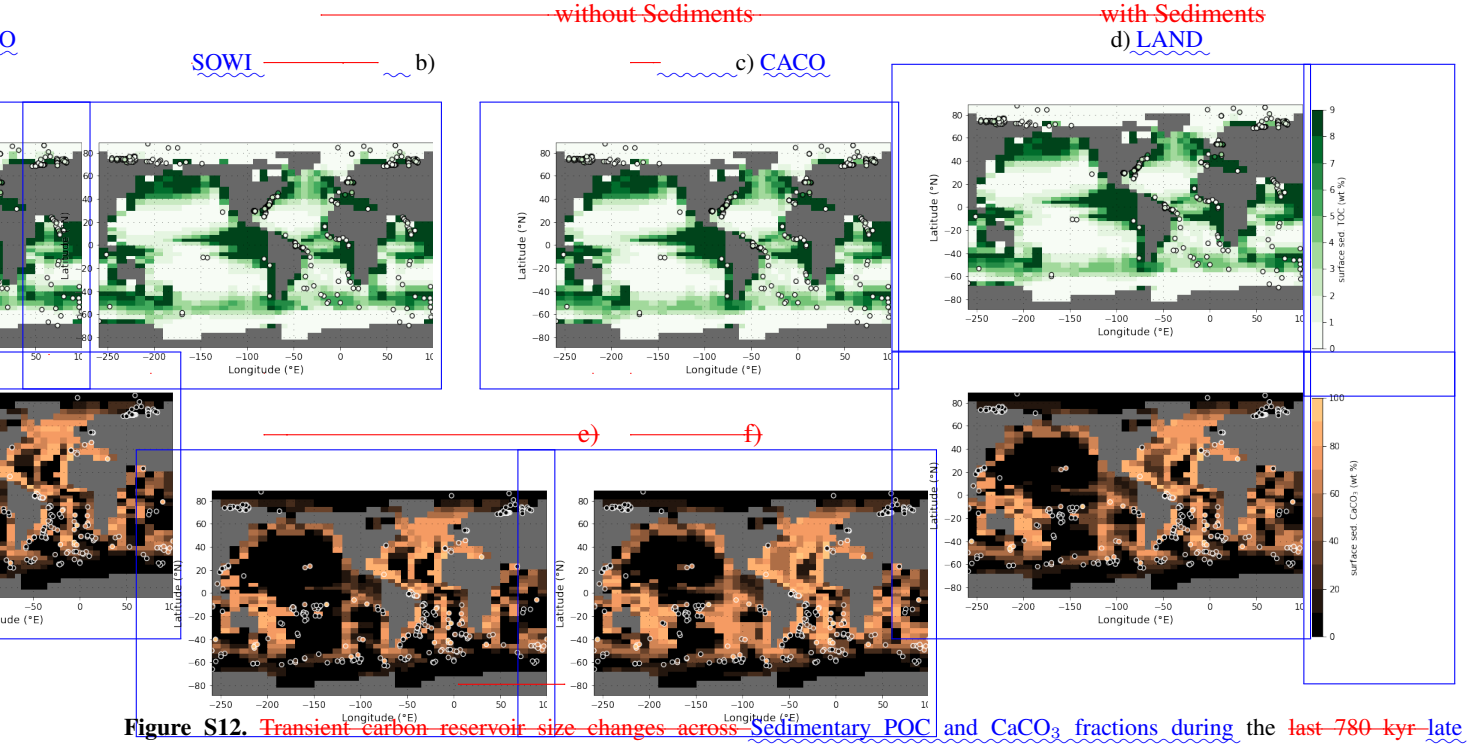

Figure S12. ~~Transient carbon reservoir size changes across~~ Sedimentary POC and $CaCO_3$ fractions during the ~~last 780 kyr~~ late Holocene (Hayes et al., 2021) as ~~simulated~~ reconstructed (circles) and in simulations ~~with the standard forcings plus additional biochemical forcings~~AERO, ~~left in a closed~~ SOWI, CACO and ~~right in an open system~~LAND (underlying maps). Shown are only data points that fall into the ~~size changes~~ local benthic grid box of ~~atmospheric~~the model. The root mean square errors of simulated and reconstructed values are (from left to right): 8.8 %, ~~terrestrial~~9.4 %, ~~marine (DIC~~ 7.6 % and ~~DOC~~7.6 % for POC (top row) and 27.2 %, ~~sedimentary (POC~~ 27.8 %, 26.2 % and 26.6 % for $CaCO_3$ ~~) and lithospheric~~ (~~organic and inorganic~~bottom row)~~carbon storage~~.

without Sediments a) $fCO2T$, $fKGAS$, $fSOWI$, $fAERO$ b) $fPIPO$, $fLAND$, $fBGC$, $fALL$

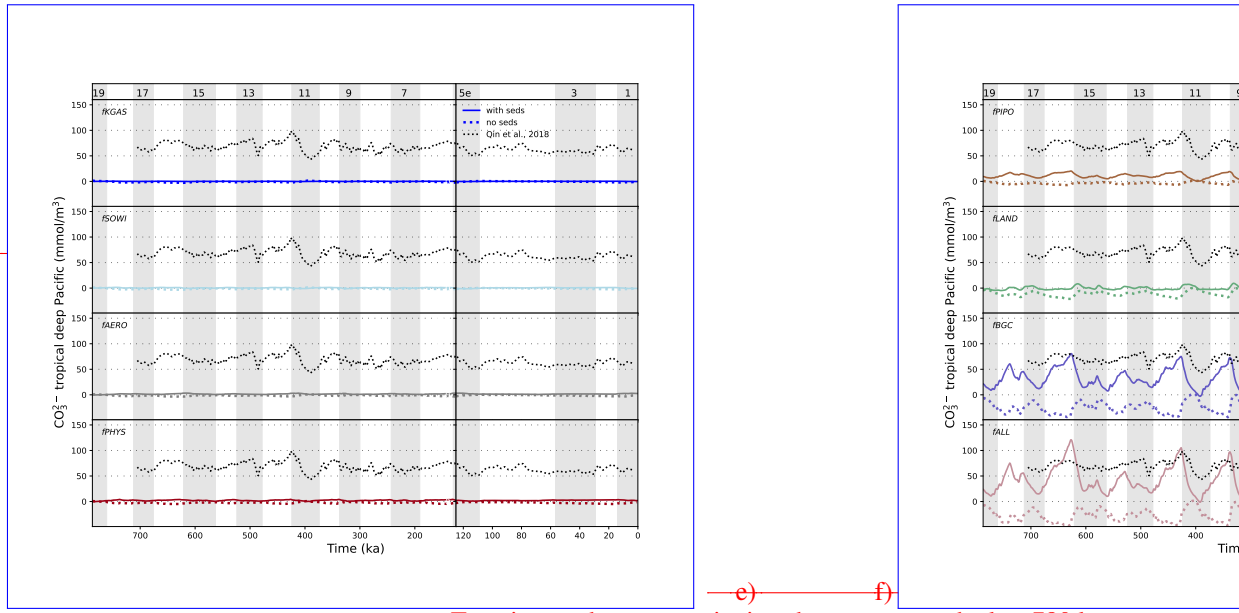

c) f)

Transient carbon reservoir size changes across the last 780 kyr as simulated in simulations with the standard forcings plus terrestrial C fluxes, left in a closed and right in an open system. Shown are the size changes of atmospheric, terrestrial, marine (DIC and DOC), sedimentary (POC and $CaCO_3$) and lithospheric (organic and inorganic) carbon storage.

Atmospheric CO_2 concentrations, DIC and carbon fluxes over the most recent full glacial cyle in simulations with additional biochemical forcings and without dynamic sediments.

Atmospheric CO_2 concentrations, DIC and carbon fluxes over the most recent full glacial cyle in simulations with combinations of additional forcings and without dynamic sediments.

Figure S13. Transient variations of CO_3^{2-} in the tropical deep Pacific as simulated in simulations and reconstructed by Qin et al. (2018).

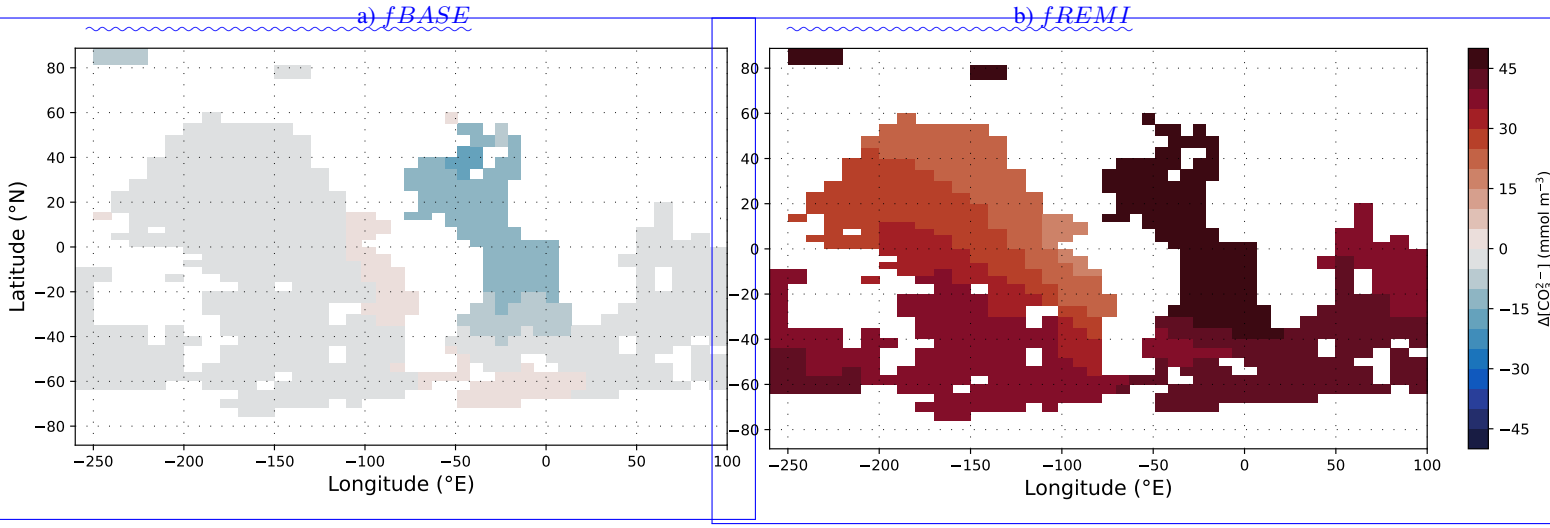

Figure S14. ~~Difference of the glacial-interglacial atmospheric CO_2 amplitude before and after the MBT in our simulations without interactive sediments compared to that~~ Selected factorial effects on simulated LGM-PI differences in ~~the reconstructed~~ deep CO_3^{2-} ~~CO_2 record (Bereiter et al., 2015, , horizontal black line)~~ (3500 m depth).

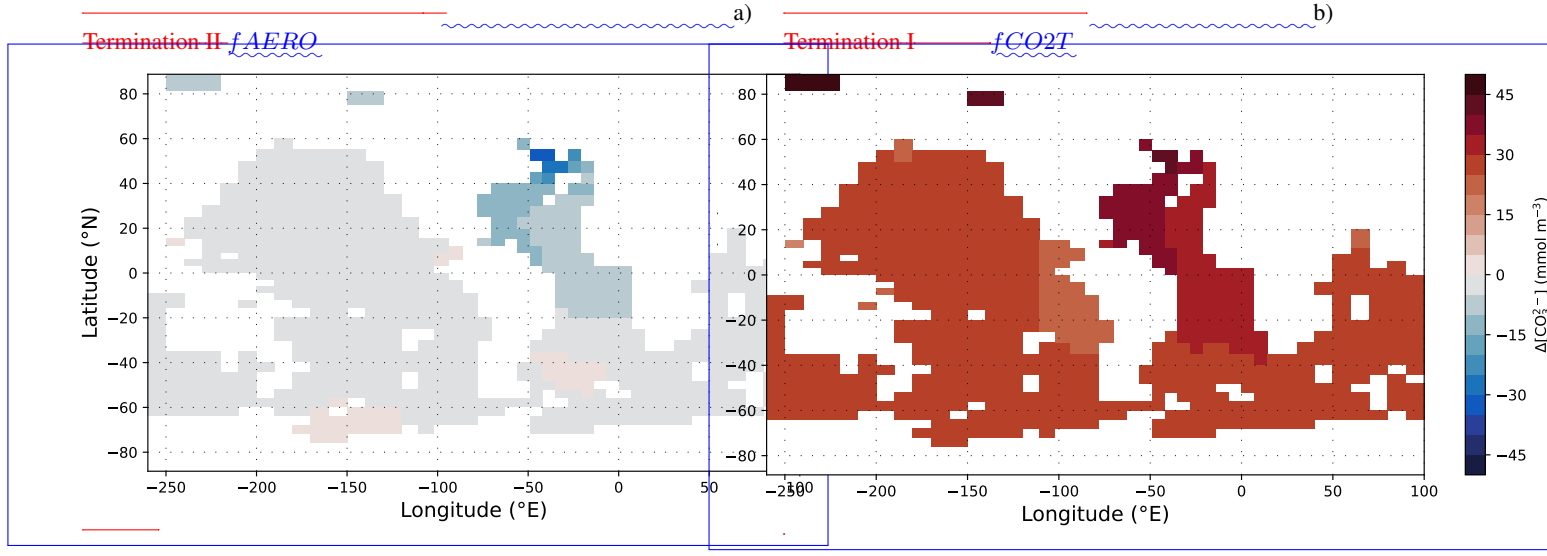

Figure S15. ~~$\delta^{18}O$-derived scaling of the prescribed forcing and the resulting~~ Selected factorial effects on simulated ~~atmospheric CO_2, normalized by the respective PI-LGM CO_2 difference,~~ LGM-PI differences in ~~selected simulations with interactive sediments (top row) and without interactive sediments~~ deep CO_3^{2-} (~~bottom row~~3500 m depth).

a) ~~Termination II~~ BASE, KGAS, SOWI, AERO

b) ~~Termination I~~ PIPO, BGC, ALL, CO2T

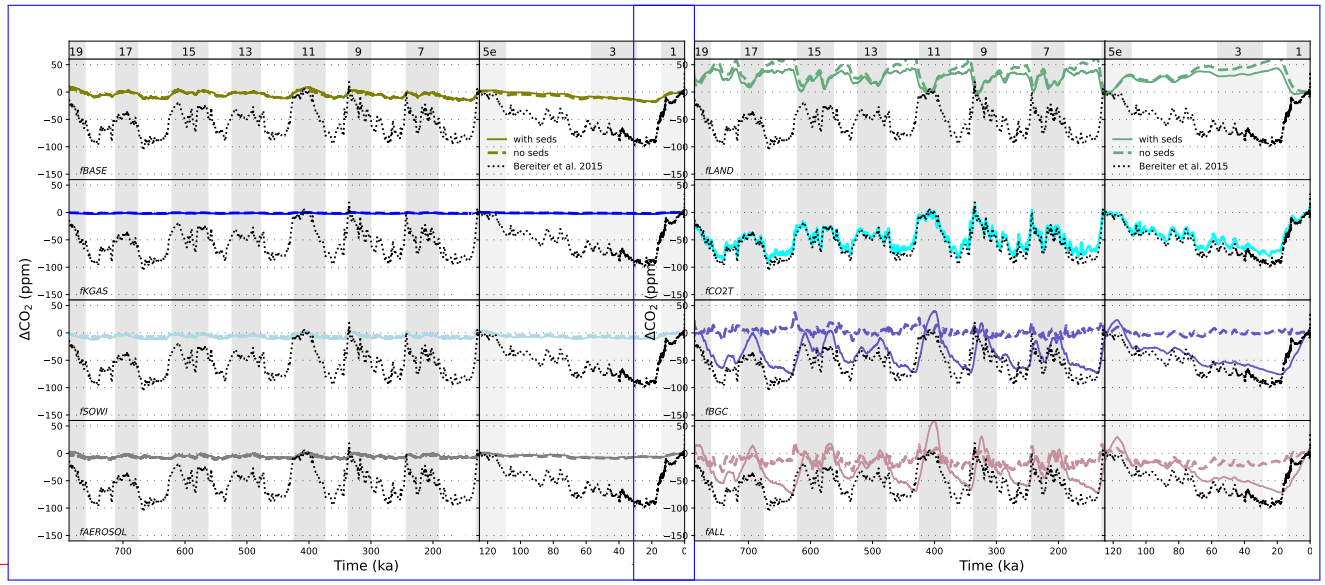

Figure S16. ~~δD-derived scaling~~ Transient variations of ~~the prescribed forcing and the resulting simulated~~ atmospheric CO_2 concentrations as simulated in the simulations not shown in Fig. 5 in the main text, ~~normalized~~ and as reconstructed by Bereiter et al. (2015). Shown is the deviation from the respective ~~PI-LGM CO_2 difference, in selected simulations with interactive sediments (top row) and without interactive sediments (bottom row)~~pre-industrial value.

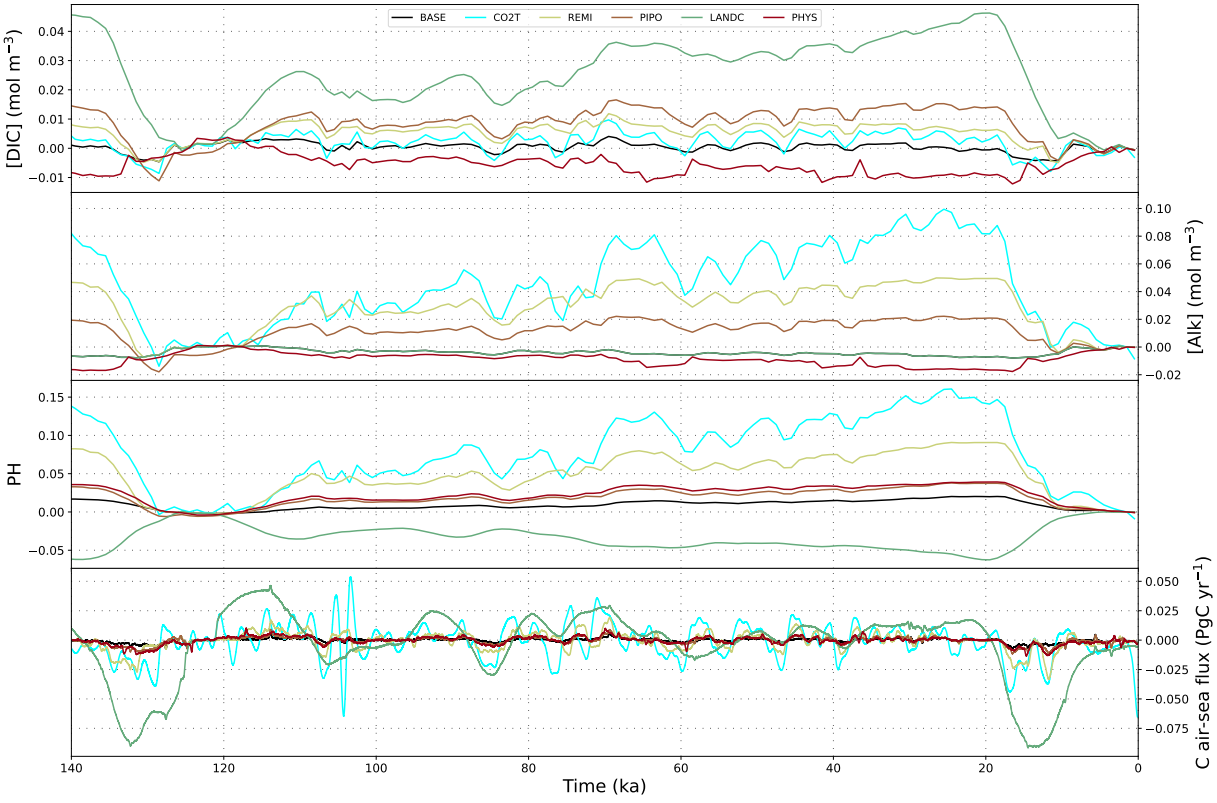

Figure S17. Globally-averaged changes in surface ocean carbonate system parameters in selected simulations without interactive sediments.

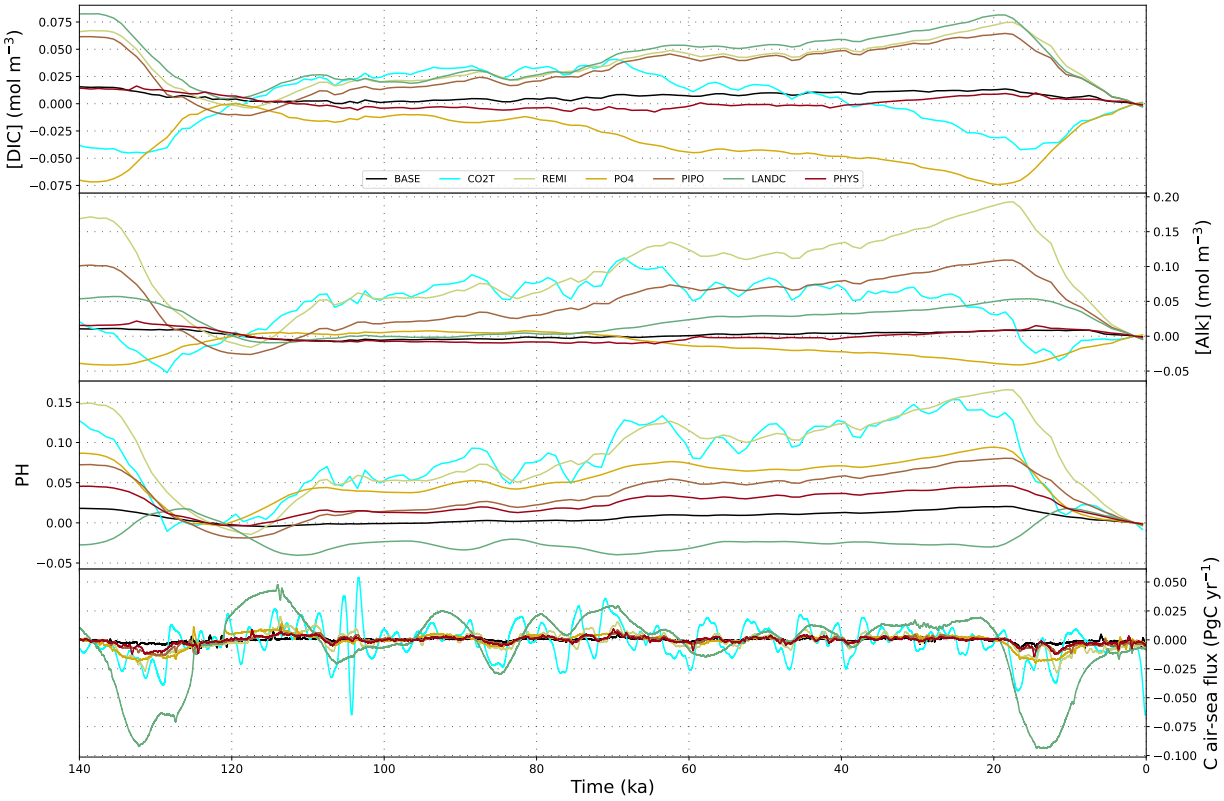

Figure S18. Globally-averaged changes in surface ocean carbonate system parameters in selected simulations with interactive sediments.

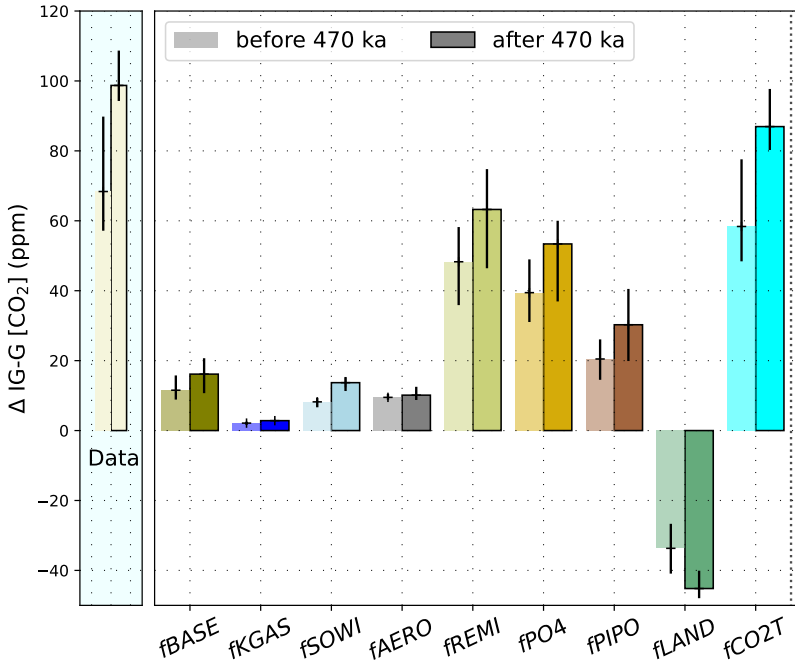

Figure S19. Difference of the glacial-interglacial atmospheric CO_2 amplitude before and after the MBT in our simulations compared to that in the reconstructed CO_2 record (Bereiter et al., 2015). For the results of the simulations without interactive sediments see Fig. S19

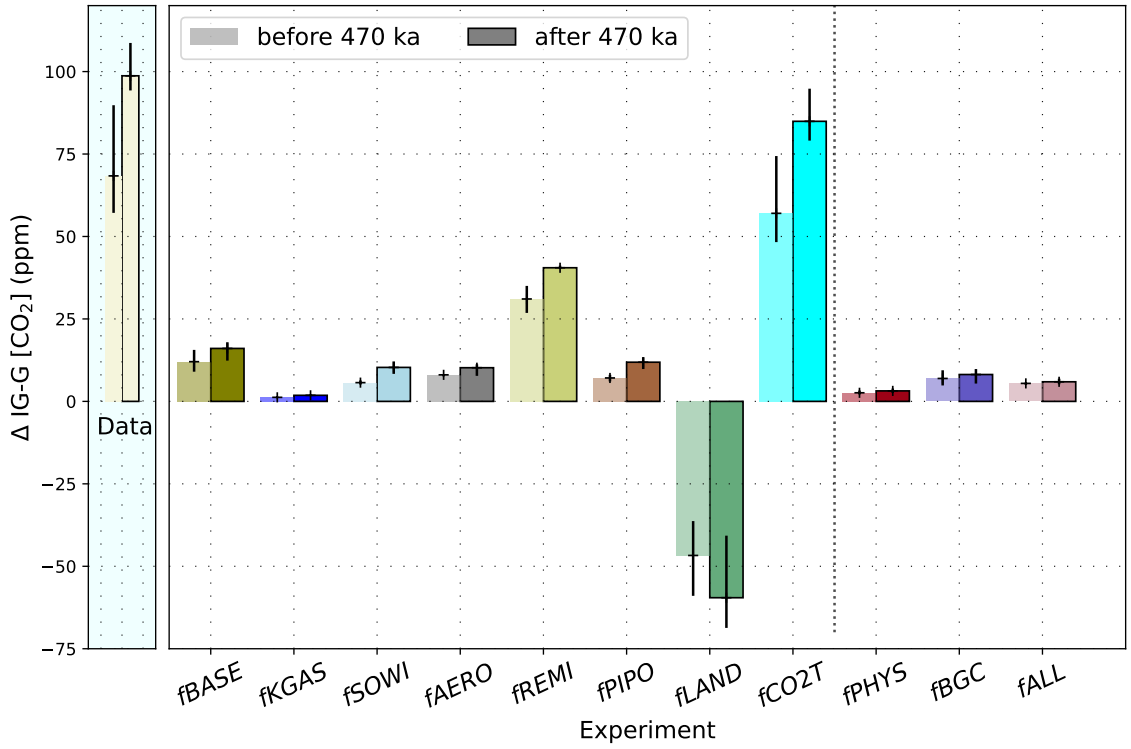

Figure S20. Difference of the glacial-interglacial atmospheric CO_2 amplitude before and after the MBT in our simulations without interactive sediments compared to that in the reconstructed CO_2 record (Bereiter et al., 2015, , horizontal black line).

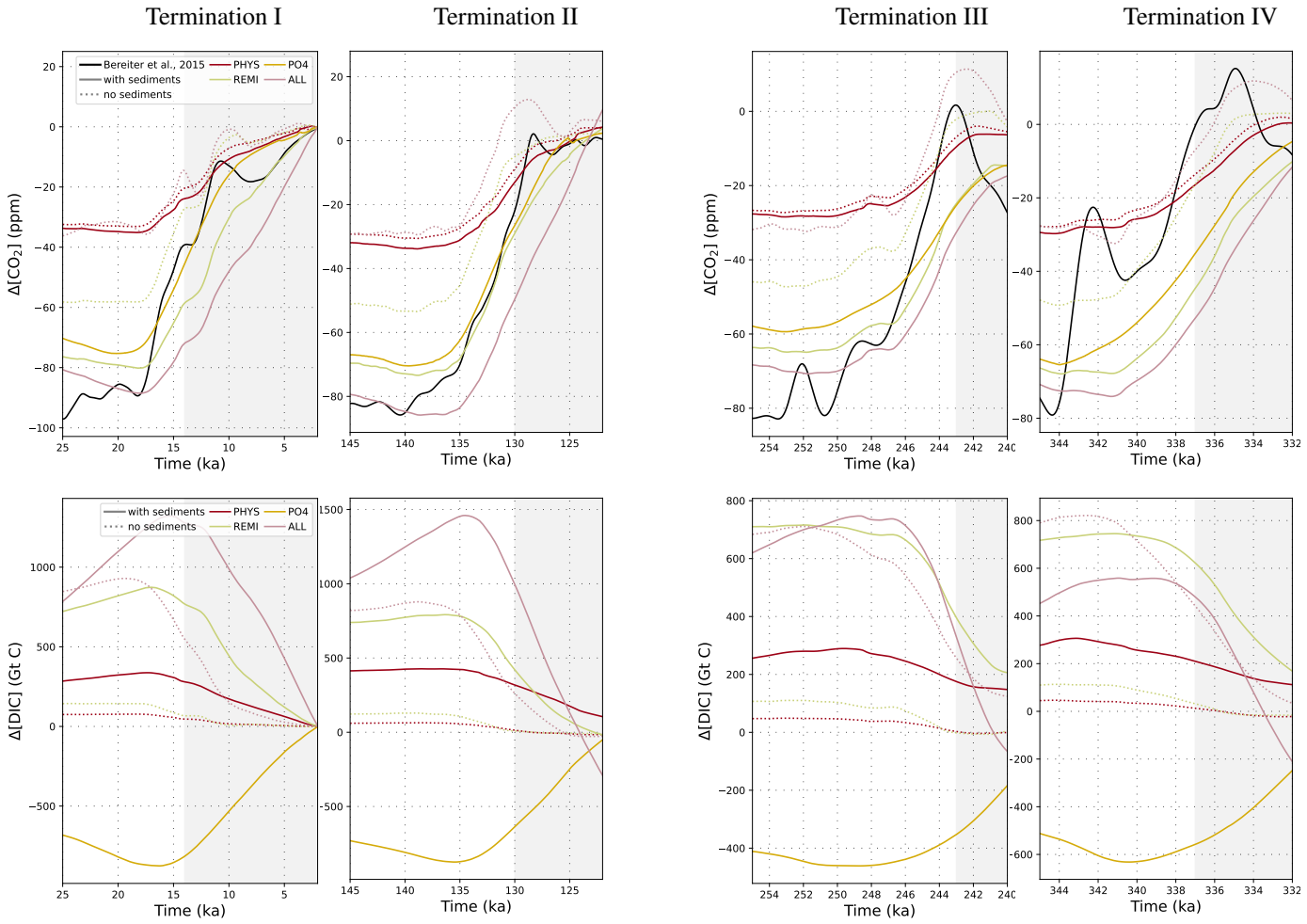

Figure S21. Reconstructed and simulated atmospheric CO_2 changes (upper row) and simulated DIC changes (lower row) across the last four deglaciations.

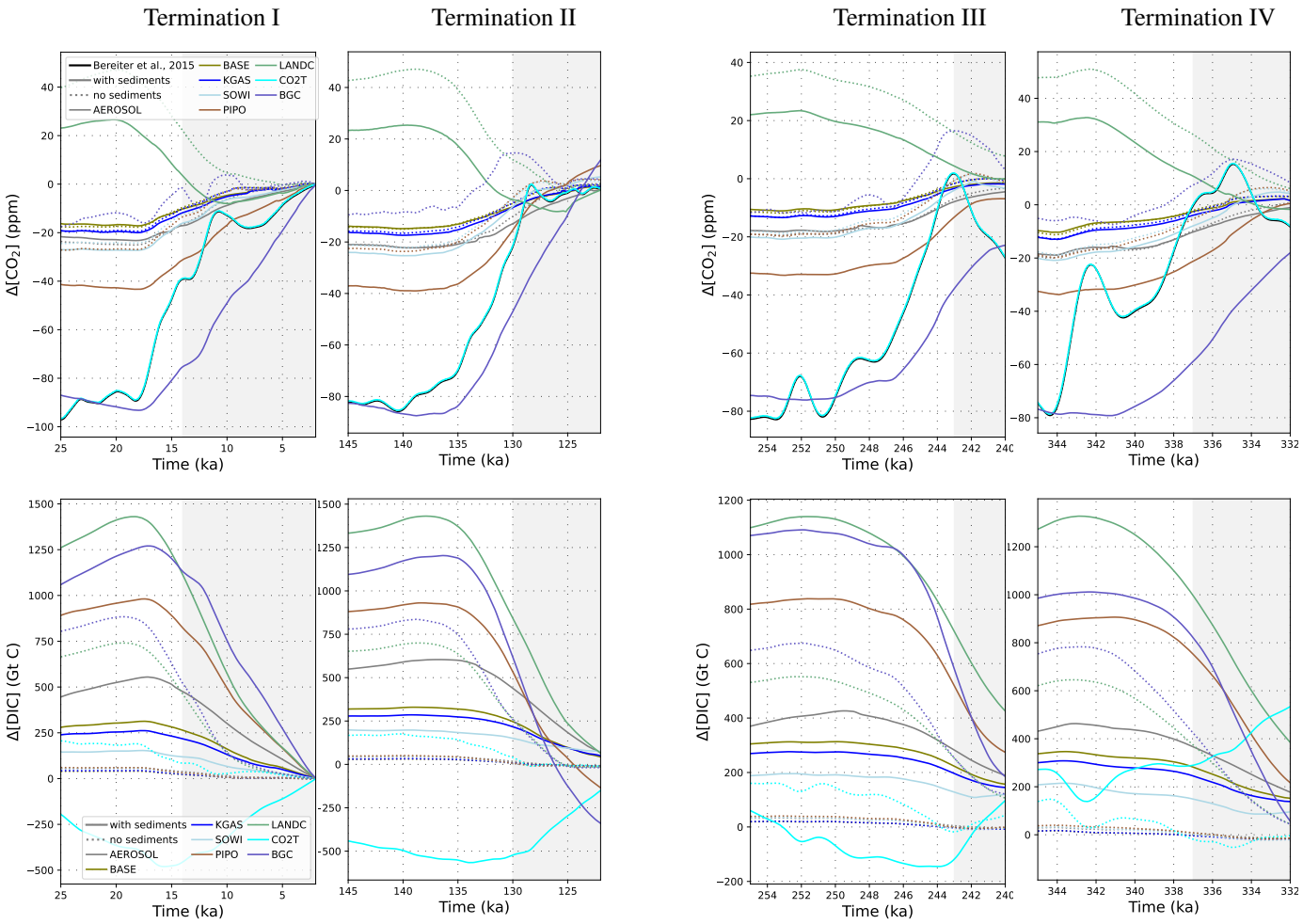

Figure S22. Reconstructed and simulated atmospheric CO_2 changes (upper row) and simulated DIC changes (lower row) across the last four deglaciations.

Table S2. ~~Globally-averaged changes in surface ocean carbonate system parameters in selected simulations without interactive sediments~~Dynamical geologic carbon cycle imbalances (marine outputs - inputs) at the end of each simulation.

~~Globally-averaged changes in surface ocean carbonate system parameters in selected simulations with interactive sediments.~~
~~Globally-averaged changes in nutrient utilization in the surface ocean across the simulated 780 kyr.~~
~~Globally-averaged changes in $PO_{4,pre}$ concentrations across the simulated 780 kyr.~~
~~The effect of step changes of plus or minus 30% of the prescribed clay flux on atmospheric CO_2 concentrations, DIC and carbon fluxes over 100 kyr.~~
~~a) 120 ka - 20 ka~~

Simulation

~~l factorial effects on simulated LGM-PI differences in deep CO_3^{2-} (3500 m depth).~~ ~~a) Atmosphere~~ height

height KGAS

~~c) PIPO~~ height SOWI

height AERO

~~δ^{13}C over the most recent glacial cycle in various reservoirs. Full lines are simulation results with different physical forcings in a closed~~

height PHOS

~~BASE~~ ~~KGAS~~ height

LAND

~~PHYS~~ ~~BGC~~ height

ht PHYS

ht BGC

ht ALL

height

~~Simulated (open system) and reconstructed (compilation from Pöppelmeier et al. (2023)) Holocene δ^{13}C distribution Pacific.~~

without Sediments

Sediments

BASE

KGAS

SOWIwit

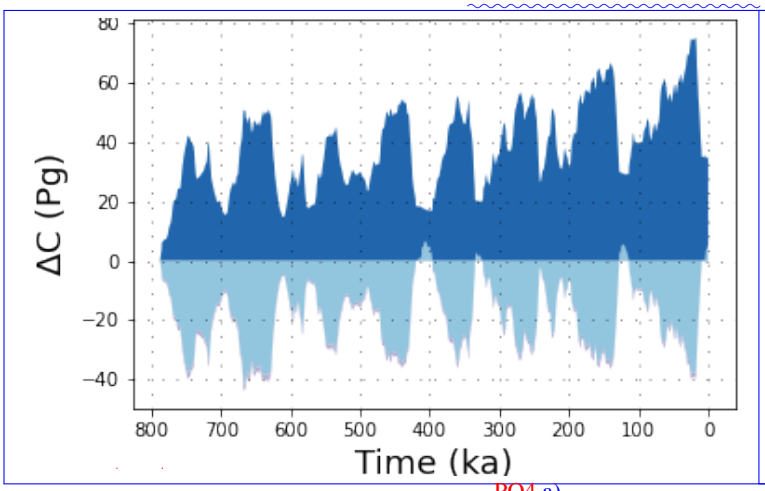

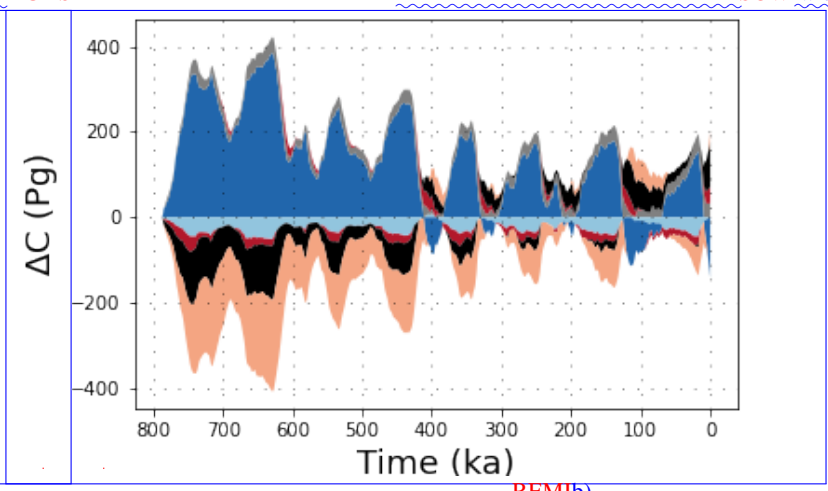

PO4 a)

REMIb)

AERO

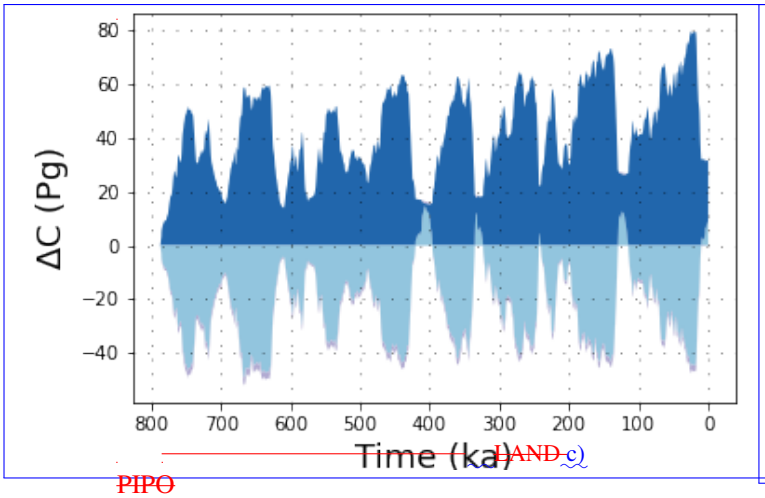

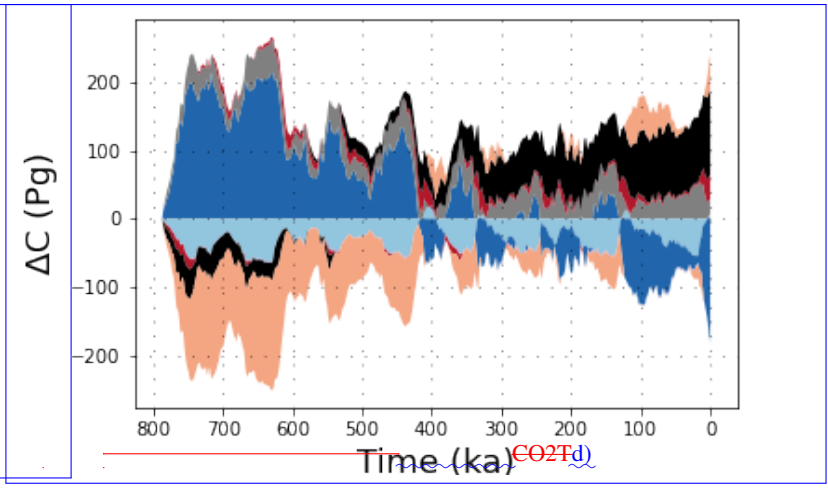

AND c)

CO2Td)

PIPO

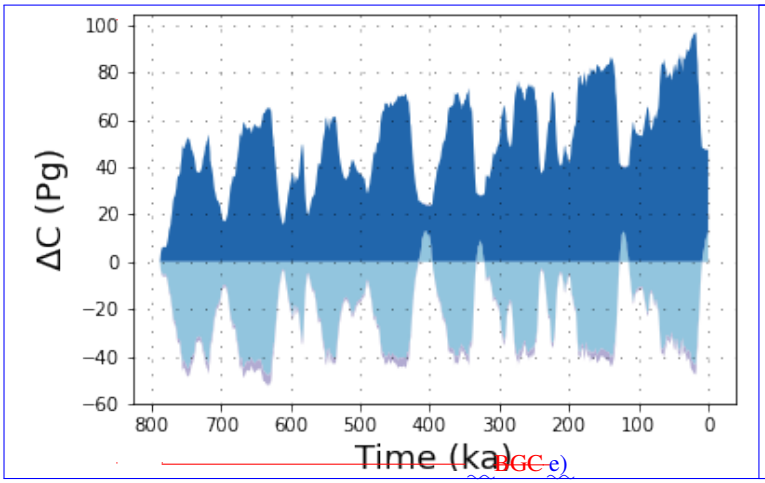

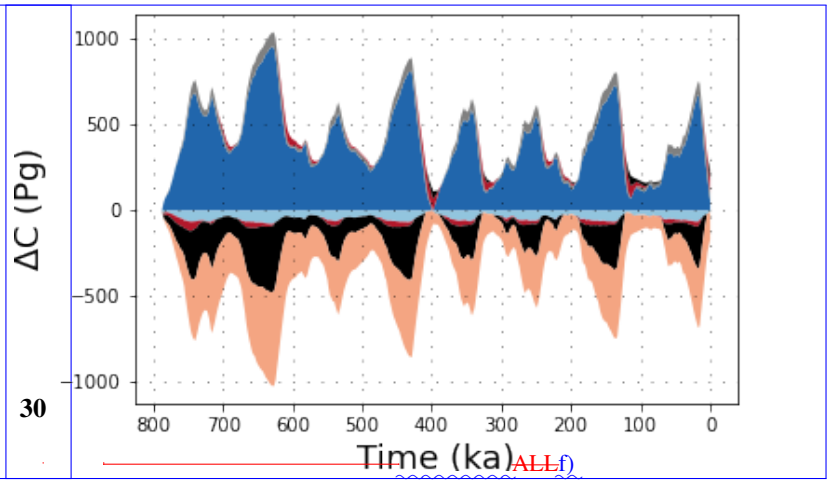

BGC e)

ALLf)

PHYS

~~BASE~~

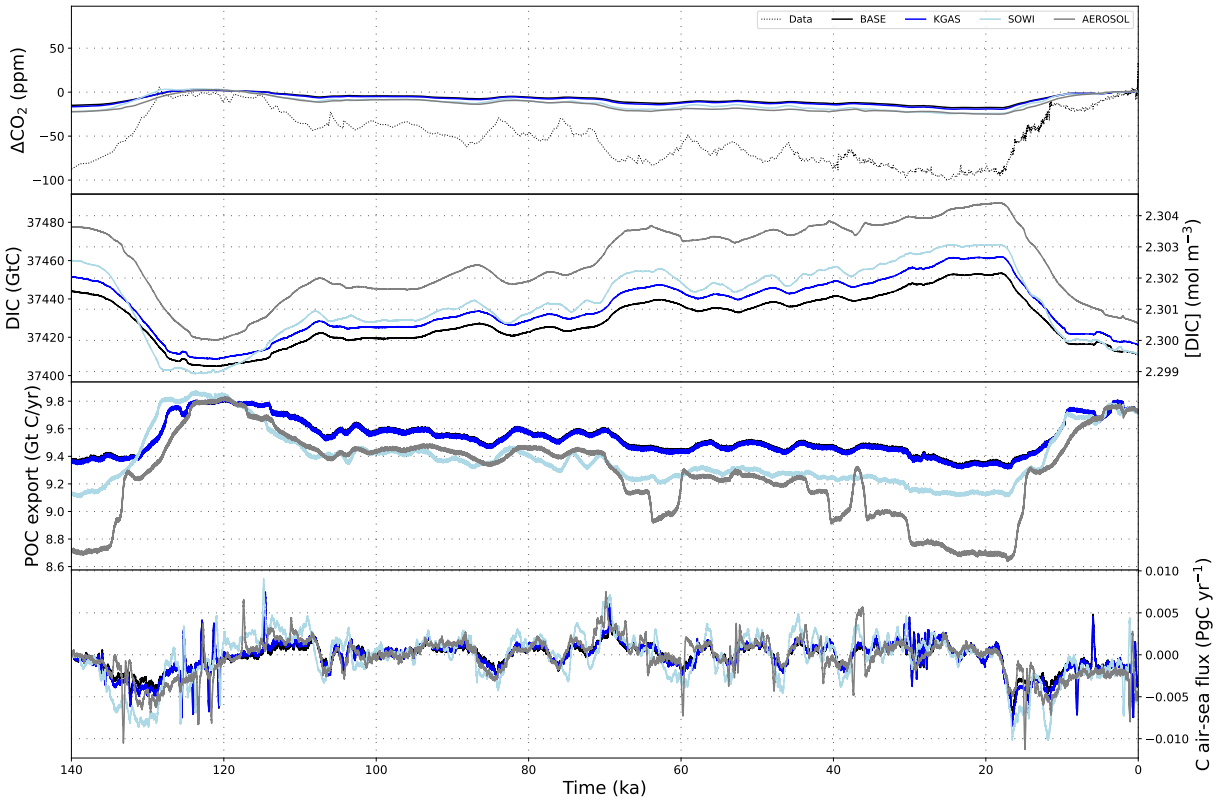

Figure S24. Atmospheric CO_2 concentrations, DIC and carbon fluxes over the most recent full glacial cyle in simulations with additional physical forcings and without dynamic sediments.

without Sediments

Sediments

KGAS

SOWIwit

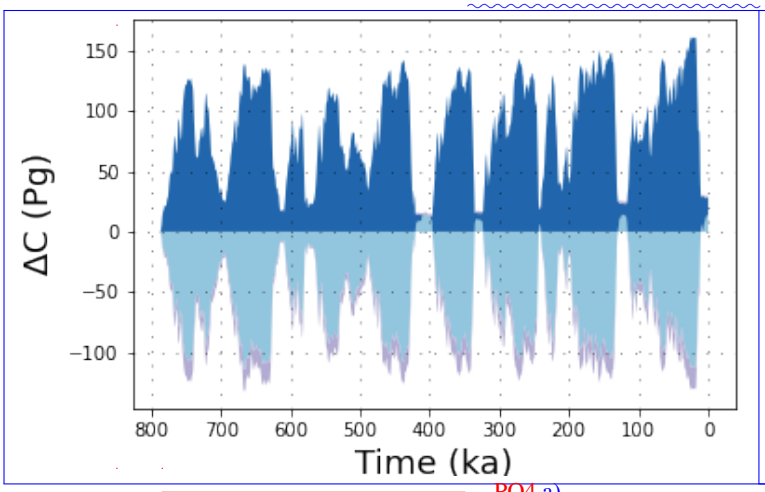

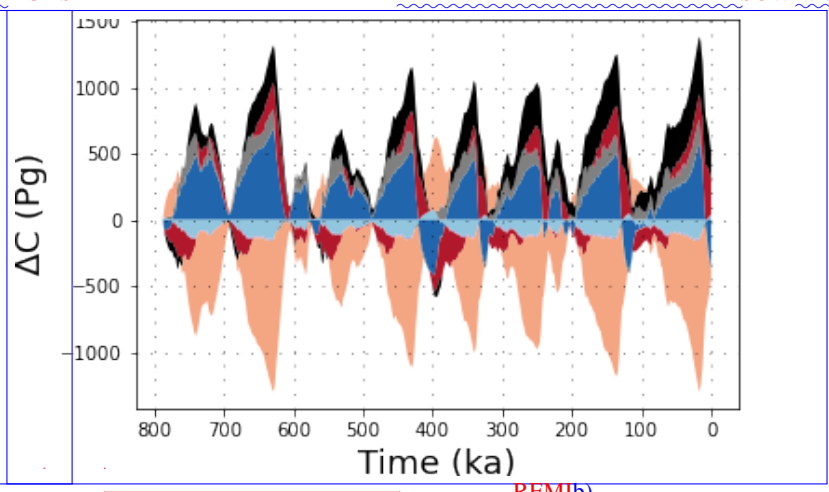

PO4 a)

REMIb)

AERO

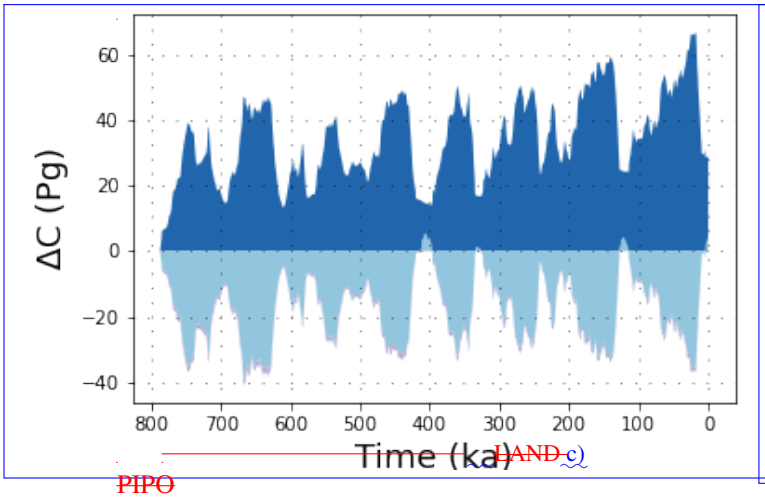

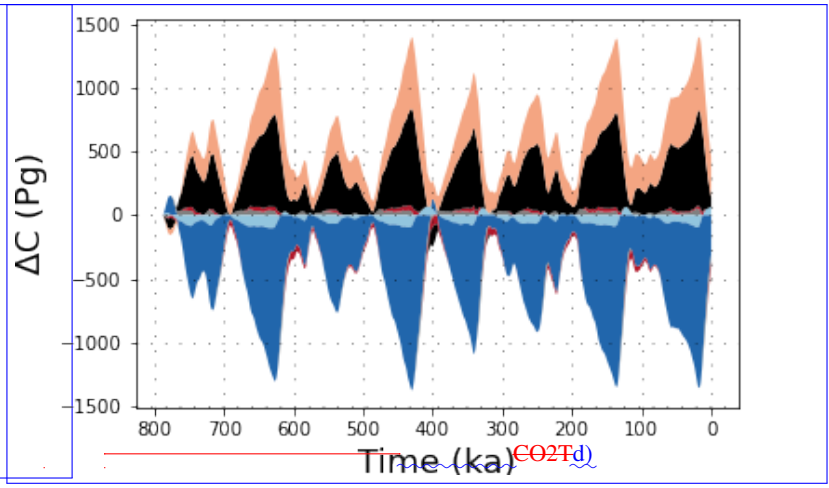

bAND c)

CO2Td)

PIPO

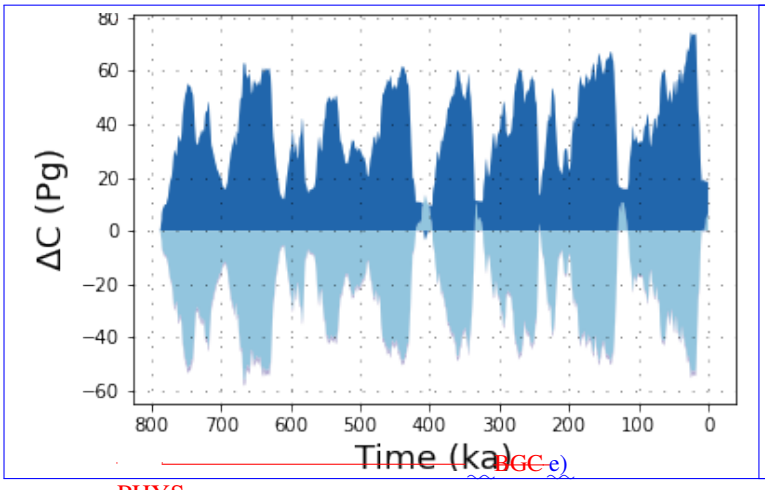

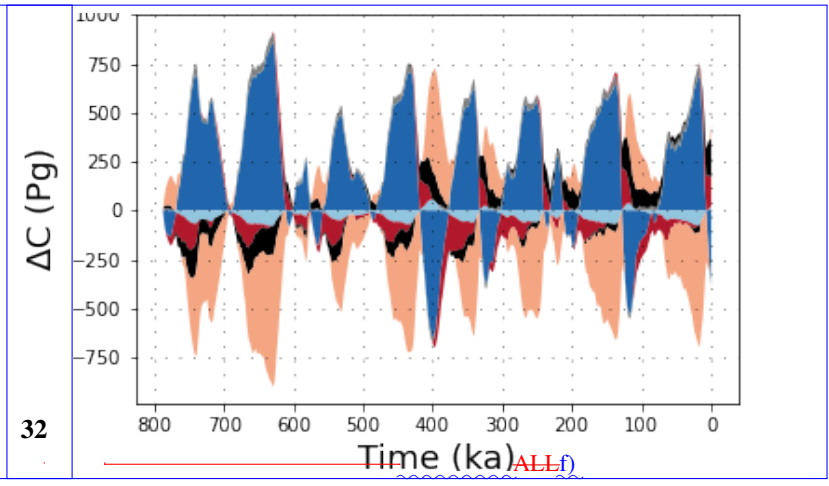

BGC e)

ALLf)

PHYS